

Measuring the Frequency of Light using Femtosecond Laser Pulses

Dissertation
der Fakultät für Physik
der Ludwig-Maximilians-Universität München

vorgelegt von
Ronald Holzwarth
aus Stuttgart

München, den 21. Dezember 2000

„Nichts auf der Welt ist so mächtig, wie eine Idee, deren Zeit gekommen ist.“

“There is nothing so powerful as an idea whose time has come.”

Victor Hugo

1. Gutachter: Prof. Dr. T. W. Hänsch
2. Gutachter: Prof. Dr. J. Habs

Tag der mündlichen Prüfung: 2.3.2001

Zusammenfassung

Im Rahmen dieser Arbeit wurde eine neue Methode zur Messung optischer Frequenzen entwickelt, angewandt und verfeinert.

Messen bedeutet vergleichen. Die SI Sekunde als maßgebliche Zeit- und Frequenzeinheit ist durch die 9.2 GHz Hyperfeinaufspaltung des Cäsium Grundzustandes definiert. Zur Präzisionsmessung optischer Frequenzen müssen also Radiofrequenzen mit optischen Frequenzen im Bereich einiger 100 THz, für die es keine Elektronik mehr gibt, verglichen werden.

Die grundlegende Idee besteht nun darin, den vom periodischen Pulszug eines moden-gekoppelten Femtosekundenlasern erzeugten Kamm equidistanter Moden als Maßstab zur Vermessung großer Frequenzlücken zu benutzen. Wendet man diese Frequenzkamm-Technik auf die Frequenzintervalle zwischen den harmonischen Schwingungen desselben Lasers an, also z. B. auf das Intervall zwischen einer optischen Frequenz f und der zweiten Harmonischen $2f$, so hat man auf denkbar einfache Weise die optische Frequenz $f = 2f - f$ selbst gemessen. Dies erfordert allerdings Frequenzkämme, die eine Breite im Bereich der optischen Frequenzen, also mehrerer 100 THz haben. Das kann entweder durch sehr kurze Pulse (5 fs) oder durch spektrale Verbreiterung durch Selbstphasenmodulation von moderat kurzen Pulsen im Bereich einiger 10 fs in Glasfasern erreicht werden. Besonders effizient funktioniert die Verbreiterung in sogenannten photonischen Kristallfaser. In diesen speziellen Glasfasern wird das Licht in einem sehr kleinen Kern (1-2 μm) geführt, der von Luftkanälen umgeben ist.

Am Ende dieser Entwicklung steht die „Ein-Laser-Frequenzkette“, die nur noch aus einem fs-Laser, einer photonischen Kristallfaser und etwas Optik besteht und die trotzdem den optischen Spektralbereich mit dem Radiofrequenz-Spektralbereich verbindet. Dabei kann praktisch jede optische Frequenz im sichtbaren und nahinfraroten Bereich mit demselben kompakten Gerät gemessen werden.

Ursprünglich gestartet wurde das Projekt „Frequenzkette“ zur Präzisionspektroskopie am 1S-2S Übergang in Wasserstoff, ein traditionsreiches Projekt unserer Arbeitsgruppe, und führte hier zur bislang genauesten optischen Frequenzmessung mit einer relativen Unsicherheit von 1.8×10^{-14} . Wasserstoff als einfachstes gebundenes System ist ein Prüfstein für die Quantenelektrodynamik, die Messung der 1S Lamb Verschiebung in Wasserstoff stellt einen der genauesten QED Tests dar. Außerdem kann aus optischen Frequenzmessungen am Wasserstoff die Rydbergkonstante sehr präzise bestimmt werden. Darauf hinaus zeigte sich sehr bald das Potential und die breite Anwendbarkeit dieser Entwicklung. So wurden im Zuge dieser Arbeit auch Präzisionsmessungen an Spektrallinien in Cäsium, Indium und Iod vorgenommen, sowie einige grundlegende Tests dieser neuen Technologie durchgeführt. Der direkte Vergleich von zwei derartigen Frequenzketten zeigte Übereinstimmung auf einem Niveau von 5×10^{-16} .

Weitere Anwendungen dieser Technologie ergeben sich nicht nur im Bereich der Präzisionsspektroskopie, sondern auch bei der Synthese von optischen Wellenformen, also Wellenzügen mit kontrollierter Phasenlage, und als Uhrwerk zukünftiger optischer Uhren.

Abstract

In the course of this work a new technique to measure the frequency of light has been developed, implemented and refined.

For all time and frequency measurements the SI second defined by the cesium ground state hyperfine splitting near 9.2 GHz is the defined standard of reference. Therefore in precision optical frequency measurements optical frequencies on the order of several 100 THz – too fast to be counted with any electronics – have to be compared with radio frequencies on the order of a few GHz.

The basic idea here is to measure differences between optical frequencies with the help of frequency combs generated by the periodic pulse trains of femtosecond lasers. The output spectrum of such a laser consists of modes equally spaced by the repetition frequency of the pulses and forms a convenient ruler in frequency space. Extending this principle to the intervals between harmonics of the same optical frequency f , in the most simple case the interval between f and $2f$, allows the absolute measurement of an optical frequency $f = 2f - f$.

To bridge the interval between an optical frequency f and its second harmonic $2f$ a broad frequency comb with a width of several 100 THz is needed. This can be achieved with very short pulses (on the order of 5 fs) or with moderately short pulses on the order of a few 10 fs via self phase modulation in an optical fiber. Especially suited for such massive broadening are so called photonic crystal fibers. Here the light is guided in a very small core (1-2 μm) surrounded by air holes.

This development culminates in the “single laser frequency chain” linking the radio frequency domain with the optical domain with the help of just one fs laser, a piece of fiber and some optics. Our optical frequency synthesizer can be used to measure not only one but almost any optical frequency with the same compact apparatus.

Originally this project has been initiated to perform precision spectroscopy on the 1S-2S transition in atomic hydrogen, a project with a long tradition in our group, and yielded what is thus far the most precise optical frequency measurement with a relative uncertainty of 1.8×10^{-14} . Hydrogen as the most simple bound system served and still serves as an important cornerstone for tests of quantum physics, the measurement of the 1S Lamb shift represents one of the most accurate QED tests. Furthermore the Rydberg constant can be determined very precisely from optical frequency measurements in hydrogen.

Soon it became obvious that this technique has a broad applicability. In this work transition frequencies in cesium, indium and molecular iodine have been measured. Besides that principle tests on this technique have been conducted. The direct comparison of two such frequency chains showed agreement on the level of 5×10^{-16} .

Further applications besides precision spectroscopy can be found in the time domain. There it is now possible with this technique to control the phase evolution of ultra short light pulses and perform optical waveform synthesis. As optical clock work for future all optical clocks a fs frequency chain transfers stability and accuracy from the optical to the rf domain.

Contents

1	Introduction	1
2	Optical frequency differences	5
2.1	Measurement toolbox	5
2.2	Femtosecond light pulses	8
2.2.1	Frequency combs	8
2.2.2	Femtosecond lasers	10
2.2.3	Broadening the comb	12
2.3	Femtosecond combs as frequency rulers	14
2.3.1	Stabilizing the comb	14
2.3.2	Test of uniformity	18
2.4	Cesium D ₁ line and fine structure constant α	25
2.5	Indium ion clock transition	30
2.6	Iodine and stable Nd:YAG lasers	35
2.6.1	Iodine frequency grid	35
2.6.2	Nd:YAG lasers	36
2.6.3	Frequency chain	39
2.6.4	Frequency measurements	41
3	Absolute optical frequencies	45
3.1	Measurement principle	45
3.2	Hydrogen 1S – 2S transition	46
3.2.1	Frequency chain from radio frequencies to vacuum UV	46
3.2.2	The fountain clock reference	49
3.2.3	Hydrogen spectroscopy	51
3.2.4	Frequency measurements	53
3.2.5	Hydrogen and fundamental constants	57
3.3	Spectral broadening in photonic crystal fibers	59
3.4	The $f : 2f$ frequency chain	65
3.4.1	$f : 2f$ Frequency chain with auxiliary laser	65
3.4.2	Single laser optical frequency synthesizer	68
3.4.3	Validation of the $f : 2f$ frequency chain	71
3.4.4	Application to Iodine	74
3.4.5	$f : 2f$ chain with a Cr:LiSAF laser	79
3.5	Applications in the time domain	83

4 Conclusion and Outlook	91
A Phase locking optical frequencies	93
B Helium Neon standard	95

Chapter 1

Introduction

For more than a century, precise optical spectroscopy of atoms and molecules has played a central role in the discovery of the laws of quantum physics, in the determination of fundamental constants, and in the realization of standards for time, frequency, and length. The advent of highly monochromatic tunable lasers and techniques for nonlinear Doppler-free spectroscopy in the early seventies had a dramatic impact on the field of precision spectroscopy [1, 2, 3].

Today, we are able to observe extremely narrow optical resonances in cold atoms or single trapped ions, with resolutions $\Delta\nu/\nu$ ranging from 10^{-13} to 10^{-15} , so that it might ultimately become possible to measure the line center of such a resonance to a few parts in 10^{18} . A laser locked to a narrow optical resonance could serve as a highly stable oscillator for a future all-optical atomic clock already passing the current state of the art radio frequency cesium fountain clocks in terms of stability [4] and probably soon in accuracy.

Highly accurate and stable optical frequency standards enable the precise measurement of fundamental constants [5, 6, 7] or investigation of their possible variation in time [8]. Advances in frequency metrology permit more accurate determination of atomic transitions in spectroscopy and offer the possibility of stringent tests of QED or general relativity. They are also needed in applications such as navigation or very long baseline interferometry [9]. Presently, twelve reference frequencies covering the visible and infrared regions of the electromagnetic spectrum are recommended by the Comité International des Poids et Mesures (CIPM) for the realization of the meter [10]. A relative standard uncertainty of below 10^{-12} for frequency standards based on atoms, molecules or ions like H [11, 12], Ca [13], CH₄ [14], In⁺ [15] and Sr⁺ [16] impressively demonstrates the potential of these optical frequency standards.

However, until recently no reliable optical “clockwork” was available that could count these rapid oscillations and provide a link between optical frequencies of hundreds of THz and the microwave frequency of current atomic clocks based on the 9.2 GHz hyperfine resonance in atomic cesium defining the SI second since 1967 and being therefore the base of all time and frequency measurements.

Most spectroscopic experiments still rely on a measurement of optical wavelengths rather than frequencies. So far unavoidable geometric wavefront distortions have made it impossible to exceed an accuracy of a few parts in 10^{10} with a laboratory-sized wavelength interferometer.

To measure optical frequencies, a few harmonic laser frequency chains have been built during the past 25 years. These frequency chains start with a cesium atomic clock and generate higher and higher harmonics in nonlinear diode mixers, crystals, and other nonlinear devices [6, 17, 18, 16]. Phase-locked transfer oscillators are needed after each step, so that such a chain traversing a vast region of the electromagnetic spectrum becomes highly complex, large, and delicate, and requires substantial resources and heroic efforts to build and operate. Most harmonic laser frequency chain are designed to measure just one single optical frequency, and very few chains reaching all the way into the visible region have been realized so far.

In 1998, our laboratory has introduced a revolutionary new approach that vastly simplifies optical frequency measurements. We have demonstrated that the broad comb of modes of a mode-locked femtosecond laser can be used as a precise ruler in frequency space [5, 19]. It has been recognized already in 1978 by J. N. Eckstein, A. I. Ferguson, and T. W. Hänsch [20] that the periodic pulse train of a pico second mode locked dye laser can be described in the frequency domain as a comb of equidistant modes. As the spectral width of these lasers scales inversely with the pulse duration only the advent of fs lasers opened the possibility to directly access THz frequency gaps [5]. We were initially surprised that the generation of femtosecond pulses in a Kerr-lens mode-locked laser is so highly reproducible that the spectral modes remain precisely equidistant out into in the far wings of the spectrum. We have since shown that this remains true even if the laser spectrum is further broadened by self phase modulation in a nonlinear optical fiber (see section 2.2.3).

Naively, for a laser cavity with dispersive optical elements, one would expect the mode frequencies to be not precisely equally spaced. As a result, a short pulse circulating inside the cavity would tend to spread and change its shape with time.

The Kerr-lens produced by the circulating light pulse in a nonlinear optical medium via the intensity dependent refractive index counteracts this tendency by periodically modulating the cavity losses. Each mode is, in fact, injection-locked by modulation sidebands of the other modes, and will oscillate in precise lock-step, as long as the cavity dispersion is sufficiently well compensated, so that the mode frequencies do not have to be pulled too far. Modes unable to follow this collective dictate cannot take advantage of the Kerr-lens and suffer high roundtrip losses in a properly designed cavity.

In the time domain, the output of a mode-locked femtosecond laser may be considered as a continuous carrier wave that is strongly amplitude modulated by a periodic pulse envelope function. If such a pulse train and the light from a cw laser are combined on a photo detector, the beat note between carrier wave and the cw oscillator is, in fact, observed in a stroboscopic sampling scheme. The detector signal will thus reveal a slow modulation at the beat frequency modulo the sampling rate or pulse repetition frequency. Similar ideas have also been discussed by V. Chebotaev [21].

Recently, extreme spectral broadening has been observed with “photonic crystal fibers” [22, 23], which manage the optical dispersion with the help of a micro-structured cladding. Meanwhile we have also shown (see section 3.4.3 and Ref. [24]) that such highly nonlinear fibers can preserve the phase coherence between successive pulses, so that frequency combs spanning more than one octave are becoming available.

This work has now culminated in a compact and reliable all-solid-state frequency “chain” which requires just a single mode-locked laser (section 3.4 and Ref. [25, 24]). As a universal optical frequency comb synthesizer it provides the long-missing simple link between optical and microwave frequencies. For the first time, small scale spectroscopy laboratories have now access to the ability to measure or synthesize any optical frequency with extreme precision. Femtosecond frequency comb techniques have since begun to rapidly gain widespread use in many laboratories around the world, with precision measurements in Ca [26], CH₄ [12], Cs [5], H [12], Hg⁺ [26], I₂ [27], and In⁺ [15] already completed or underway.

A high degree of mutual phase coherence has even been observed for pairs of white light continuum pulses produced by focusing the light from an amplified Ti:sapphire femtosecond laser at two separate spots inside a nonlinear medium, despite complications such as self-focusing, stimulated Raman and Brillouin scattering or shockwave formation [28]. Similar experiments with high harmonics produced in gas jets [29] suggest that it may eventually become feasible to extend absolute optical frequency measurements into the extreme ultraviolet and soft x-ray region.

In the first experiment of its kind, we have applied the frequency comb of a mode-locked femtosecond laser to measure the frequency of the cesium D₁ line (section 2.4 and Ref. [5]). This frequency provides an important link for a new determination of the fine structure constant α . More recently, we have measured the absolute frequency of the hydrogen 1S-2S two-photon resonance in a direct comparison with a cesium atomic fountain clock to within 1.8 parts in 10^{14} , thus realizing the most accurate measurement of an optical frequency to date [12]. The hydrogen 1S-2S resonance with its natural line width of only 1 Hz has long inspired advances in high resolution laser spectroscopy and optical frequency metrology.

Hydrogen as the most simple bound system served and still serves as an important cornerstone for tests of quantum physics, the measurement of the 1S Lamb shift represents one of the most accurate QED tests. During the past few years, precision spectroscopy of hydrogen has yielded a Rydberg constant that is now one of the most accurately known fundamental constants and even hadronic structure [30] can be studied. Nonetheless, after more than a century of spectroscopic experiments, the hydrogen atom still holds substantial challenges and opportunities for further dramatic advances. In the future, it may reveal possible slow changes of fundamental constants or, with the antihydrogen experiments now under preparation at CERN [31], conceivable differences between matter and antimatter.

The same femtosecond frequency comb techniques that are about to revolutionize optical frequency metrology are also opening new frontiers in ultrafast physics. Here two very different fields of optical physics namely the ultrafast and the ultrastable can

benefit from each other. So far we have explored the regularly spaced comb of cw frequencies generated by the periodic pulse train of a fs laser. In the time domain however such a fs pulse can be interpreted as a amplitude modulated carrier wave. Looking at this in some detail one finds that the group velocity of the pulse in the cavity that governs the pulse envelope differs from the phase velocity of the carrier (as discussed in section 2.2.1 and illustrated in Fig. 2.4) and therefore there is a pulse to pulse phase shift of the pulse versus the envelope. Control of the phase evolution of few cycle light pulses, as recently demonstrated [25, 32], provides a powerful new tool for the study of highly nonlinear phenomena that should depend on the phase of the carrier wave relative to the pulse envelope, such as above threshold ionization, strong field photoemission, or the generation of soft x-ray attosecond pulses by high harmonic generation.

As a starting point in this text possibilities to measure optical frequency differences will be introduced and why it is important to do so. Then fs frequency combs will be thoroughly examined as a powerful tool for this task. With the help of this tool measurement applications in cesium, indium and iodine will be presented together with some physics along the way. In the second part we will concentrate on absolute optical frequency measurements. The first implementation of such a chain used for a determination of the Hydrogen 1S-2S transition will be discussed. Then photonic crystal fibers will be introduced and a “single laser frequency chain” will be described. Furthermore this chain has been tested and applied to the measurement of iodine lines. Finally an applications of this frequency domain technique in the time domain, namely controlling the phase evolution of a fs pulse train, will be discussed.

The “Garching frequency chain” team consists at the moment of Th. Udem (PhD Dec. 1997), J. Reichert (PhD June 2000) and myself. In the summer of 2000 a new PhD student M. Zimmermann has joined our team. Most experiments discussed in this work have been carried out by changing members of this team and several other collaborators as mentioned throughout the text.

Chapter 2

Optical frequency differences

2.1 Measurement toolbox

While it has been extremely difficult in the past to measure an absolute optical frequency, a small frequency difference or gap between two laser frequencies can be measured rather easily by superimposing the two beams on a photodetector and monitoring a beat signal. The first experiments of this kind date back to the advent of cw He-Ne-lasers in the early 1960s. Modern commercial fast photodiodes and microwave frequency counters make it possible to directly count frequency differences up to the order of 100 GHz.

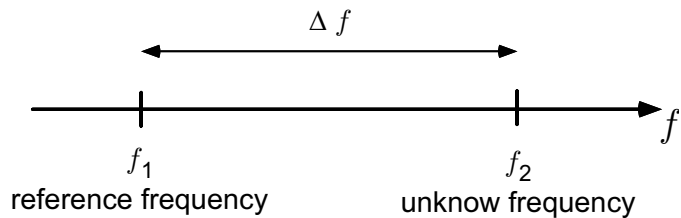


Figure 2.1: A typical situation in frequency metrology, a well known reference frequency and an unknown frequency tens or hundreds of THz apart.

Since the gap between the endpoint of a traditional harmonic laser frequency chain and an unknown optical frequency to be measured can easily amount to tens or hundreds of THz, there has long been a strong interest in methods for measuring much larger optical frequency differences.

Motivated by such problems in precision spectroscopy of atomic hydrogen, a general solution for the measurement of large optical frequency gaps has been introduced in 1988 by T.W. Hänsch and D. McIntyre with the invention of the optical frequency interval divider (OFID) which can divide an arbitrarily large frequency difference by a factor of precisely two [33]. An OFID receives two input laser frequencies f_1 and f_2 . The sum frequency $f_1 + f_2$ and the second harmonic of a third laser $2f_3$ are created in

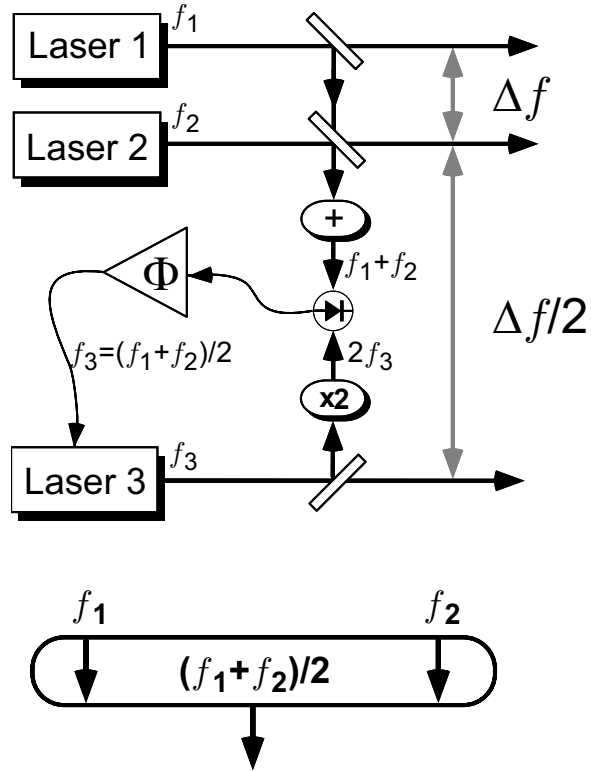


Figure 2.2: Principle of the divider stage. Throughout the remainder of this text divider stage will be denoted by the oval divider stage symbol.

nonlinear crystals. The radio frequency beat signal between them at $2f_3 - (f_1 + f_2)$ is used to phase-lock the third laser at the midpoint $f_3 = (f_1 + f_2)/2$. Phase-locking of two optical frequencies is achieved electronically by locking the phase of their beat signal to zero or, to reduce $1/f$ noise, to a given offset radio frequency, provided by a local oscillator. Techniques of conventional radio frequency phase-locked loops can be applied, some details are collected in appendix A. With a divider chain of n cascaded OFIDs, the original frequency gap can be divided by a factor 2^n .

Another more compact setup to measure frequency gaps on the order of a few THz is an optical frequency comb generator (OFCG) based on the very efficient creation of side bands in a large index electro optic phase modulator. To enhance the efficiency an electro optic modulator is placed inside a Fabry-Perot cavity. To further reduce losses a monolithic resonator can be formed by placing high reflectivity coatings on the end facets of the electro optic crystal. The cavity can be locked to the carrier wave by adjusting temperature and a dc offset applied to the crystal. If the modulation frequency matches the free spectral range of this optical resonator, the side bands are again in resonance and create further side bands. This technique has been pioneered by M. Kurogi in the group of M. Ohtsu (Tokyo, Japan) [34, 35, 36]. Some details including different locking schemes and further references can be found in the PhD thesis of Th. Udem [37].

The width of such a comb is limited by dispersion. The refractive index in the crystal depends on wavelength and therefore the modes of the resonator do not match the modulation side bands far away from the carrier.

To measure optical frequency differences beat signals can be observed between cw lasers and sidebands on different sides of the carrier and frequency gaps on the order of 8 THz can be bridged in this way. To measure larger gaps, a chain of OFIDs can be followed by an OFCG.

Typical parameters for such an OFCG that has been set up in our laboratory by M. Kourogi are: a free spectral range (FSR) of 3.16 GHz which corresponds to a 21 mm long LiNbO_3 crystal, a dc offset voltage up to 1000 V can be applied and a rf power of 2 W at 6.32 GHz ($= 2 \times \text{FSR}$) is coupled into the rf resonator for modulation. This OFCG has been used in our laboratory in various experiments in the “prior-fs” time [30, 37, 38, 39].

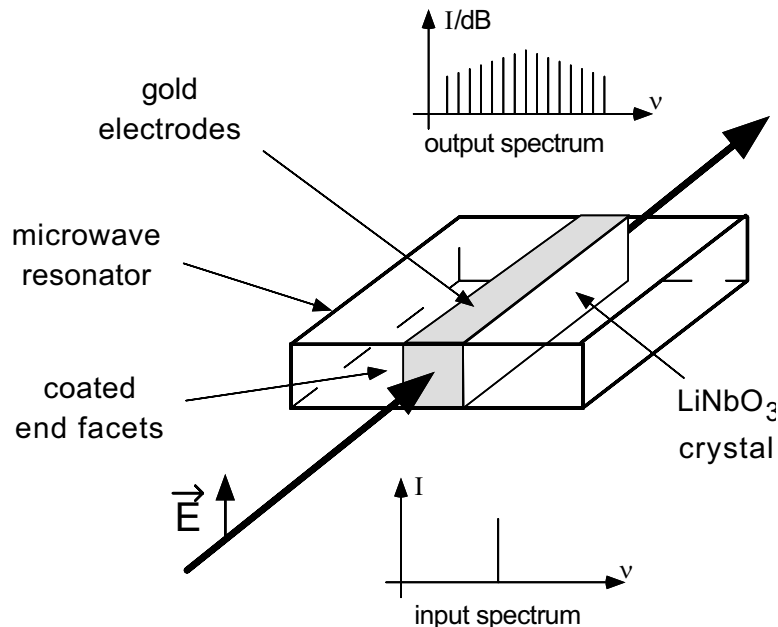


Figure 2.3: Principle of an optical frequency comb generator (OFCG). Side bands are created efficiently in an electro optic crystal.

As the latest and most powerful addition to this optical frequency difference measurement toolbox let us now turn our view to the frequency combs actively generated by mode-locked femtosecond laser.

2.2 Femtosecond light pulses

2.2.1 Frequency combs

The use of mode-locked lasers as active optical comb generators was already reported over 20 years ago [20] with picosecond pulses. As the spectral width of such a comb scales inversely with the (Fourier limited) pulse duration, its application was limited to comparatively small frequency differences like the 1028 MHz fine structure splitting of the sodium 4d level [20]. This route was further pursued in the seventies and eighties [40, 41, 42, 43], but the attainable bandwidths were never sufficiently large to make it a widespread technique for optical frequency metrology. Broadband femtosecond Ti:sapphire lasers have existed since the beginning of the 1990s, but only our recent experiments at Garching have shown conclusively that such lasers can play a crucial role in this field [19, 24].

To understand the mode structure of a fs frequency comb and the techniques applied for its stabilization one can look at the idealized case of a pulse circulating in a laser cavity with length L as a carrier wave at f_c that is subject to strong amplitude modulation described by an envelope function $A(t)$. This function defines the pulse repetition time $T = f_r^{-1}$ by demanding $A(t) = A(t - T)$ where T is calculated from the cavity mean group velocity: $T = 2L/v_{gr}$. Because of the periodicity of the envelope function the electric field at a given place (e.g. at the output coupler) can be written as

$$E(t) = A(t)e^{-2\pi i f_c t} + \text{c.c.} = \sum_q A_q e^{-2\pi i (f_c + q f_r) t} + \text{c.c.} \quad (2.1)$$

As the envelope function $A(t)$ is strictly periodic it has been written as a Fourier series

$$A(t) = \sum_q A_q e^{-2\pi i q f_r t} \quad (2.2)$$

where A_q are Fourier components of $A(t)$. Equation 2.1 represents a comb of laser frequencies with spacing f_r . Since f_c is not necessarily an integer multiple of f_r the modes are shifted from being exact harmonics of the pulse repetition frequency by an offset $f_o < f_r$:

$$f_n = n f_r + f_o \quad n = \text{a large integer} \quad (2.3)$$

This equation links two radio frequencies f_r and f_o with the optical frequencies f_n . While f_r is readily measurable, f_o is not easy to access unless the frequency comb contains more than an optical octave [44]. In the time domain the frequency offset is obvious because the group velocity differs from the phase velocity inside the cavity and therefore the carrier wave does not repeat itself after one round trip but appears phase shifted by $\Delta\varphi$ as shown in Fig. 2.4. The offset frequency is then calculated from $f_o = \Delta\varphi/T2\pi$ [40, 42, 44].

One might argue that no laser has linewidth zero and that one should treat the carrier not as a ideal single frequency wave f_c but as a source with general line width function $C(t)$. Even if no technical noise would be present, there would still be some sort of

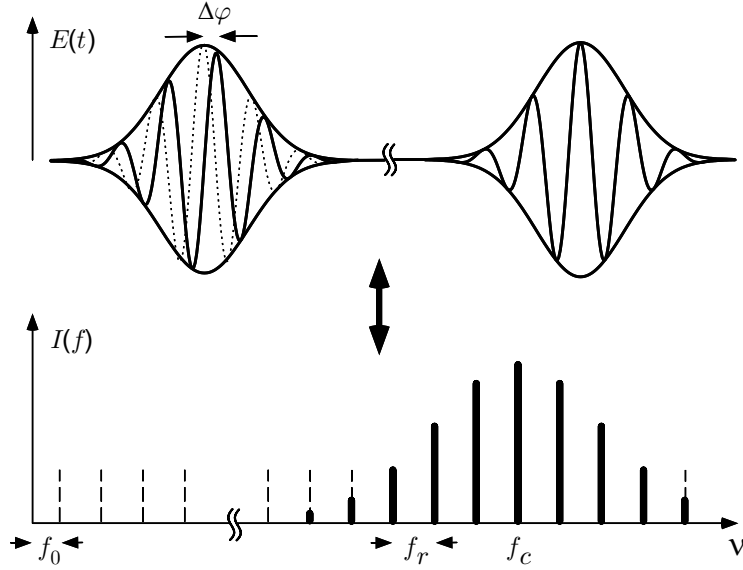


Figure 2.4: Two consecutive pulses of the pulse train emitted by a mode locked laser and the corresponding spectrum. The pulse to pulse phase shift $\Delta\varphi$ results in a offset frequency $f_0 = \Delta\varphi/2\pi T$ because the carrier wave at f_c moves with the phase velocity v_p while the envelope moves with the group velocity v_g .

fundamental Schawlow-Townes limit connected with the line width of each mode. As long as we still have the periodicity of $A(t)$ Eqn. 2.1 reads then as

$$E(t) = A(t)C(t) + \text{c.c.} \quad (2.4)$$

Fourier transforming $E(t)$ brings us into the frequency domain and back ($\omega = 2\pi f$):

$$E(\omega) = \frac{1}{\sqrt{2\pi}} \int_{-\infty}^{+\infty} E(t)e^{i\omega t} dt \quad E(t) = \frac{1}{\sqrt{2\pi}} \int_{-\infty}^{+\infty} E(\omega)e^{-i\omega t} d\omega \quad (2.5)$$

With the help of the convolution theorem

$$\sqrt{2\pi}A(t)C(t) = \frac{1}{\sqrt{2\pi}} \int_{-\infty}^{+\infty} (A(\omega) \otimes C(\omega)) e^{-i\omega t} d\omega \quad (2.6)$$

we get

$$E(\omega) = \frac{1}{\sqrt{2\pi}}(A(\omega) \otimes C(\omega)) = \frac{1}{\sqrt{2\pi}} \int_{-\infty}^{+\infty} A(\omega')C(\omega - \omega') d\omega' + \text{c.c.} \quad (2.7)$$

The Fourier transforms of $A(t)$ and $C(t)$ are given by

$$A(\omega) = \sqrt{2\pi} \sum_{n=-\infty}^{+\infty} A_n \delta(\omega - n\omega_r) \quad (2.8)$$

$$C(\omega) = \frac{1}{\sqrt{2\pi}} \int_{-\infty}^{+\infty} C(t)e^{i\omega t} dt \quad (2.9)$$

and therefore

$$E(\omega) = \sum_{n=-\infty}^{+\infty} A_n C(\omega - n\omega_r) + \text{c.c.} \quad (2.10)$$

This sum represents a periodic spectrum in frequency space with periodicity $f_r = 1/T$. The mode shape function is duplicated by the strong amplitude modulation induced by Kerr lens mode locking. Assuming the simplified case of a carrier wave $C(t) = e^{-i2\pi f_c t}$ brings us back to Eqn. 2.1. A chirp of the pulse may be hidden in the complex Fourier components A_n . Note that the only assumption necessary to create a precisely equidistant comb is the periodicity of the envelope function.

In the time domain, the output of a mode-locked femtosecond laser may be considered as a continuous carrier wave that is strongly amplitude modulated by a periodic pulse envelope function. If such a pulse train and the light from a cw laser are combined on a photo detector, the beat note between the carrier wave and the cw oscillator is, in fact, observed in a stroboscopic sampling scheme. The detector signal will thus reveal a slow modulation at the beat frequency modulo the sampling rate or pulse repetition frequency. A similar idea based on the stroboscopic sampling scheme has been reported previously by Chebotayev et al. [21].

The important fact to learn from this chapter is that such a fs frequency comb has two degrees of freedom which are the repetition frequency f_r and the offset frequency $f_0 < f_r$. Depending on the application one or both degrees of freedom have to be stabilized. Furthermore the fast amplitude modulation of the Kerr lens keeps the inter mode spacing constant even across a vast spectrum of modes. As the spectral width of these pulsed lasers scales inversely with the pulse duration the advent of fs lasers has opened the possibility to directly access THz frequency gaps.

2.2.2 Femtosecond lasers

So far we have discussed some frequency domain properties of femtosecond light pulses. Now let us briefly review how these pulses are generated and how they travel in matter. This has been subject of various textbooks, the overview given here is mainly taken from the books of Rulliere [45] and Diels [46] as well as from the PhD theses of A. Kasper [47] and J. Reichert [38].

As optical pulses travel in a transparent medium we can observe linear dispersive and nonlinear effects. The wavelength dependence of the light propagation factor

$$k(\omega) = \omega \frac{n(\omega)}{c} \quad (2.11)$$

(or of the refractive index respectively) leads to dispersive broadening of the pulses in the time domain while the nonlinear power dependent refractive index

$$n = n_0 + n_2 I(r, t) \quad (2.12)$$

changes the spectral and spatial properties of the pulse via the Kerr lens effect and self phase modulation respectively.

To get some insight into the dispersive properties of short pulses we apply a Taylor expansion to $k(\omega)$ around ω_0

$$k(\omega) = k(\omega_0) + \frac{\partial k}{\partial \omega} \Big|_{\omega_0} (\omega - \omega_0) + \frac{1}{2} \frac{\partial^2 k}{\partial \omega^2} \Big|_{\omega_0} (\omega - \omega_0)^2 + \dots \quad (2.13)$$

The linear term does not change the envelope function of the pulse (i. e. the pulse length), linear dispersion just translates the pulse in time. All higher terms change the pulse duration, lead by the quadratic term, the group velocity dispersion (GVD) $k'' = \partial^2 k(\omega_0)/\partial \omega^2$. It measures (in first order) the spreading of a pulse as it travels with the group velocity

$$v_g = \frac{\partial \omega}{\partial k} = k'(\omega_0)^{-1} = \frac{c}{n + \omega \frac{\partial n}{\partial \omega}} \quad (2.14)$$

i.e. the GVD represents the wavelength dependence of the group velocity:

$$k'' = \frac{\partial^2 k}{\partial \omega^2} = \frac{\partial}{\partial \omega} (v_g^{-1}) \quad (2.15)$$

The GVD is usually stated in fs^2 per cm. In the literature the GVD is sometimes denoted by $\beta_2 = k''$ or a dispersion parameter D is introduced with $D = \frac{\partial}{\partial \lambda} (v_g^{-1}) = -\frac{2\pi c}{\lambda^2} k''$ in units of $\text{ps}/(\text{km nm})$ [48]. For optical elements where the light travels a path length z the integrated contribution $D_2 = k'' z$ is sometimes stated as GVD in fs^2 .

Higher order terms (third, forth ... order dispersion) are getting relevant for very short pulses where a wide spectral bandwidth is covered.

For stable mode-locked operation of a short-pulse laser two conditions must be fulfilled. The soliton-like pulse must be able to travel back and forth in the laser cavity without being dispersed and there must be a mechanism to form the pulses i.e. to mode-lock many cw modes. With Kerr-lens mode-locking this pulling is achieved by exploiting a Kerr-lens that persists only in the presence of an intense short pulse due to the intensity dependent nonlinear index of refraction as a fast amplitude modulator. The cavity is designed to have less loss if the Kerr-lens is present. The result is a short pulse with a stable envelope that bounces back and forth between the cavity end mirrors. In Kerr-lens mode-locked lasers [50] a combination of prism pairs or specially designed mirrors [51] as illustrated in Fig. 2.5, are used to compensate for the positive group velocity dispersion $k''(\omega_m)$ (GVD) of the laser crystal and mirrors etc. The remaining perturbations of the regular grid of modes, due to a imperfect compensation of the GVD and the presence of higher order terms, are zeroed by mode pulling. The achievable pulse length is determined by the total number of modes that can contribute to the pulse. The broader the frequency comb the shorter is the shortest possible pulse length, ideally reaching the so-called Fourier limit. In fact, the spectral width is usually limited by the width over which the GVD and higher order terms can be compensated for by mode pulling [52, 53].

The first flash lamp pumped Nd:glass and Nd:YAG mode-locked laser appeared in the mid sixties with less than 100 ps in duration and demonstrated one of the most

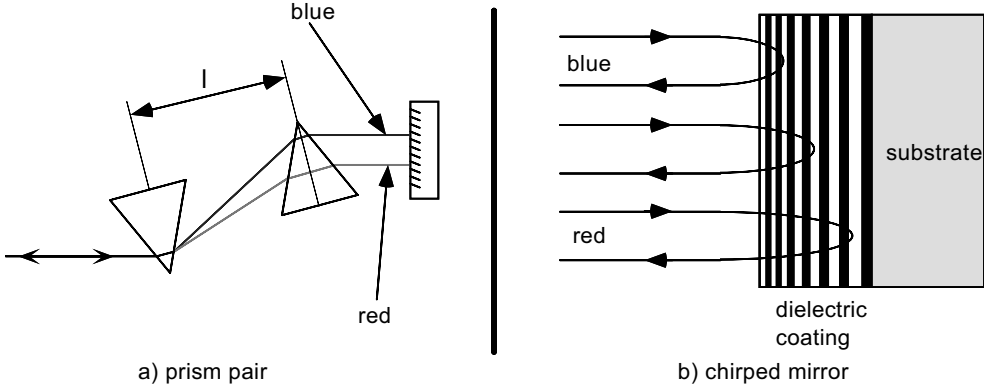


Figure 2.5: Two possibilities to introduce negative group velocity dispersion (“red pulses have a longer optical path than blue pulses”) into a laser cavity: a) through a prism pair and b) through so called chirped mirrors.

powerful interference phenomena in nature [46, 54]. The cw operation of dye lasers with broad bandwidth triggered the second generation of mode-locked lasers. Optical pulses shorter than 1 ps could be produced and improvements in the cavity design allowed breaking of the 100 fs barrier. Intracavity dispersion control by means of Brewster angled prism pairs was the next major breakthrough in 1984 [55]. This early work culminated in the production of 27 fs pulses from a Rhodamine 6G dye laser emitting around 620 nm [56]. The development of new solid state laser materials led to the emergence of third generation laser sources with the discovery of self-mode locking in Ti:sapphire lasers [57], its explanation as being due to Kerr-lens mode-locking [50], and development of the design to produce ≈ 10 femtosecond pulses [58]. Recently pulses shorter than 6 fs have been created directly from a Ti:Sapphire laser oscillator [52, 53] with the help of special dispersion-compensating mirrors. Ti:sapphire lasers nowadays represent convenient laboratory work horses and are commercially available in a variety of pulse length, repetition rates and peak powers.

2.2.3 Broadening the comb

At the high peak intensities of femtosecond laser pulses nonlinear effects due to the $\chi^{(3)}$ nonlinear susceptibility are considerable even in standard silica fibers. The output spectrum of a femtosecond laser can be broadened significantly via self phase modulation in an optical fiber therefore increasing its useful width even further beyond the time-bandwidth limit of the laser. The following considerations follow closely the excellent book of Agrawal [48].

In a dispersion and absorption free environment the intensity dependent refractive index¹ $n(t) = n_o + n_2 I(t)$ leads to a self induced phase shift after the pulse has propagated the length l along the fiber:

$$\Phi_{NL}(l, t) = -n_2 I(t) \omega_c l / c \quad \text{with } I(t) = |A(t)|^2. \quad (2.16)$$

¹Note that n_2 and $\chi^{(3)}$ are connected through $n_2 = \frac{3}{4n^2 \epsilon_0 c} \chi^{(3)}$ [48]

The nonlinear phase shift has its maximum at the pulse center $I(t_0) = I_0$ and increases with the propagated distance l . The maximal phase shift amounts to

$$\Phi_{max} = I_0 n_2 l \frac{\omega_c}{c} = \frac{l}{L_{NL}} \quad (2.17)$$

where the nonlinear length L_{NL} has been introduced as the effective propagation distance at which $\Phi_{max} = 1$.

This time dependent phase shift leads to a frequency modulation that is proportional to the time derivative of the self induced phase shift $\dot{\Phi}_{NL}(t)$. For fused silica with its positive Kerr coefficient $n_2 \approx 3 \times 10^{-16} \text{ cm}^2/\text{W}$ [48] the leading edges of the pulses are creating frequencies shifted to the red ($\dot{\Phi}_{NL}(t) < 0$) while the trailing edges causes blue shifted frequencies to emerge. Self-phase modulation modifies the envelope function according to

$$A(t) \longrightarrow A(t)e^{i\Phi_{NL}(t)}. \quad (2.18)$$

Self phase modulation thus produces a chirp without making the pulse longer! This means that additional frequency components are created and the pulse can in principle be compressed afterwards. Because $\Phi_{NL}(t)$ has the same periodicity as $A(t)$ the comb structure of the spectrum is not affected.

In the real world however there is dispersion and the GVD broadens the pulses as they travel along the fiber. Effective self-phase modulation however takes place when the so called dispersion length L_D is much smaller then the nonlinear length L_{NL} whose ratio is given by [48]

$$R = \frac{L_D}{L_{NL}} = \frac{n_2 \omega_c I_o T_o^2}{c |k''(\omega_c)|} \quad (2.19)$$

where T_o is the initial pulse duration. In the dispersion dominated regime, $R \ll 1$, the pulses will disperse before any significant nonlinear interaction can take place while for $R \gg 1$ dispersion can be neglected as an inhibitor of self-phase modulation. We are considering of course the case of a physical fiber longer than either $L_D = T_o^2 / |k''(\omega_c)|$ or $L_{NL} = c / n_2 \omega_c I_o$.

We see that spectral broadening of the comb is achieved by imposing a large frequency chirp on each of the pulses. Provided that the coupling efficiency into the fiber is stable, the periodicity of the pulse train is maintained. The discussion of section 2.2.1 is thus equally valid if the electric field $E(t)$ as measured for example at the fiber output facet instead of the laser output coupler.

Note that self phase modulation can be seen as the temporal pendant to the Kerr-lens effect.

As an example Fig. 2.6 illustrates spectral broadening of 73 fs pulses from a Mira 900 system (Coherent Inc.) in a standard single mode fiber (Newport FS-F). The low power curve in the left part of the figure resembles the input pulse with very little nonlinear interaction with the fiber. The high power curve illustrates the broadening, 280 mW average power have been coupled through the fiber. The right part of Fig. 2.6 illustrates how the “-53dB” point that has been shown to supply enough power per mode to enable phase locking of cw sources moves out with increasing power.

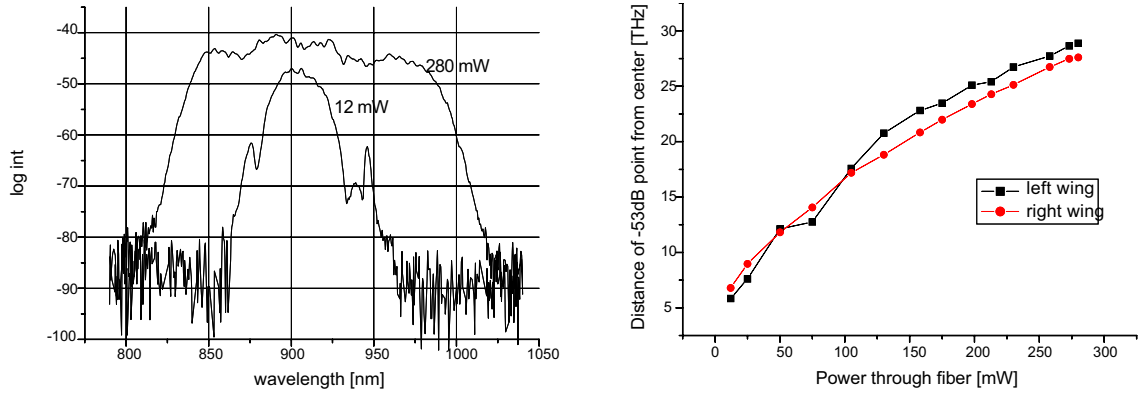


Figure 2.6: Spectral broadening of 73 fs pulses in a standard single mode fiber. Left: no broadening with 12 mW average power coupled through the fiber, with 280 mW broadening to more than 50 THz. Right: the broadening is almost symmetrical to the center of the initial pulse.

This broadened frequency comb has been thoroughly tested in section 2.3.2 and has been used for the experiments in sections 2.5 and 3.2. Another example of spectral broadening in a standard single mode fiber will be discussed in section 3.5. New possibilities of spectral broadening in fibers with special dispersion properties will be discussed in section 3.3.

2.3 Femtosecond combs as frequency rulers

2.3.1 Stabilizing the comb

We have seen above that such a femtosecond frequency comb has two free parameters, i.e. the repetition frequency f_r and the offset frequency f_0 . For most applications it is desirable to fix one of the modes in frequency space and phase-lock the pulse repetition rate simultaneously. Furthermore, the laser spectrum is subject to acoustic and other technical noise that needs to be suppressed. For this purpose it is necessary to control the phase velocity (more precisely the round trip phase delay) of that particular mode and the group velocity of the pulses (more precisely the round trip group delay) independently.

A piezo driven folding mirror as depicted in Fig. 2.7 is changing the cavity length but leaves $\Delta\varphi$ approximately constant as the additional path in air does have a negligible dispersion. Also the offset frequency $f_0 = \Delta\varphi f_r / 2\pi$ is almost untouched by changing the cavity length as f_r is usually changed by a few 100 Hz in order to reach every desired position in frequency space with one of the modes. Fig. 2.8 illustrates this in a exaggerated way with a simple “rubber band” model.

A mode-locked laser that uses two intracavity prisms to produce the negative group velocity dispersion ($\partial^2\omega/\partial k^2 < 0$) necessary for Kerr-lens mode-locking provides us

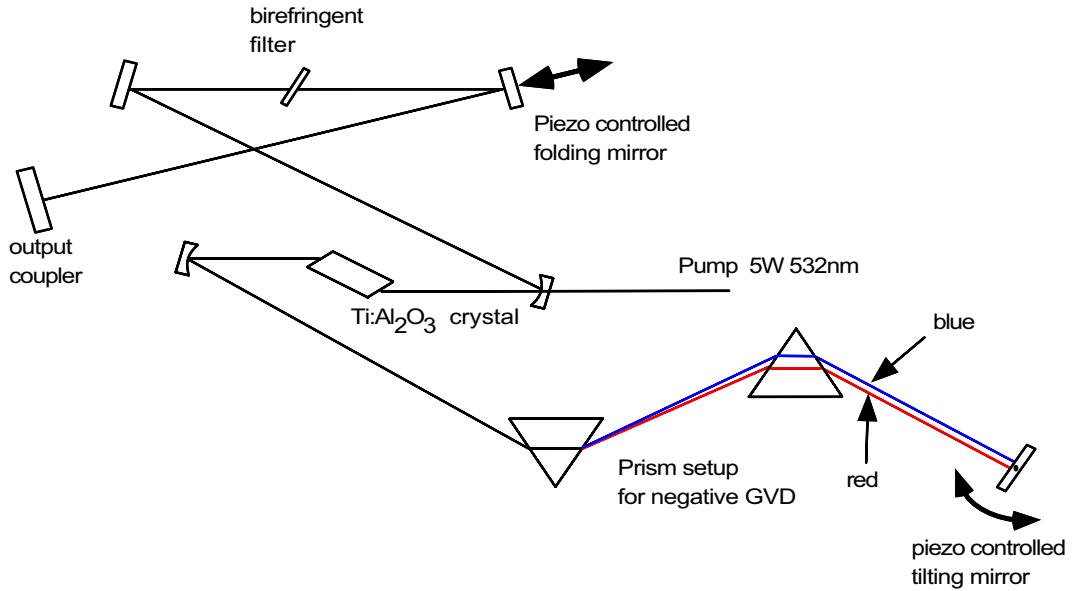


Figure 2.7: Setup of a typical fs laser (following a Mira 900 system (Coherent Inc.)). The possibilities to stabilize the frequency comb include changing the cavity length and tilting the end mirror

with a means for independently controlling the pulse repetition rate. We use a second piezo-transducer to slightly tilt the mirror at the dispersive end of the cavity about a vertical pivot that ideally corresponds to the mode f_n (see Fig. 2.7). We thus introduce an additional phase shift $\Delta\Phi$ proportional to the frequency distance from f_n , which displaces the pulse in time and thus changes the round trip group delay. In the frequency domain one could argue that the length of the cavity stays constant for the mode f_n while higher (lower) frequency modes experience a longer (shorter) cavity (or vice versa, depending on the sign of $\Delta\Phi$). This leads to a changes in f_0 and f_r but leaves the mode on the pivot axis constant as shown in Fig. 2.9. Our first fs laser system that we used in various experiments reported here is a Mira 900 system (Coherent Inc.). It delivers 73 fs pulses at a repetition rate of 76 MHz. It uses

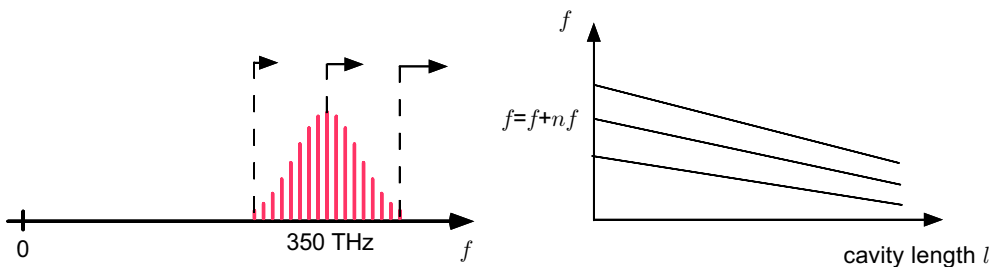


Figure 2.8: A decreasing cavity length pulls the modes apart like mounted on a rubber band. Note that the pulling is not uniformly.

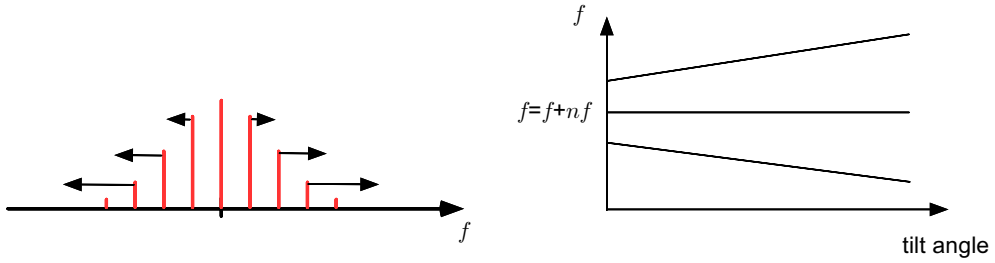


Figure 2.9: Slightly tilting the end mirror at the dispersive end of the laser cavity changes the mode spacing.

prisms for GVD compensation and can be tuned with a Lyot filter (and different mirror sets) between 750 and 1000 nm. It is pumped by a frequency doubled diode pumped Nd:YVO₄ laser (model Verdi, Coherent Inc.)

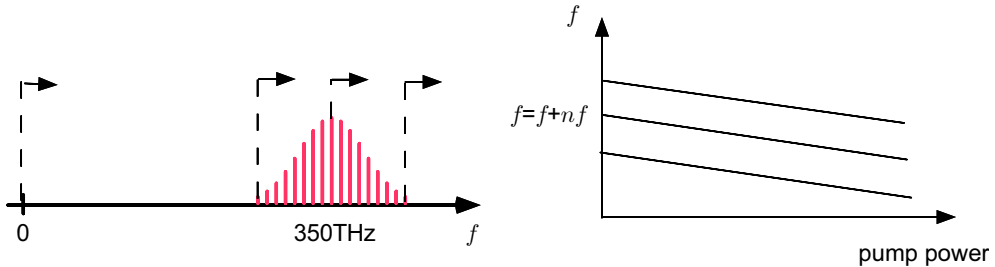


Figure 2.10: Changing the pump power efficiently changes the offset frequency f_0

In the case where only dispersion compensation mirrors are used to produce the negative group velocity dispersion one can modulate the pump power or manipulate the Kerr lens by slightly tilting the pump beam. Primarily this changes the pulse energy of the fs laser and via the Kerr lens nonlinearity mainly the phase delay is affected. This can be derived with the master equation for nonlinear pulse evolution [49].

That is just what is needed to control the pulse repetition rate f_r and the offset frequency f_0 separately: A separate control of the round trip group delay T and the round trip phase delay [44]. Another method that we have used to stabilize the offset frequency f_0 was to translate the laser crystal along the axis of the cavity mode. This changes the integrated power inside the crystal with the same effect but it is reversed at the point where the focus is centered inside the crystal.

Yet another possibility to adjust the offset frequency f_0 is to insert additional glass into the laser cavity e.g. by moving prisms already present for GVD compensation or by inserting a wedge into the laser cavity. The phase difference between carrier and envelope $\Delta\varphi$ experiences a shift during propagation through a dispersive transparent medium $\delta\varphi = (k(\omega_0) - \omega_0 v_g^{-1})l$ where l is the propagation length, v_g the group velocity and k the propagation constant $k(\omega) = \omega n(\omega)/c$. With $v_g^{-1} = \frac{\partial k}{\partial \omega} = \frac{n + \omega \frac{\partial n}{\partial \omega}}{c}$ we arrive at $\delta\varphi = -\frac{\omega_0^2}{c} \frac{\partial n}{\partial \omega}$ and finally $\delta\varphi = 2\pi(\partial n/\partial \lambda)\delta l$ where $\partial n/\partial \lambda = -0.018 \mu\text{m}^{-1}$ for fused

silica at $\lambda = 790$ nm [59]. According to $f_0 = \Delta\varphi f_r / 2\pi$ we expect $\delta f_0(\delta l) = -0.018 f_r \delta l$. This has actually been verified in our Vienna experiments (Ref. [32] and section 3.5). Note that putting more glass into the cavity moves the comb in the same direction as increasing the power.

The second fs laser system that we used in several experiments is based on a Ti:sapphire 25 fs ring laser with a high repetition rate (GigaOptics, model GigaJet). We have modified the original setup by mounting one of the mirrors on a translation stage for coarse control of the repetition rate and another mirror on a piezo transducer for fine tuning and phase locking of the repetition rate. Furthermore we have inserted an electro optic modulator into the pump beam for fine adjustment and phase locking of the offset frequency. For this purpose we used an electro optic amplitude modulator (EOM) from Gsänger (model LM 0202). The pump power can only be changed by about 10 % without terminating mode-locked operation. This changes the slipping frequency beat signal f_0 by about 60 MHz. This range is enough for phase locking but it is not enough to place f_0 at any desired frequency within $f_{rep}/2$ of a few hundred MHz. Therefore we included in our setup a fused silica wedge at Brewster's angle. This also gives access to the offset frequency f_0 and can be used to preset f_0 to the desired position (e.g. 64 MHz as in most of our experiments) and phase lock it with via pump modulation. By double folding the cavity more bounces are obtained on the chirped mirrors so that we can actually add the fused silica wedge in the first place. The full system is depicted in Fig. 2.11 and more details on the experimental parameters of this laser will be given in section 3.4.

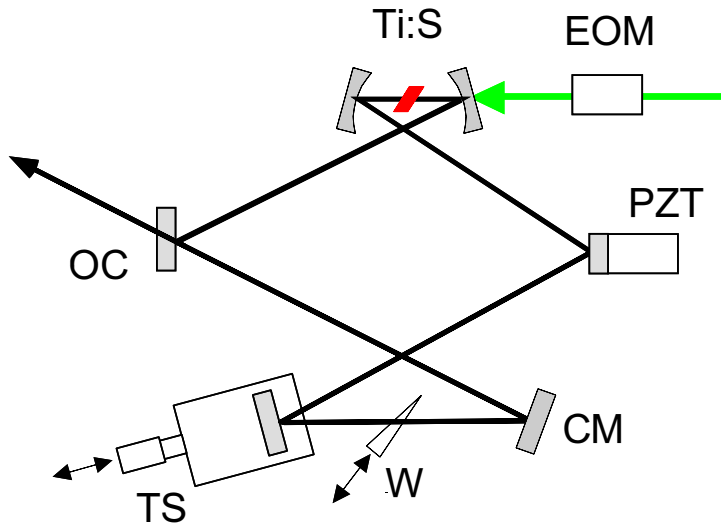


Figure 2.11: The high repetition rate laser. It has been operated with repetition frequencies of 625, 750 and 950 MHz. Piezo transducer (PZT) and translation stage (TS) are used for coarse adjustment and locking of the repetition rate f_r , fused silica wedge (W) and an electro optic intensity modulator (EOM) are used for coarse adjustment and locking of the offset frequency f_0 . All mirrors except the output coupler (OC) are chirped.

Note that a distinct advantage of the pump beam modulation technique is a much higher servo bandwidth than is attainable with piezo transducers. It should in fact only be limited by the life time of the upper level in Ti:sapphire of $2.2\mu\text{s}$. Furthermore stabilizing f_0 with the help of pump power modulation even reduces amplitude noise from the fs laser ass will be discussed in section 3.5.

Now one question remains to be answered: how do we get experimental access to f_r and especially f_0 ? The repetition rate f_r is readily picked up with a fast photo detector. The question how to access f_0 will be answered in section 3.4.

2.3.2 Test of uniformity

If there is one essential thing to a frequency comb used as a ruler in frequency space it is the uniform mode spacing. There have been many objections that our simple picture of this precisely equally spaced comb will fail due to dispersion or other effects. We have found that the frequency comb is equally spaced even after further spectral broadening in a standard single mode fiber at the level of a few parts in 10^{18} .

To check whether the frequency comb emitted by a mode-locked laser can satisfy the exceptional demands of an all optical clock we have performed a series of experiments. All of them make use of an optical frequency interval divider as illustrated in Fig. 2.2. This optical interval divider is realized with three grating stabilized laser diodes [60] that can be phase-locked to modes of the mode-locked laser by controlling the injection current and the tilt angle of an external grating that is used to achieve single mode operation. Phase-locking of two laser frequencies is achieved by stabilizing their radio frequency beat signal to zero or, to reduce $1/f$ -noise, to a precisely known reference frequency [61], the so called local oscillator, using standard techniques for electronic phase-locked loops. Some details are collected in appendix A. A low noise beat signal between a particular mode and the laser diode is detected with an Si avalanche photo

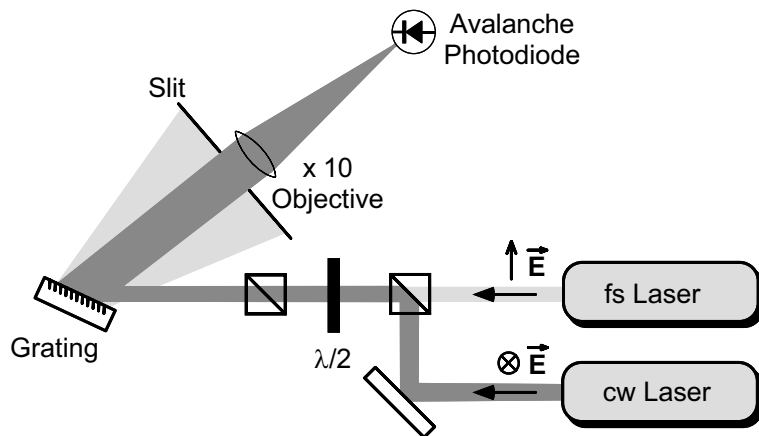


Figure 2.12: Setup for obtaining a low noise beat signal. Some of the modes in the vicinity of the cw laser are preselected with the help of a grating.

diode. The beams of the two lasers are superimposed with orthogonal polarizations and mixed with a $\lambda/2$ plate and a polarizing beam splitter. With the help of an optical grating some of the modes in the vicinity of the laser diode frequency are preselected as shown in Fig. 2.12. Even though the signal to noise ratio achieved is typically around 30 dB in a bandwidth of 1 MHz it is possible that single optical cycles are lost by the phase locked loop. To prevent such cycle slipping events from entering our data we continuously measure the in-lock beat frequencies with a bandwidth (10 MHz bandpass) that differs from the input bandwidth of the phase locked loop (40 MHz lowpass). If the deviation from the given local oscillator frequency is larger than some threshold we do not include this data point in the evaluation even though some of the rejected data points are probably not connected with cycle slip events. This cycle slip detection scheme is actually used for all phase locked loops throughout the following experiments.

In a first experiment, as sketched in figure 2.13, we have phase-locked two laser diodes at 822.8 nm and 870.9 nm to two modes of the mode-locked laser separated by more than 20 THz. The local oscillator frequencies were 20 MHz with one laser having a positive and the other a negative frequency offset. If the number of modes in between the two diode laser frequencies, which we did not count in this experiment, happens to be an odd number we expect another mode of the frequency comb right at the center between the two laser diodes. A third laser diode is then phase-locked at 20 MHz below the center mode of the frequency comb. With the help of an optical interval divider we can verify that the central mode is at the expected position in frequency space confirming the uniform distribution of the modes in the frequency comb. Because of the frequency conversions used for setting up the divider stage we expect a beat frequency of twice the local oscillator frequency. We have measured this frequency with a radio frequency counter (Hewlett Packard model 53132A) using gate times of 1, 10 and 100

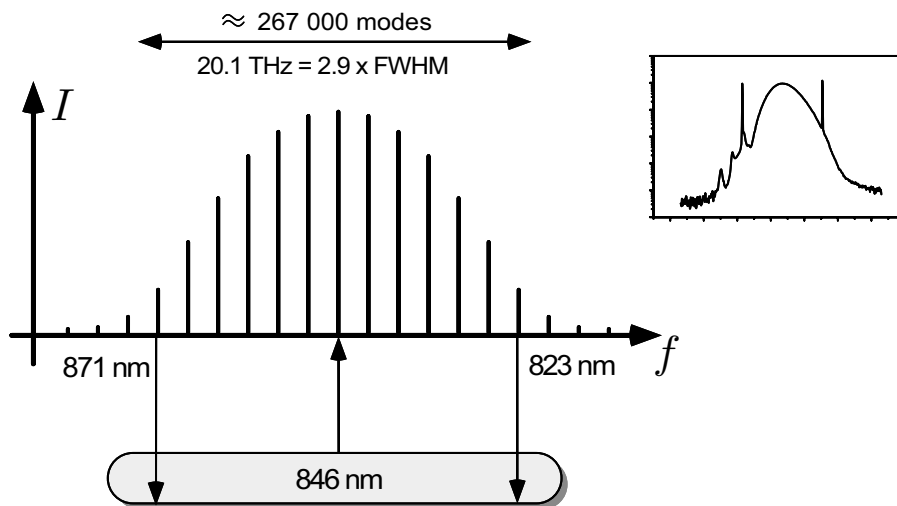


Figure 2.13: Setup for the test of a fs frequency comb. The inset shows the spectrum on a log scale. The two peaks denote the phase locked laser diodes at -30 dB.

seconds which yields a resolution of 1 mHz, 0.1 mHz and $10 \mu\text{Hz}$ respectively. The radio frequency counter and the local oscillators were all referenced to the same local cesium clock (HP 5071A, Hewlett Packard). In combination with the 1 second gate time a cycle slipping threshold of 0.5 Hz seemed to be sufficient. The result did not change significantly when this value was decreased. For the other measurements it was then appropriate to reduce the threshold in proportion to the inverse of the gate time as a possible cycle slip is averaged over this period. The weighted average of the results obtained using the various gate times calculates to a $-0.59 \pm 0.48 \text{ mHz}$ deviation from the expected 40 MHz. This verifies the uniform distribution of the modes within a relative precision of 3.0×10^{-17} .

In a second experiment we have reduced the frequency difference between the laser diodes to 4.15 THz and locked them asymmetrically with respect to the spectrum of the frequency comb. The measurement is performed in the same way as with the 20 THz frequency gap but with a gate time of 10 seconds only. With 1703 remaining frequency readings after rejecting 326 suspected cycle slipping events we find a frequency deviation from 40 MHz of $-0.70 \pm 0.61 \text{ mHz}$.

To prove that optical frequency combs emitted by mode-locked lasers are useful tools for the precise determination of large optical frequency differences it is not sufficient to verify the comb spacing. In addition one has to show that the mode separation can be measured or stabilized to the precision needed. To verify that the mode separation equals the pulse repetition rate, which can be easily measured or phase-locked, we have performed an actual frequency difference measurement. We have tuned the peak of the spectrum of the mode-locked laser to the center between the 845 nm and the 855 nm laser diode and the local oscillators set with the same sign as above. We use 328 modes of an OFCG separated by the modulation frequency of $f_{mod} = 6.321\,4 \text{ GHz}$ to phase-lock the centered laser diode precisely $328 \times f_{mod} - 100 \text{ MHz} = 2.073\,319\,2 \text{ THz}$ apart from the 855 nm laser diode (to 849.974 nm). By locking the 845 nm diode laser frequency 54205 modes of the mode-locked laser above the 855 nm laser diode (to 845.007 nm) a beat signal of 44.1 MHz is expected at the divider stage if the pulse repetition rate is set to 76.5 MHz with a phase locked loop. The short term stability of the mode-locked laser cavity helps to avoid the increase in phase noise due to the large frequency multiplication factor.

To reduce noise in the detection process we detected the 100th harmonic of the pulse repetition rate with a fast detector and phase locked it to 7.65 GHz provided by a synthesizer (Hewlett-Packard model 8360). With a total of 1859 non rejected readings and 166 suspected cycle slippings at a counter gate time of 10 seconds we find a frequency deviation from 44.1 MHz of $2.2 \pm 2.5 \text{ mHz}$. This confirms that the pulse repetition rate equals the mode separation with an accuracy of at least 6.0×10^{-16} . The four fold larger statistical uncertainty as compared with the result above may be due to additional phase fluctuations caused by the OFCG.

These first results have been published in Optics Letters [19] and have been discussed in the preceding PhD thesis of J. Reichert.

As mentioned above the frequency comb emitted directly from the laser can be broadened significantly via self phase modulation in an optical fiber therefore increasing its

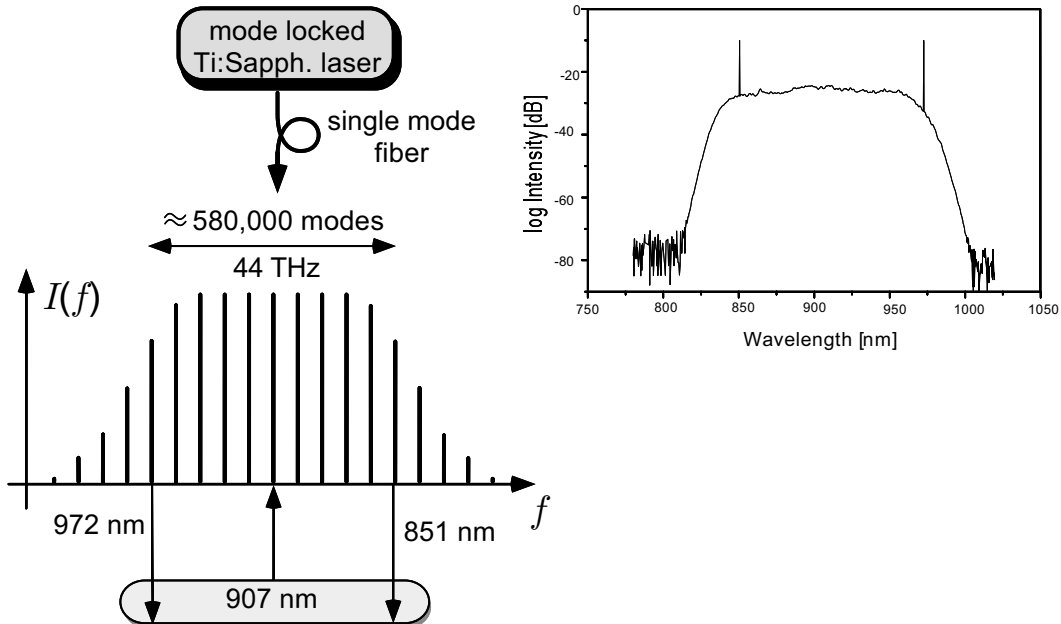


Figure 2.14: Comparison of the broadened fs comb and an optical interval divider (oval symbol). The inset (right) shows on a logarithmic intensity scale the observed spectrum. The peaks mark the position of the 972 nm and 851 nm laser diodes and the comb was generated with a Mira 900 system (Coherent Inc.) delivering 73 fs pulses at a 75 MHz repetition rate.

useful width even further beyond the time-bandwidth limit of the laser. In our case we have increased the useful range of our Mira 900 system from 20 THz to about 50 THz (see Fig. 2.6). And again the question arises whether or not this broad frequency comb is equally spaced and can therefore be used as a ruler to measure frequency differences. One might get especially suspicious about the modes created in the fiber that have never seen the fast amplitude modulating Kerr lens.

To test this we have also compared this broadened fs comb with a divider stage as illustrated in Fig. 2.14. In order to achieve a spectrum broad enough to phase-lock both laser diodes we have coupled at least 200 mW average power from our Mira 900 fs laser through a standard single mode fiber (Newport FS-F). The spectrum of the Mira pulses has been centered at 907 nm. The divider stage as shown in Fig 2.2 has been implemented with three grating stabilized diode lasers [60] at 972 nm, 851 nm and the midpoint 907 nm. Each of this laser diodes has been phase-locked to an appropriate mode of the frequency comb. The 907 nm laser diode defines the midpoint, the other two span a frequency interval of 44.2 THz. Two A-cut KNbO₃ crystals heated in ovens to approx. 130°C have been used for SHG and sum frequency generation.

As above we have detected the beat signal between the SHG and sum radiation with an avalanche photo diode and counted with a radio frequency counter (Hewlett Packard model 53132A). Different gate times of 1, 10 and 100 seconds have been used which yield a resolution of 1 mHz, 0.1 mHz and 10 μHz respectively. The radio frequency

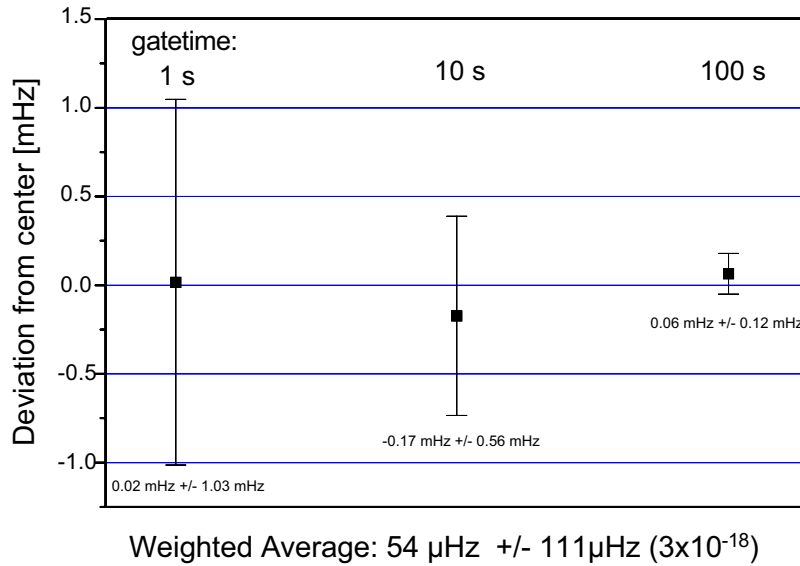


Figure 2.15: Result of the comparison divider stage vs. fs comb. Approx. 20 000 sec of data have been collected for each point.

gate time	mean deviation from 40 MHz	relative deviation	approved readings	cycle slip threshold
1 s	$0.017 \pm 1.03 \text{ mHz}$	2.3×10^{-17}	20083	0.5 Hz
10 s	$-0.173 \pm 0.562 \text{ mHz}$	1.3×10^{-17}	2028	50 mHz
100 s	$0.064 \pm 0.115 \text{ mHz}$	2.6×10^{-18}	199	5 mHz

Table 2.1: Results from the set-up of figure 2.14 with statistical uncertainties derived from the data.

counter and the local oscillators were all referenced to the same local cesium clock (HP 5071A, Hewlett Packard). For 1 second gate time we used a cycle slipping threshold of 0.5 Hz. For longer gate times this threshold has been reduced accordingly. The results of this measurement are summarized in table 2.1 and Fig. 2.15. We find agreement with the expected beat frequency of 40 MHz within $54 \pm 111 \mu\text{Hz} (3 \times 10^{-18})$.

The analysis shows that the scatter of data points consists of a nearly Gaussian distribution and a few outlying points. These points tend to scatter only to the low frequency side of the 40 MHz beat signal. We believe that these points, which lead to increased statistical uncertainty and shifts of the mean frequency, are due to cycles that have been lost by the counter connected to the divider stage. Unlike the phase locked beat signals the 40 MHz beat signal provided by the divider stage was not phase locked but measured with only one bandwidth (10 MHz bandpass). This effect has been even stronger for the 20 THz interval described above. Here we tried to keep the temperature as stable as possible by leading a steady flow of cool air across our table which substantially reduced this tendency to undetected cycle slips. Note that possible drifts of the ambient temperature may cause Doppler-shifts by slowly

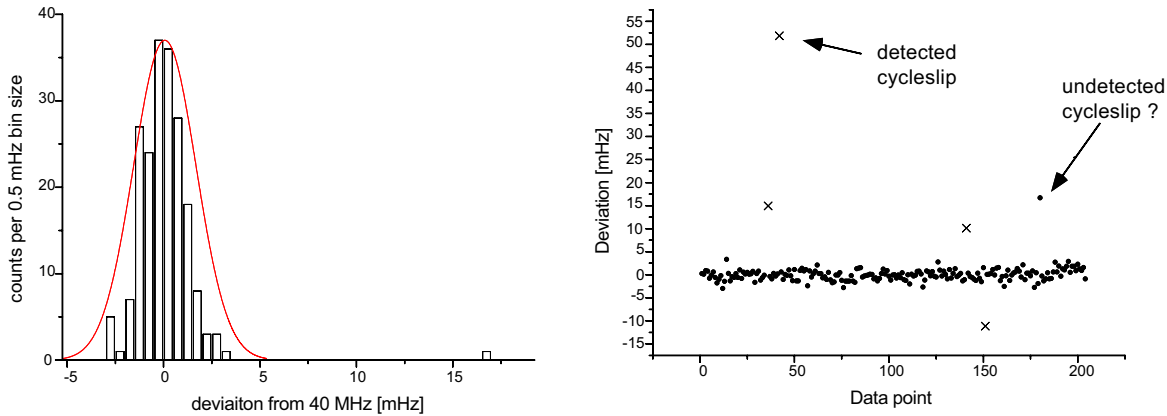


Figure 2.16: 100 s gate time data with detected cycleslips (cross). Note the one data point that is 15 mHz away. This might be an undetected cycle slip. 199 data points have been evaluated to find for the mean value $0.06 \text{ mHz} \pm 0.12 \text{ mHz}$. The normal distribution doesn't fit very well due to one outlying point.

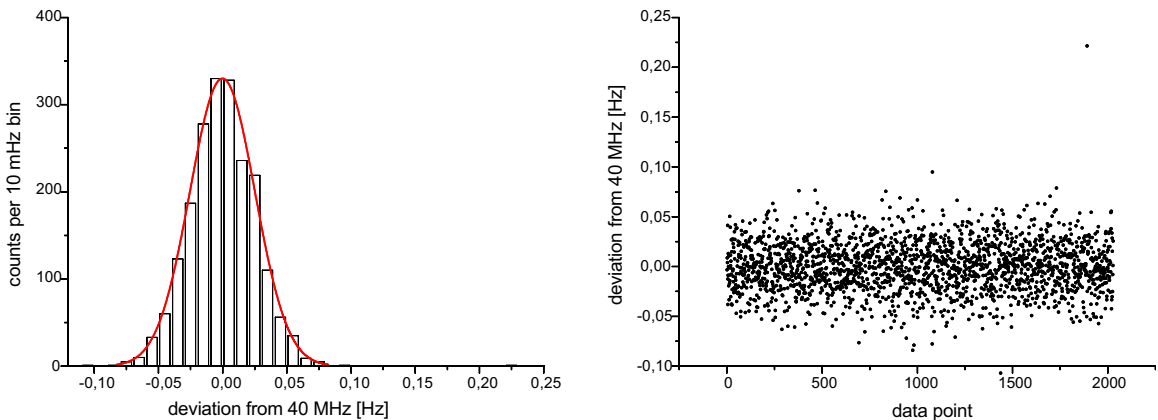


Figure 2.17: 10 s gate time data. Again 1 data point is quite far off.

changing the mirror separation by about 20λ per Kelvin at a distance of 1 meter. In our experiment this effect may cause a systematic shift of 6 mHz provided the ambient temperature changes by 1 Kelvin within a measurement time of one hour. The (worst case) specified systematic uncertainty of the frequency counter is 4 mHz, 0.4 mHz and $40 \mu\text{Hz}$ for the gate times of 1, 10 and 100 seconds respectively.

The undetected cycle slips limit the accuracy at this point. In order to reliably work at this level of accuracy this (among other problems) has to be solved. One way is to count the same beat signal with two different detection bandwidths. If the two counters disagree by more than the cycle slip threshold the data point is rejected. To observe drifts associated with changing ambient temperature or slow drifts in the servo electronics (drifting locking points etc.) tighter phase locks which would lead to increased stability of the counted beat note would be mandatory.

When measuring large optical frequency differences with fs frequency combs we are in

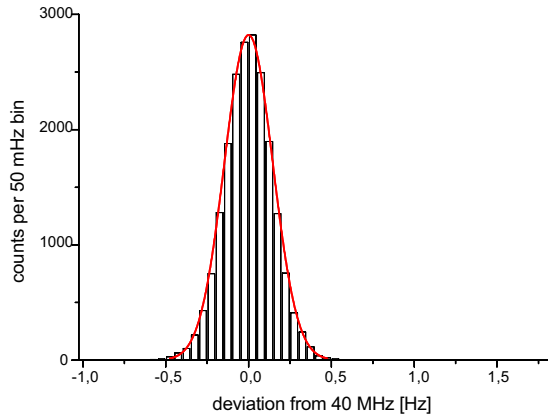


Figure 2.18: Distribution of 1 s gate time data.

fact using the fs laser as a multiplication device that multiplies an input signal not only by 2 or 10 or 100 but by 10^5 to 10^6 . To phase-lock the pulse repetition rate to a signal provided by a synthesizer one faces thus the problem of noise multiplication. It is well known that the total noise intensity grows as N^2 when a radio frequency is multiplied by a factor of N [62]. Fortunately the laser cavity acts as a filter and prevents the high frequency noise components from propagating through the frequency comb [44].

This strict periodicity gives an quite amazing insight in the nature of ultrashort pulses and even people working in both connected fields (i.e. ultrashort pulses and frequency metrology) seemed to be not totally convinced about this point.

Following our initial success in using fs lasers other groups started working in this area too, in particular S. Diddams, D. Jones S. Cundiff and J. Hall. With a commercial 12 fs laser (KMLabs) spectrally broadened in a single mode fiber they bridged a 104 THz gap between a iodine stabilized YAG laser at 1064 nm and a laser stabilized to the rubidium two photon transition at 778 nm [63]. Also H. Telle and coworkers at the Physikalisch Technische Bundesanstalt (PTB) started to use fs frequency combs for optical frequency measurements [64].

2.4 Cesium D_1 line and fine structure constant α

The first example for an optical frequency measurement using fs frequency comb techniques is the determination of the frequency of the cesium D_1 line. Here we are facing the situation discussed above of a well known reference frequency, in our case a transportable methane stabilized He-Ne laser, and an unknown frequency.

We compare the frequency of the cesium D_1 line at 895 nm with the 4th harmonic of the methane stabilized He-Ne laser operating at $3.4 \mu\text{m}$ (88 THz). This laser was set up at the Institute of Laser Physics in Novosibirsk, Russia [65], and has been calibrated previously in 1996 at the Physikalisch Technische Bundesanstalt Braunschweig/Germany (PTB) for a measurement of the hydrogen 1S - 2S absolute frequency [6]. In the summer of 1999 (one year after the experiment) we calibrated the standard again in a direct comparison with a cesium fountain clock in our lab (section 3.2 and appendix B), with

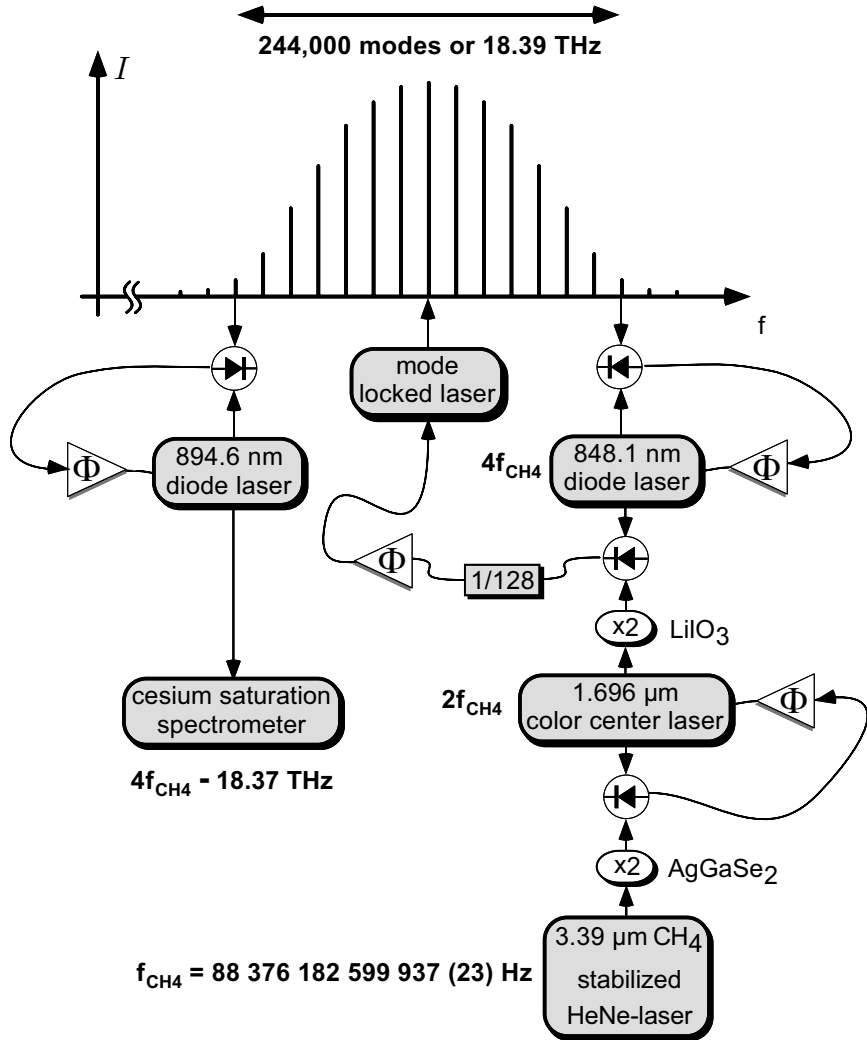


Figure 2.19: Frequency chain used for the determination of the cesium D_1 line.

$f_{He-Ne} = 88\ 376\ 182\ 599\ 976\ (10)\ Hz$ [12]. This value deviates from the previous one by 39 Hz (1.6 combined standard deviations) most likely because the operating parameters were not exactly maintained over the years. This deviation on the 10^{-13} level does not influence the measurements presented here.

The experiment, that is sketched in figure 2.19, is operated as follows: First the color center laser is phase-locked to the second harmonic of the He–Ne standard by controlling the beat frequency between them with an electronic phase-locked loop. This forces the beat frequency to oscillate in phase [61] with a reference frequency of a few MHz (not shown in the figure) provided by a cesium atomic clock. The frequency of the color center laser is then known as precisely as the He–Ne standard. Next two grating-stabilized laser diodes [60] at 848 nm and 895 nm are locked to two suitable modes of the femtosecond frequency comb after their absolute frequencies have been checked coarsely with a wavemeter. As described below, the number of modes between the laser diodes is controlled to be an integer multiple of 20. A low noise beat signal (signal to noise ratio > 30 dB in 400 kHz resolution bandwidth), necessary for phase-locking, is created with the help of a grating that preselects some of the modes in the vicinity of the laser diode frequencies. From the measured spectral intensity of the frequency comb we estimate the power of the modes in use to 40 nW. The mode to which the 848 nm laser is phase-locked is stabilized to the second harmonic of the color center laser (fourth harmonic of the He–Ne standard). This is done with the help of a piezo mounted folding mirror of the mode locked laser that controls the beat frequency between the 848 nm laser diode and the second harmonic of the color center. Because of the rather low servo bandwidth of about 10 kHz at this stage we use a large range ($\pm 16\pi$) digital phase detector [61], as we do for locking the diode lasers, and a digital by 128 divider that increases the maximum allowable phase fluctuations by a factor of 128. We continuously monitor the in-lock beat signals for possible lost cycles with additional counters operated at a different bandwidth, discarding data points that are off by more than 0.5 Hz from the given reference frequency. In the phase-locked condition the frequency of the laser that probes the cesium transition f_{895} is related to other known frequencies by

$$f_{895} = 4f_{HeNe} - nf_r \pm 128f_{ref} - 280\text{MHz}. \quad (2.20)$$

where $f_{HeNe} = 88\ 376\ 182\ 599\ 937(23)\ Hz$ denotes the frequency of the methane stabilized He–Ne laser. By changing the reference frequency f_{ref} used for phase-locking the 848 nm laser diode, we scan the frequency of the 895 nm laser diode. Exchanging the input signals of the phase detector allows the use of both signs in Eqn. (2.20). The offset of 280 MHz is due to the remaining reference frequencies used for phase-locking. The pulse repetition rate f_r of the free running laser is measured with a radio frequency counter (signal to noise ratio > 60 dB in a resolution bandwidth of 400 kHz).

As frequency comb generator we have utilized a commercial Kerr-lens mode-locked Ti:sapphire laser (Coherent Mira 900, 73 fs $\approx 1.5 \times$ Fourier limited pulses, 76 MHz repetition rate), pumped by a 5 W diode-pumped frequency-doubled single-frequency Nd:YVO₄ laser (Coherent Verdi). The same laser setup has been used in section 2.3.2 to test the regular mode spacing.

The cesium D_1 line was observed in a 7.5 cm long cell (Ophos Instruments Inc.) at room temperature. To probe the cesium D_1 transition we use a saturation spectrometer with two linearly polarized counter propagating laser beams with equal intensities ($10 \mu\text{W}/\text{cm}^2$). The pump beam redistributes the occupation number mainly by pumping the atoms to the other ground state hyperfine level so that the absorption of the probe beam is decreased. By chopping the pump beam the difference in absorption is detected with a lock-in amplifier. Because one beam can change the absorption of the other only through atoms whose Doppler shift is the same for both beams we detect only atoms that do not move along the laser beam axis. With this Doppler free method we observe 4 hyperfine components of the single stable isotope ^{133}Cs for the transitions from the ground states $F_g = 3$ and $F_g = 4$ to the upper states $F_e = 3$ and $F_e = 4$. The observed linewidth of about 6 MHz (FWHM) was somewhat larger than the natural linewidth of 5 MHz. This is believed to be caused by the short term frequency fluctuations of the phase locked lasers, allowed by the large range phase detectors. The cross over resonances were not visible due to the large separation of the excited state hyperfine components. Stray magnetic fields are reduced by a double cylindrical μ -metal shielding to values below $2 \mu\text{T}$ along the laser beam axis. The transversal field component has not been measured but is assumed to be much smaller. We find the line center of the resonances by fitting a Lorentzian with a linear background to it as shown in figure 2.20.

In order to obtain the correct frequency f_{895} the exact number of modes n between the two phase-locked laser diodes at 848 nm and 895 nm has to be determined. We could neither unambiguously identify the modes with our wavemeter nor did we want to rely solely on previous measurements in order to exclude the $f_r \approx 75$ MHz ambiguity. The observation of a frequency shift $n \times \delta f_r$ of one of the modes after changing f_r by δf_r may be a difficult because it demands a resolution of δf_r to distinguish between the mode number n and $n \pm 1$. The shift $n \times \delta f_r$ could not be chosen too large if one has to track it with a phase locked diode laser. To uniquely determine n of the

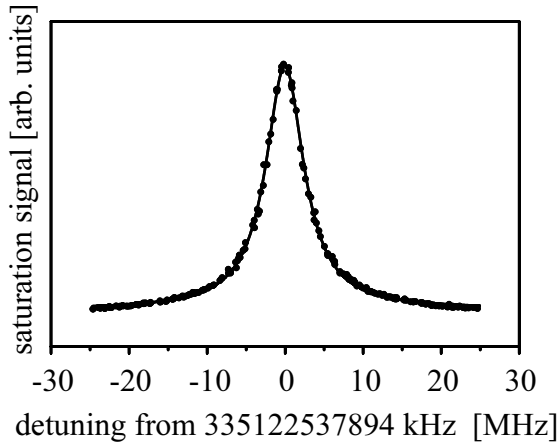


Figure 2.20: The $F_g = 4 \rightarrow F_e = 4$ component of the cesium D_1 transition with fitted Lorentzian.

order of 244,000 we employ a cavity that is stabilized to have a free spectral range of exactly 20 times the pulse repetition rate. On resonance this cavity transmits every 20th mode of the frequency comb increasing the pulse repetition rate by a factor of 20. Then the beat signals between the frequency comb and one of the laser diodes are no longer separated by $f_r \approx 75$ MHz but by $20f_r \approx 1.5$ GHz sufficient to be unambiguously identified by our wavemeter. To validate our mode number counting scheme we have phase locked two laser diodes 26,500 modes apart and checked the resulting frequency difference with an optical frequency comb generator [34]. Since then a larger mode spacing is now allowing identification with a common laser wavemeter.

The ground state hyperfine splitting as calculated from our result is 36 kHz for $F_e = 3$ and 27 kHz for $F_e = 4$ too large compared to the definition of the SI second. We attribute this deviation to systematic uncertainties due to imperfections of the magnetic field shielding. Because of different gyromagnetic ratios Zeeman shifts are present depending on the Zeeman level that is mostly depleted by the pump beam. Imperfections of the polarization of the beams and small polarization modulations caused by the chopped pump beam may lead to unsymmetric pumping of the M_F levels. In the worst case the $M_F = 4 \leftrightarrow M_F = 3$ component is probed leading to a Zeeman shift of 40 kHz where the sign depends on the nature of the polarization imperfections. We expect smaller shifts for transitions connecting the same total angular momentum than for transitions between $F = 4$ and $F = 3$ because the difference of the gyromagnetic ratios is smaller and mostly unshifted $M_F = 0$ components will be probed. We have corrected for this systematic effect by adding 36 kHz to the $F_g = 4 \rightarrow F_e = 3$ and subtracting 27 kHz from the $F_g = 3 \rightarrow F_e = 4$ transition forcing the ground state hyperfine splitting to the defined value and obtain from a total of 112 recorded lines:

$$f_{D1}^{F_g=3 \rightarrow F_e=3} = 335\ 120\ 562\ 838 \text{ kHz} \quad (2.21)$$

$$f_{D1}^{F_g=3 \rightarrow F_e=4} = 335\ 121\ 730\ 526 \text{ kHz} \quad (2.22)$$

$$f_{D1}^{F_g=4 \rightarrow F_e=3} = 335\ 111\ 370\ 206 \text{ kHz} \quad (2.23)$$

$$f_{D1}^{F_g=4 \rightarrow F_e=4} = 335\ 112\ 537\ 894 \text{ kHz} \quad (2.24)$$

This procedure does not alter our result of the hyperfine centroid but the resulting excited state hyperfine splitting. The systematic uncertainty is estimated by the maximum expected Zeeman shift of 40 kHz for the absolute frequencies and twice that value (systematic uncertainties may add up) for the upper state hyperfine splitting. Other systematic effects like the AC–stark effect, light pressure induced line–shape modifications [73], spurious selective reflection signals and collisional shifts [74] shifts are estimated to be much smaller. The statistical uncertainty is around 10 kHz. Our results for the hyperfine centroid

$$f_{D1} = 335\ 116\ 048\ 807\ (41) \text{ kHz}, \quad (2.25)$$

and for the upper state hyperfine splitting

$$f_{6P_{1/2}}^{HFS} = 1\ 167\ 688\ (81) \text{ kHz}, \quad (2.26)$$

are in good agreement with previous values obtained by others $f_{D1} = 335\,116\,062$ (15) MHz [71] and $f_{6P_{1/2}}^{HFS} = 1\,167.54$ (32) MHz [75]. The uncertainties of the frequencies given in Eqn. 2.24 are estimated in the same way to be 41 kHz.

Our measurement of the cesium D_1 line provides an important link for a new determination of the fine structure constant α , one of the most fundamental constants of nature. Because α scales all electromagnetic interactions, it can be determined by a variety of independent physical methods [112]. Different values measured with comparable accuracy disagree with each other by up to 3.5 standard deviations and the currently most accurate value from the electron $g - 2$ experiment relies on extensive QED calculations [66]. The 1998 CODATA² value [67] $\alpha^{-1} = 137.035\,999\,76$ (50) (3.7×10^{-9}) follows the $g - 2$ results. To resolve this unsatisfactory situation it is most desirable to determine a value for the fine structure constant that is comparable in accuracy with the value from the $g - 2$ experiment but does not depend heavily on QED calculations. A promising way is to use the photon recoil shift of some atomic resonance together with the accurately known Rydberg constant R_∞ [6] according to:

$$\alpha^2 = \frac{2R_\infty}{c} \frac{h}{m_e} = 2R_\infty \times \frac{2cf_{rec}}{f_{D1}^2} \times \frac{m_p}{m_e} \times \frac{m_{Cs}}{m_p} \quad (2.27)$$

In addition to the Rydberg constant a number of different quantities, all based on intrinsically accurate frequency measurements, are needed.

Experiments are underway in Stanford in S. Chu's group to measure the photon recoil shift $f_{rec} = f_{D1}^2 h / 2m_{Cs}c^2$ of the cesium D_1 line. A preliminary result is given in the PhD thesis of B. Young [68]. Together with the proton-electron mass ratio m_p/m_e , that is known to 2×10^{-9} [69] and even more precise measurements of the cesium to proton mass ratio m_{Cs}/m_p in Penning traps, that have been reported recently [70], a new value for the fine structure constant $\alpha^{-1} = 137.035\,992\,4(41)$ is obtained from Eqn. 2.27.

The results presented here have been published in Physical Review Letters [5] and are also discussed in the preceding PhD thesis of J. Reichert [38].

²The Committee on Data for Science and Technology (CODATA) publishes regularly a self-consistent set of recommended values of the basic constants and conversion factors of physics and chemistry for international use. The most recent recommendations have been published in 1986 and 1998 [67].

2.5 Indium ion clock transition

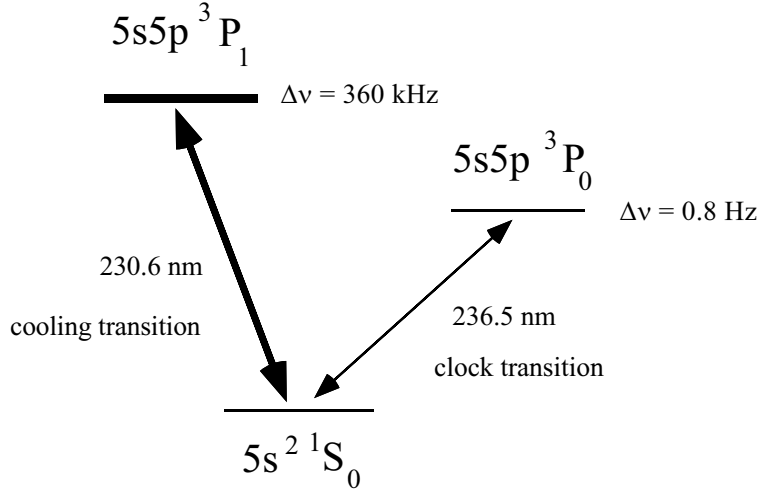


Figure 2.21: Indium energy level scheme.

In collaboration with the group of H. Walther and his Indium team (E. Peik, J. von Zanthier, A. Nevsky, Th. Becker, M. Eichenseer, Ch. Schwedes) we have investigated the $5s^2 1S_0 - 5s5p ^3P_0$ transition at 237 nm in a single trapped In^+ ion. This is a promising candidate for a high performance optical frequency standard [80, 81, 82, 83]. By comparison with our CH_4 stabilized He–Ne laser we have measured its frequency to within 1.8 parts in 10^{13} . This transition with a natural linewidth of only 0.8 Hz [83] has a line quality factor of $Q = \nu/\Delta\nu = 1.6 \times 10^{15}$. The two states participating in the hyperfine-induced $J = 0 \rightarrow J = 0$ transition couple only weakly to perturbing external electric or magnetic fields. In particular, they are insensitive to electric quadrupole shifts caused by the field gradient of the trap. The particle can be kept in the trap free of collisions for an almost infinite time and brought to near-rest by laser cooling. Thus, transit-time broadening and first-order Doppler effects can be eliminated and the second-order Doppler effect can be reduced to negligible values [82, 83]. With these characteristics taken into account, a residual uncertainty of 10^{-18} for a frequency standard based on a single stored In^+ ion is expected [84, 80].

In a first experiment [39, 38], we reported the measurement of the absolute frequency of the In^+ clock transition using two optical reference frequencies, a methane-stabilized He–Ne laser at $3.39 \mu\text{m}$ and a Nd:YAG laser at 1064 nm whose second harmonic was locked to a hyperfine component in molecular iodine. The measurement inaccuracy of 3.3 parts in 10^{11} was limited by the degree of uncertainty to which the iodine reference was known.

Here we report on a new precise measurement of the absolute frequency of the $1S_0 - ^3P_0$ transition using a phase-coherent frequency chain which links the 237 nm radiation (1 267 THz) of the In^+ clock transition to the He–Ne laser at $3.39 \mu\text{m}$ (88 THz) alone. In this case the accuracy of the measurement is only limited by the much

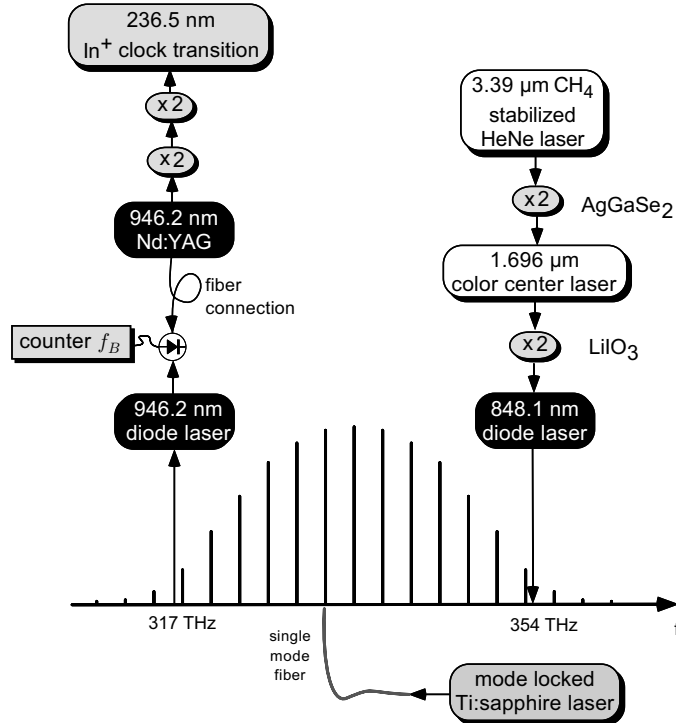


Figure 2.22: Frequency chain connecting the Indium clock transition with the He–Ne secondary frequency standard .

smaller uncertainty of the $\text{CH}_4/\text{He-Ne}$ reference. The present experimental setup of the frequency chain is illustrated in Fig. 2.22. A $\text{NaCl}:\text{OH}^-$ color center laser at 1.70 μm is phase-locked to the second harmonic of the methane-stabilized He-Ne laser at 3.39 μm . A 848 nm laser diode is then locked to the second harmonic of the color center laser. This is accomplished by first stabilizing it to a selected mode of the frequency comb of a Kerr-lens mode-locked Ti:sapphire femtosecond laser (Coherent model Mira 900), frequency-broadened by a standard single-mode silica fiber (Newport FS-F), and then controlling the position of the comb in frequency space [11]. A radio-frequency divider, dividing by 128, helps to overcome the limited servo bandwidth that controls the comb position. In chapter 2.3.2 we have demonstrated that this frequency comb is regularly spaced and meets the exceptional requirements of high-precision spectroscopy. The 76 MHz pulse repetition rate, which sets the mode separation, is phase-locked [44] to a commercial cesium clock (Hewlett-Packard model 5071 A) which is constantly calibrated using the time disseminated by the Global Positioning System. Each mode of the comb is therefore known with the same fractional precision as the He-Ne standard, i.e. within 1.1 parts in 10^{13} . A diode laser at 946 nm is phase-locked to another selected mode of the comb, positioned $n = 482\,285$ modes or 37 THz to lower frequencies from the initial mode at 848 nm. The mode number n is determined from our previous measurement [39]. We know the transition frequency already to within a few kHz, so the mode number can be determined by demanding n to be integer. The beat frequency with the 946 nm Nd:YAG laser, whose 4th harmonic excites the In^+

clock transition, is counted with a commercial radio-frequency counter (HP 53131A). Again our cycle slip detection scheme comes into play. For the absolute frequency measurement, the in-lock beat signals of the chain are continuously monitored with additional counters for possible lost cycles [11], see appendix A. Points that are off by more than 0.5 Hz from the phase-locked beat signal are discarded. With the frequency chain in lock, the unknown $^{115}\text{In}^+ - ^1S_0 - ^3P_0$ clock transition frequency f_{In^+} at 237 nm is related to the known frequency of the He-Ne standard f_{He-Ne} through

$$f_{In^+} = 16 \cdot f_{He-Ne} - 4 \cdot (f_{beat} + n \cdot f_r) - f_{LO}. \quad (2.28)$$

Here f_{beat} is the frequency of the beat signal at 946 nm detected by a photodiode and recorded by a radio-frequency counter in a 1 sec interval, f_r denotes the repetition rate of the mode-locked femtosecond laser, n is the number of modes separating the two selected modes of the comb, and $f_{LO} = 1\,632\text{ MHz}$ contains all contributions from the local oscillator frequencies employed for the phase-locks.

The He-Ne secondary optical frequency standard was set up at the Institute of Laser Physics in Novosibirsk, Russia [65], and has been calibrated previously (1996) for a measurement of the hydrogen $1S - 2S$ absolute frequency [6] as described in section 2.4. In the present experiment conducted in October 1999 we have used the result of a more recent calibration (see appendix B) that was obtained 4 months earlier from a direct comparison with a cesium fountain clock in our lab, with $f_{He-Ne} = 88\,376\,182\,599\,976(10)\text{ Hz}$ [12]. This value deviates from the previous one by 39 Hz (1.6 combined standard deviations), most likely because the operating parameters were not exactly maintained over the years in the two experiments. Unlike in the previous calibration, this time the laser was not moved between its calibration and the measurement.

Within several days of measurement we recorded 6 214 excitations of the 3P_0 level by scanning the 946 nm Nd:YAG clock laser over the $\text{In}^+ - ^1S_0 - ^3P_0$ resonance. Excitation of the 3P_0 state is detected by optical-optical double resonance invented by Dehmelt (shelving spectroscopy) [84]: after applying the clock laser for 15 ms the laser exciting the $^1S_0 - ^3P_1$ cooling transition is turned on for 40 ms to probe the population of the ground state. If no fluorescence photons are counted on the $^1S_0 - ^3P_1$ transition, the cooling laser is kept on for up to ten further 40 ms intervals to wait for the decay of the metastable state and an excitation event is recorded. The frequency of the clock laser is typically changed in steps of 80 Hz (at 946 nm) and 16 excitation attempts are made at each frequency. Scanning of the Nd:YAG master laser is synchronized with detection of the beat signal f_{beat} at 946 nm and the counters used for detection of lost cycles. All counters as well as the AOM driving synthesizers are referenced to our local cesium atomic clock.

Figure 2.23 shows the 3P_0 excitation probability as a function of the beat frequency f_{beat} for a typical measurement session, collecting 674 quantum jumps to the 3P_0 state. During the measurement session 21 excitation spectra were recorded where the investigated scanning range varied slightly from spectrum to spectrum. The width of the distribution is due to short-term and mid-term frequency instabilities of the Nd:YAG laser,

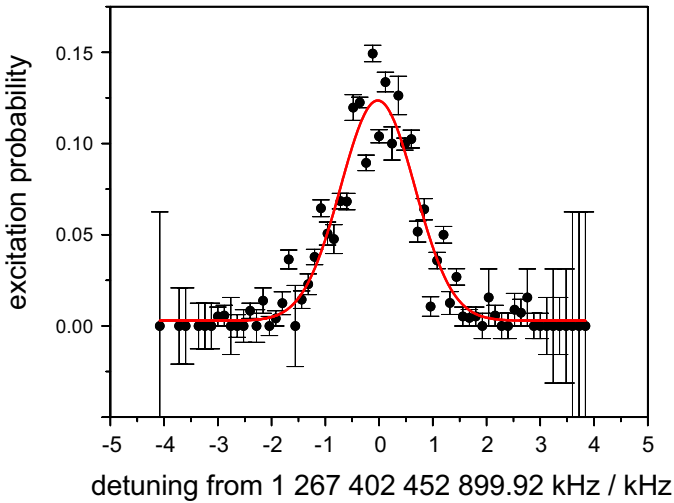


Figure 2.23: Indium line obtained in a sample session. Excitation probability in a 40 ms interval at 1 mW/cm² ($\approx 10^4 I_{sat}$), line width in this sample is 1.7 kHz (FWHM) from fitted Gaussian.

the methane standard, and the frequency chain. A weighted fit to a Gaussian function is used to determine the line center. By averaging the beat frequency at line center for the eleven measurement sessions performed we obtain $f_{beat} = 49\,174\,925(42)$ Hz (see Fig. 2.24). From this value we determine the absolute frequency f_{In^+} of the $^{115}\text{In}^+ \text{ }^1S_0 - \text{ }^3P_0$ clock transition according to Eq. (2.28):

$$f_{In^+} = 1\,267\,402\,452\,899.92(0.23) \text{ kHz.}$$

The uncertainty of 1.8 parts in 10^{13} is derived from a quadratic addition of the uncertainty of the measurement ($4 \Delta f_{beat}$) and the uncertainty in the He-Ne standard calibration ($16 \Delta f_{He-Ne}$). Both contributions are due to the limited reproducibility of the He-Ne standard.

Systematic frequency shifts of the clock transition are negligible at the present level of accuracy. The magnetic field dependence is -636 ± 27 Hz/G for the $|F = 9/2; m_F = 9/2\rangle \rightarrow |F = 9/2; m_F = 7/2\rangle$ component that we excite [83], where we adjust the magnetic field to zero with a precision of a few times 10 mG. Other systematic frequency shifts such as the quadratic Stark or second-order Doppler shift are orders of magnitude smaller than the Zeeman shift at the temperatures to which the ion is cooled in our trap ($T \sim 150 \mu\text{K}$) [83].

The new result is well within the error bars of our previous measurement, where we obtained a value of $1\,267\,402\,452\,914(41)$ kHz for the clock transition [39]. Compared with that value, the new measurement represents an improvement in accuracy of more than 2 orders of magnitude. It now stands as the most accurate measurement of an optical transition frequency in a single ion.

The linewidth of the exciting laser is still too large to finally explore the accuracy range beyond current cesium atomic clocks. Note that the measurement time τ needed to

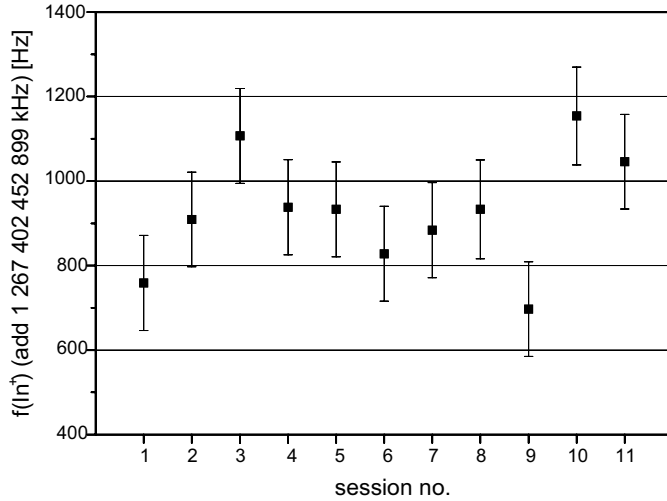


Figure 2.24: Result of the Indium measurement. From a total of 11 runs we derive a mean value for the clock transition of $f_{I_n} = 1\ 267\ 402\ 452\ 899\ 916\ (232)\ \text{Hz}$

average down to a certain accuracy scales as $\tau \sim 1/\sqrt{\text{linewidth}}$. Work is in progress and recently laser linewidth on the order of one Hz in several seconds have been achieved by the Indium team.

The low systematic uncertainties of the indium ion make it a promising candidate for an oscillator in a future all optical clock. However, an optical clock consists not only of a stable oscillator (“the pendulum”) but also of a counter that counts the oscillations per time unit, the “clockwork”. This can be done by a fs frequency chain as described in this text.

A further interesting feature of our frequency chain is the fact that it can be used to compare two narrow optical transition frequencies with each other, e.g. the clock transition in indium with the hydrogen 1S - 2S transition. In particular, this may allow investigation of possible variations of fundamental constants in time as recently proposed in [8].

The results presented here have been published in Optics Letters [15].

2.6 Iodine and stable Nd:YAG lasers

2.6.1 Iodine frequency grid

Another excursion into the wonderful world of precision spectroscopy and stable lasers brings us to iodine stabilized lasers.

Here we have compared two different laser systems in terms of stability and accuracy and find that iodine stabilized lasers are convenient and easy to handle secondary optical frequency standards in the 10^{-12} reproducibility range. Recent values obtained from other groups for the transitions under investigation have been confirmed and partly improved.

High resolution saturated absorption spectroscopy of molecular iodine hyperfine transitions delivers a convenient natural frequency grid in the range from the near infrared to the limit of the iodine molecule dissociation near 500 nm. The absence of an electrical dipole moment leading to extremely small perturbation by external electromagnetic fields [85, 86] as well as strong and relatively narrow natural linewidths of hyperfine structure (HFS) transitions make molecular iodine ideally suited as a secondary optical frequency standard where the ultimate of precision is not needed. More than 100 000 Iodine lines have been catalogued by Gerstenkorn and Luc by Fourier transform spectroscopy [87], which, in spite of its versatility, does not resolve the Doppler broadened HFS transitions. In recent years different groups have carried out precise absolute frequency measurements of a number of iodine lines at 532 nm [88, 27], 540 nm, 778 nm [89], 633 nm [89, 90].

Although playing in another league as compared to the ion trap experiments and despite the fact that fs frequency chains as discussed in this text allow us to synthesize almost any optical frequency with unprecedented precision, iodine stabilized lasers are still widely used as simple and reliable wavelength standards.

Up to now practical length metrology is performed mainly by using the red line of the iodine stabilized He-Ne laser at $\lambda = 633$ nm with a relative standard uncertainty of 2.5×10^{-12} [90]. With the use of diode-pumped, frequency-doubled Nd:YAG lasers emitting at $\lambda = 532$ nm, it becomes possible to develop a new optical secondary frequency standard in the green part of the visible spectrum. Compact in size, these lasers exhibit low intrinsic frequency and amplitude noise, high power levels and long expected life time. Moreover, within the tuning range of the doubled frequency at 532 nm lie a number of iodine absorption lines which are strong and relatively narrow so that they can be used as reference lines and for the frequency stabilization of the laser. So far, iodine stabilized Nd:YAG lasers have demonstrated a remarkably low Allan standard deviation³, reaching the level of 5×10^{-15} at 1000 s [92]. This is already more than 2 orders of magnitude better than the iodine stabilized He-Ne systems at 633 nm [93]. These lasers can therefore possibly replace the low power He-Ne - or

³The Allan variance or Allan standard deviation is often used to characterize frequency stability. It is given by $\sigma^2(\tau) = \frac{1}{M} \sum_{k=1}^M \frac{(f_{k+1} - f_k)^2}{2f_0^2}$ where f_k are consecutive measurements with gatetime τ , f_0 is the mean frequency. More details can be found in Ref [91]

costly Ar⁺ - laser in this spectral range. Presently, several groups are investigating a number of features of these laser systems, at Stanford University, the Joint Institute for Laboratory Astrophysics (JILA), Boulder, the Bureau International des Poids et Mesures (BIPM), Paris, the Institute of Laser Physics (ILP), Novosibirsk, including different methods of frequency stabilization [94, 95], measurements of hyperfine line separations or frequency intervals between absorption lines [96, 97, 92] and absolute optical frequency measurements [98, 99, 27]. As a result of these efforts, the Comité Consultatif des Longueurs (CCL) meeting in 1997 recommended the frequency of one particular component, the a₁₀ hyperfine structure (HFS) component of the R(56)32-0 transition, for the realization of the metre with a relative standard uncertainty of 7×10^{-11} [10].

2.6.2 Nd:YAG lasers

In order to explore the potential of the I₂ stabilized Nd:YAG laser at 532 nm as a secondary frequency standard a direct comparison of different laser systems is beneficial. Different independent measurements of the absolute frequency of the R(56)32-0 line will help to identify possible systematic errors. Here we present a frequency comparison of two independent iodine stabilized frequency-doubled Nd:YAG lasers at 532 nm and an absolute frequency measurement of the laser frequencies locked to different HFS components of the R(56)32-0 and P(54)32-0 iodine absorption line. The absolute frequencies have again been determined using a phase-coherent frequency chain which links the I₂ stabilized laser frequency to our CH₄-stabilized He-Ne laser at 3.39 μm . This laser has been calibrated before the measurements against an atomic cesium fountain clock. Details are given in appendix B.

For the frequency measurements two independent laser systems were used, one set up at the Institute of Laser Physics (ILP), Novosibirsk, Russia, the other at the

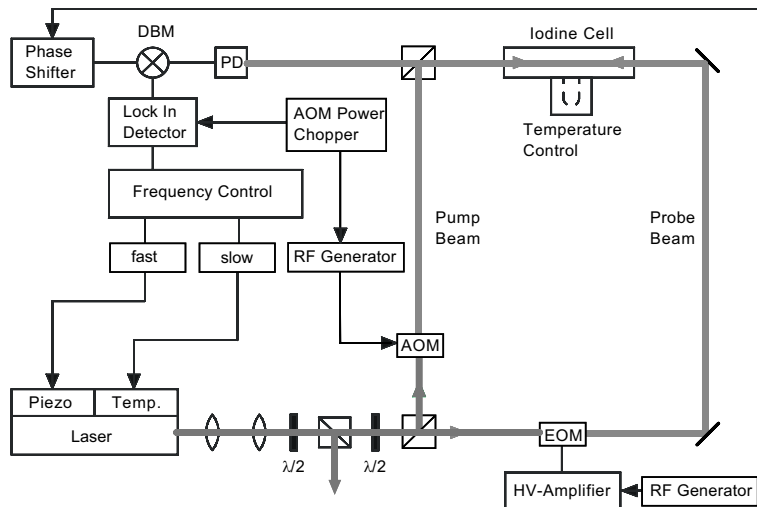


Figure 2.25: The PTB iodine spectrometer. See text for details.

Physikalisch-Technische Bundesanstalt (PTB), Braunschweig, Germany. Both lasers employ saturated absorption techniques for stabilizing the laser onto a selected hyperfine component in molecular iodine.

The PTB Nd:YAG laser system shown in Fig. 2.25 is based on model 142 of Lightwave Electronics Co.. Within the frequency tuning range of this laser two major iodine lines, R(57)32-0 and P(54)32-0, can be addressed. The PTB system uses two servo-loops to stabilize the laser frequency: a slow thermal and a fast piezo-mounted transducer (PZT) with bandwidths of approximately 10 Hz and 10 kHz, respectively. To lock the laser onto a selected I_2 line the phase modulation method is employed [100]. The probe beam is modulated at 2.05 MHz by an electro optic modulator (EOM), the pump beam is frequency shifted by an acousto-optical modulator (AOM). The driving AOM RF power is chopped in order to cancel frequency offsets introduced by the Doppler background or residual amplitude modulation, using a lock-in detection scheme. The transmitted probe beam signal is detected by a photodiode (PD) and mixed with the EOM RF in a double balanced mixer (DBM). A detailed description of the set-up is given in [101]. The frequency stability of the laser has been analyzed at PTB by locking two identical systems to independent iodine cells and observing the beat frequency between them. The root Allan variance of the beat follows a $2 \times 10^{-13}/\sqrt{Hz\tau}$ dependence for measurement times $\tau \leq 100$ sec and reaches a minimum value of 3×10^{-14} at $\tau = 100$ s.

The ILP iodine spectrometer 2.26 is based on a home-made diode-pumped Nd:YAG laser at 1064 nm with intracavity frequency doubling. The laser uses a Nd:YAG crystal with one surface spherical and dichroically coated to serve as resonator mirror and input mirror for the pumping beam. The crystal is mounted on a PZT for fast frequency control. The flat output mirror is also mounted on a PZT and used for probe frequency

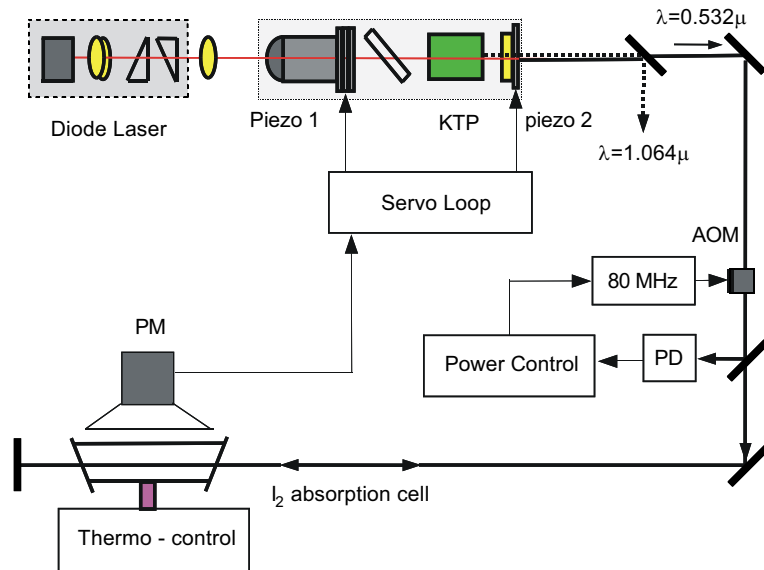


Figure 2.26: The ILP iodine spectrometer.

modulation. The small size of the mirror and the PZT allows to reduce contributions of high-order harmonics to the probe frequency modulation. For intracavity frequency-doubling a KTP crystal is used which, together with a Brewster plate, serves as a Lyot filter. This provides single-frequency operation and the possibility to frequency tune the laser for more than 500 GHz by changing the temperature of the KTP crystal. The length of the laser resonator is about 18 mm so that the whole system remains compact and stable. With 700 mW of pumping power, 30 mW in the fundamental beam at 1064 nm and up to 20 mW in the second harmonic at 532 nm are generated. The 532 nm laser radiation, after passing an acousto-optical modulator (AOM), is directed into an external I_2 fluorescence cell. The iodine pressure in the cell is controlled via the temperature of a cold finger. A photomultiplier (PM) detects the fluorescence signal over a solid angle of almost 0.2π . The laser frequency is modulated at 455 Hz with an amplitude of about 500 kHz. In order to lock the laser to an I_2 saturation absorption resonance, a third harmonic synchronous detection of the probe modulation is employed which minimizes the influence of Doppler background. The frequency stability of the laser has been investigated at ILP with the help of two identical systems locked to two different iodine cells. The root Allan variance of the beat frequency between the two I_2 locked lasers reaches a minimum of 5×10^{-14} at $\tau = 300$ s - 1000 s.

In order to investigate the reproducibility of the two iodine spectrometers, a frequency comparison of the ILP and the PTB laser was made. The frequency intervals between hyperfine components of the P(54)32-0 line (1105) for the three best isolated components were measured, using both lasers and the matrix method [102]: one laser was stabilized to a selected component of this line while the other was successively stabilized to the a_1 , a_{10} , and a_{15} component. All frequency intervals were measured several times at different days.

In order to check for systematic errors on the measured frequencies due to iodine cell impurities, we interchanged in the ILP system three different iodine cells (cells 16/98PTB, 13/97PTB, and 5/98PTB, respectively). The PTB laser system used a 50 cm cell 2/98PTB throughout the measurements, which is too long to be used in the ILP set-up. The result was: $(\nu_{16/98} - \nu_{13/97}) = 1.6$ (0.4) kHz, $(\nu_{16/98} - \nu_{5/98}) = 2.7$ (0.8) kHz and $(\nu_{2/98} - \nu_{13/97}) = 1.0$ (0.7) kHz. For most measurements, iodine cell 13/97PTB was used. In addition, we checked for systematic frequency shifts due to variation of laser power, probe modulation amplitude, beam alignment and iodine pressure. The temperature of the cells could be changed between -20 °C and $+10$ °C, with a stability of better than 0.05 K and an accuracy of better than 1 K. Again one system was operated under unchanged conditions to serve as a reference while the parameters of the other laser were varied. The PTB laser is sensitive to geometrical alignment of the counter-propagating pump and probe beams and to residual amplitude modulation resulting in a total standard uncertainty of about 2 kHz. Due to the fluorescence detection technique the ILP laser is less sensitive to geometrical effects which shift the line center. At present the estimated total standard uncertainty of 1.1 kHz of this laser is limited by the uncertainty to which the absolute temperature of the cold finger of the iodine cell is known.

Taking into account all available data of frequency differences obtained during the

course of the matrix measurements, and correcting for different iodine pressures, different iodine cells and different HFS-separations, we derive a combined frequency reproducibility of the two laser systems in the experiment of 1.1 ± 0.7 kHz (at 532 nm). This is a notable result, given the fundamental differences between the two iodine spectrometers as far as saturated absorption signal detection, laser frequency stabilization and laser set-ups are concerned.

2.6.3 Frequency chain

In order to measure the optical frequencies of the iodine spectrometers, we employed a frequency chain which links the Nd:YAG laser frequencies to our CH₄ stabilized He-Ne laser at 3.39 μm shown in Fig. 2.27. This laser has already been described in the preceding sections and more details can be found in appendix B.

The frequency chain works as follows: to the second harmonic of the He-Ne laser at 3.39 μm a NaCl:OH⁻ color center laser at 1.70 μm is phase locked. To the second harmonic of the color center laser a laser diode at 848 nm is then stabilized. This is accomplished by first locking the laser diode to a selected mode of the frequency comb of a Kerr-lens mode-locked Ti:sapphire femtosecond laser (Coherent model Mira 900), frequency-broadened in a standard single-mode silica fiber (Newport FS-F), and then controlling the position of the comb in frequency space as described in section 2.3.1. A 128 prescaler helps to overcome the limited servo bandwidth that controls the comb position. At the same time the mode separation of 76 MHz is controlled by a local cesium atomic clock [44]. With one mode locked to the 4th harmonic of the CH₄ standard and at the same time the pulse repetition rate (i.e. the mode separation) fixed [44], the femtosecond frequency comb provides a dense grid of reference frequencies known with the same fractional precision as the He-Ne standard [19, 11]. With this tool a frequency interval of about 37 THz is bridged to lock a laser diode at 946 nm to the frequency comb, positioned $n = 482\,285$ modes to lower frequencies from the initial mode at 848 nm.

In extension to this frequency chain we installed an optical frequency interval divider [33] to extrapolate to 1064 nm. The center frequency of the optical divider stage is given by the Nd:YAG laser at 946 nm laser with its frequency determined via the beat note with the comb locked laser diode at 946 nm. The higher input frequency of the divider stage is set by a diode laser at 852 nm which is heterodyned with another diode laser at 852 nm, also phase locked to the frequency comb. The lower input frequency of the divider stage is determined by the iodine stabilized Nd:YAG laser at 1064 nm. While scanning the frequency doubled 1064 nm Nd:YAG laser over the iodine line the two beat notes at 852 nm and 946 nm are measured with a rf counter. They are then used to determine the absolute frequency of the 1064 nm Nd:YAG laser. Another beat signal is observed between the fundamental wave of the two YAG systems. All phase locked beats are again checked with additional counters for lost cycles.

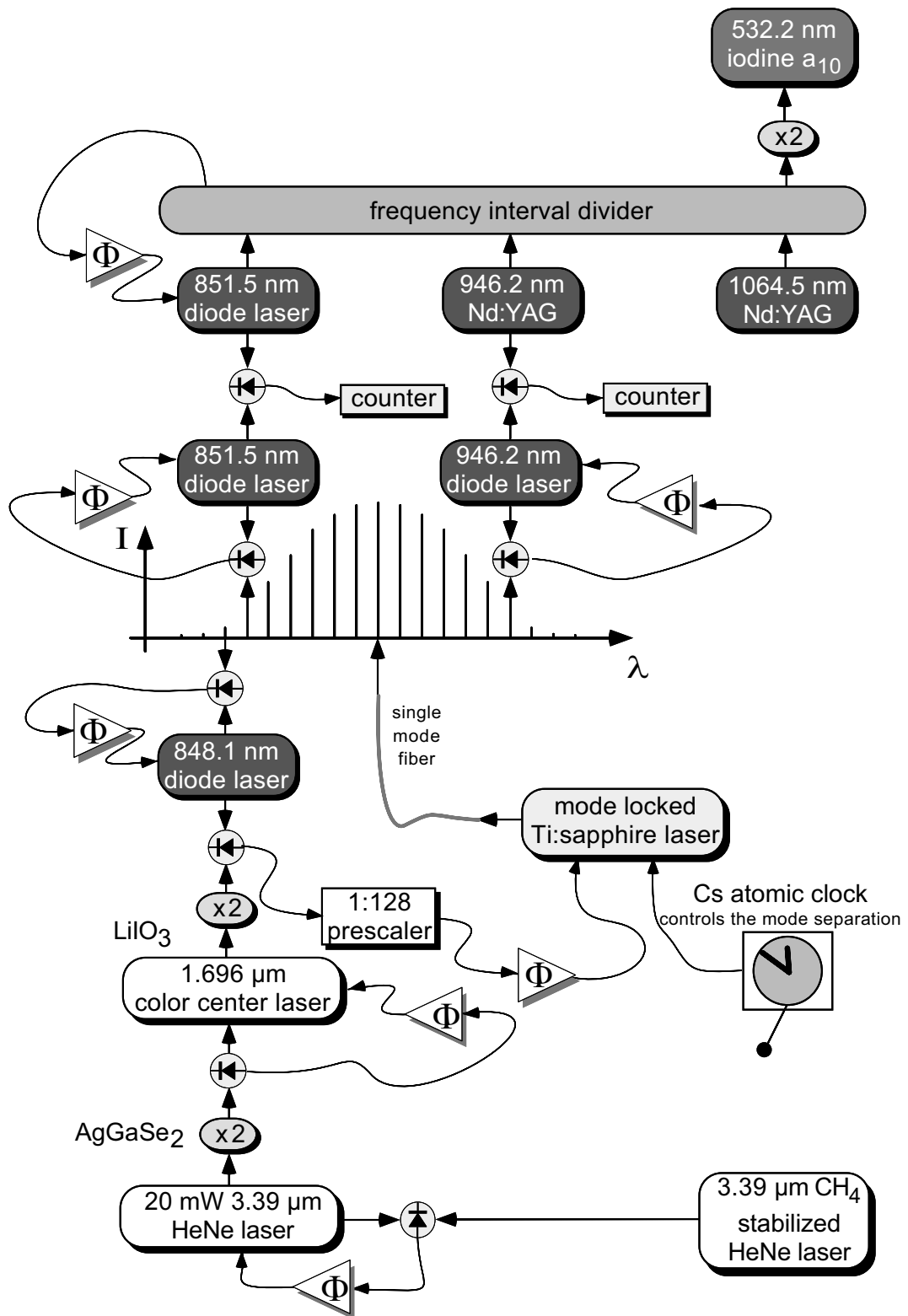


Figure 2.27: frequency chain for iodine measurement.

2.6.4 Frequency measurements

With the frequency chain in lock the unknown frequencies f_{532} of the investigated iodine lines at 532 nm are related to the known frequency of the He-Ne standard f_{He-Ne} and the comb mode separation f_{rep} through:

$$f_{532} = 8 \cdot f_{He-Ne} - 4 \cdot \Delta f_{946} - 2 \cdot \Delta f_{852} - 4 \cdot n_1 \cdot f_{rep} + 2 \cdot n_2 \cdot f_{rep} - f_{LO} \quad (2.29)$$

Here Δf_{946} and Δf_{852} are the beat signals at 946 nm and 852 nm, respectively, n_1 and n_2 are the number of modes separating the two selected modes of the comb at 946 nm and 852 nm from the comb mode at 848 nm and f_{LO} collects the frequencies of all local oscillator employed in the phase-locks.

In a first experiment, the frequency of the a_{10} HFS component of the R(56)32-0 iodine absorption line has been measured. This line is recommended by the Comité International des Poids et Mesures (CIPM) for the realization of the metre [10]. Since the PTB laser is not tunable to this frequency, the experiment has been carried out with the ILP laser only. Using cell 13/97PTB with the parameters $T = -5^\circ\text{C}$ ($p = 2,42$ Pa), $P = 1,7$ mW, $I = 80$ mW/cm² the result is (see Fig. 2.28):

$$f_{a10}(1110) = 563\,260\,223\,507.8 (1.1) \text{ kHz}$$

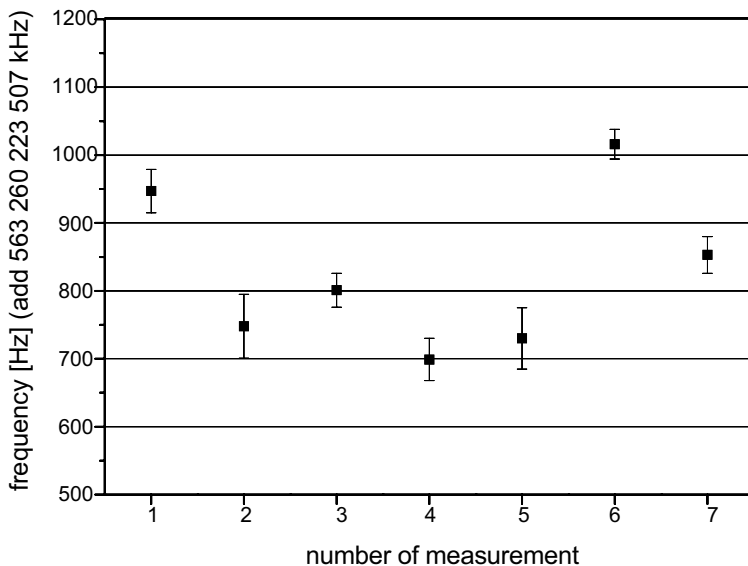


Figure 2.28: Results of 6 sessions measuring line 1110 component a_{10} . The statistical mean value is 563 260 223 507 828 (45) Hz. Approx. 800 sec of data have been collected per session.

The contributions to the estimated standard uncertainty of this frequency are 1.1 kHz from the spectrometer, 80 Hz from the He-Ne standard and 15 Hz from the rf reference

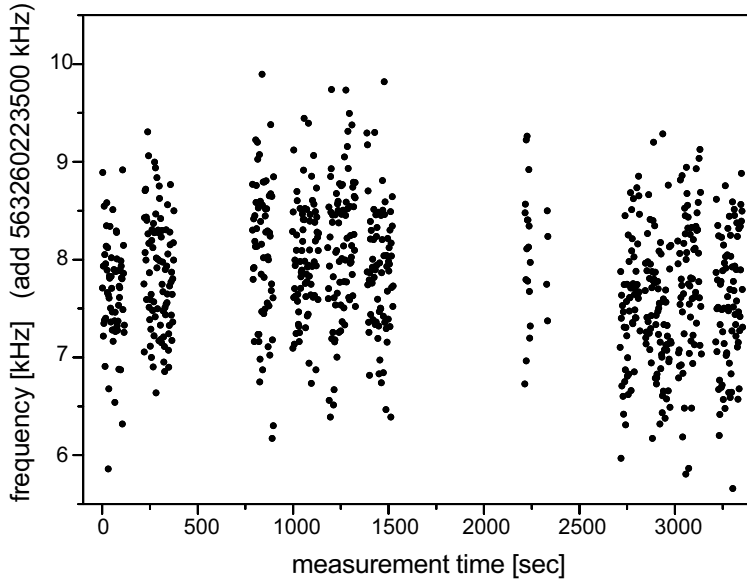


Figure 2.29: Details of the 3rd session. A total length of the session is 3355 sec, it yielded 924 data points at 1 sec gate time of which 160 cycle slips have been eliminated. This leaves us with 764 valid data points. The Allan variance at 1 sec is 1.1×10^{-12} . The mean value is 563 260 223 508 801 (25) Hz

source	correction [kHz]
power shift -340 Hz/mW	-0.6
iodine cell shift	-1.1
pressure shift -4.2 kHz/Pa	-8.2
total correction	- 9.9

controlling the mode spacing of the frequency comb. For a given cell, the frequency uncertainty is mainly determined by the limited reproducibility of the ILP standard. As the frequency uncertainty of the iodine cell is concerned the lower limit is given by the 1.1 kHz uncertainty of the frequency measurement itself. The upper limit is difficult to determine since it strongly depends on the impurities of the cell and these are difficult to assess. For a set of iodine cells the one with the smallest impurities will lead to the highest measured transition frequency of a given iodine line. Therefore, we extrapolate our results to PTB cell number 16/98. Nevertheless, we cannot exclude that higher frequencies of a given iodine line will be measured in the future. This would lead to a blue shifted value.

To be able to compare our result for the a_{10} component of the (R56)32-0 transition (line 1110) with previously published data [92], we extrapolate further to an iodine pressure at -20 °C ($p = 0.46$ Pa). In this case we obtain:

$$f_{a10}(1110, \text{ext}) = 563\,260\,223\,517.7 (1.1) \text{ kHz} \quad (2.30)$$

This value is shifted by about 46.7 kHz to higher frequencies from the value published in [92]. However, our result is in good agreement with a more recent measurement of this transition, where an absolute frequency of $f_{a10}(R56) = 563\,260\,223\,514(5)$ kHz was obtained [27]. The result (2.30) agrees also within error bars with the value stated for the recommended line [10].

In the same manner, using only the ILP laser, the absolute frequencies of the hyperfine component a_1 of the P(54)32-0 iodine absorption line (1105) has been measured. The result as measured with parameters stated above is:

$$f_{a1}(1105) = 563\,212\,634\,608.7(1.1) \text{ kHz} \quad (2.31)$$

Within one session the hyperfine components a_1 , a_{10} and a_{15} of the P(54)32-0 iodine absorption line were measured. 500 s of data have been collected per component.

Again, extrapolating to cell 16/98PTB and an iodine pressure at -20 °C ⁴ we obtain:

$$f_{a1}(P54) = 563\,212\,634\,618.6(1.1) \text{ kHz} \quad (2.32)$$

$$f_{a10}(P54) = 563\,213\,206\,155.3(1.1) \text{ kHz} \quad (2.33)$$

$$f_{a15}(P54) = 563\,213\,492\,579.2(1.1) \text{ kHz} \quad (2.34)$$

As the uncertainty introduced by the use of different iodine cells is concerned we refer to the discussion above.

These results were confirmed by an independent measurement using both iodine spectrometers, locked to the same HFS components of the P(54) line. While the ILP laser frequency was counted in the manner described above, the PTB laser frequency - shifted by an AOM - was determined by additionally counting the beat signal between the two oscillators. The pressure in the cells was kept equal, setting the temperature of the cold fingers of both cells to T = -5 °C. After extrapolating to cell number 16/98 and to an iodine pressure at -20 °C, the results for the PTB laser system agree with the results 2.32 - 2.34 but error bars were now increased due to the lower reproducibility of the PTB laser.

The absolute frequencies of the P(54)32-0 iodine line have been measured independently for the first time. We have found that the frequency separations between the three HFS components are in a good agreement with previously published data [92]. However, the frequency distance between the a_{10} component of the (R56)32-0 line and the a_1 , a_{10} and a_{15} components of the (P54)32-0 line is about 7 kHz higher than stated in [92].

In order to verify this result, we measured the frequency gap using a different technique: while one ILP laser was locked to the R(56)32-0: a_{10} transition another ILP Nd:YAG laser with slightly worse characteristics was first locked to the same transition to subtract frequency shifts due to the use of different iodine cells and then alternately locked to the a_1 , a_{10} and a_{15} component of the P(54)32-0 line. The beat frequency between the two lasers of about 47 GHz was detected by a fast photodetector (New Focus

⁴The pressure shift measured in the ILP laser system is -4.2 kHz/Pa.

model 1006) and measured by mixing the signal down with a Rb-clock synchronized high-frequency synthesizer and harmonic mixer. Within the uncertainty of the two measurements, the results of the absolute frequency measurement using the frequency chain were confirmed (see Fig. 6). According to this measurement, the frequency differences between the a_{10} HFS component of the (R56)32-0 line and the a_1 , a_{10} and a_{15} HFS component of the (P54)32-0 line are:

$$\Delta f_{a_{10}:(R56)-a_1:(P54)} = 47\,588\,898 (2) \text{ kHz} \quad (2.35)$$

$$\Delta f_{a_{10}:(R56)-a_{10}:(P54)} = 47\,017\,360 (2) \text{ kHz} \quad (2.36)$$

$$\Delta f_{a_{10}:(R56)-a_{15}:(P54)} = 46\,730\,937 (2) \text{ kHz} \quad (2.37)$$

Since systematic frequency shifts due to the use of different iodine cells can be neglected in this measurement, the total uncertainty is given by the combined uncertainty of the two ILP standards corresponding to about 2 kHz.

This result was further confirmed by an independent measurement at PTB using two Nd:YAG lasers from Innolight GmbH with dual wavelength output. In the experiment the two lasers were stabilized to the I_2 transitions R(56)32-0 and P(54)32-0 in the manner described above but the beat signal between them was now measured in the infrared. The 23.5 GHz signal was detected using an IR photo detector. Evaluating the data, it was found that both measurements agree to within 0.3 kHz.

These results validate the world of iodine stabilized lasers, very useful and widely used as laboratory wavelength standards. Accuracy in the kHz region (2×10^{-12}) is feasible and higher stability than radio frequencies can be achieved.

The team responsible for these measurements includes H. Schnatz and F. Riehle from PTB, P. V. Pokasov, M. N. Skvortsov and S. N. Bagayev from Novosibirsk, A. Y. Nevsky, J. von Zanthier and H. Walther from our institute as well as the frequency chain team.

The work presented here has been submitted to Optics Communications for publication [103].

Chapter 3

Absolute optical frequencies

3.1 Measurement principle

For the absolute measurement of optical frequencies one has to determine frequencies of several 100 THz in terms of the definition of the SI second represented by the cesium ground state hyperfine splitting of 9.2 GHz.

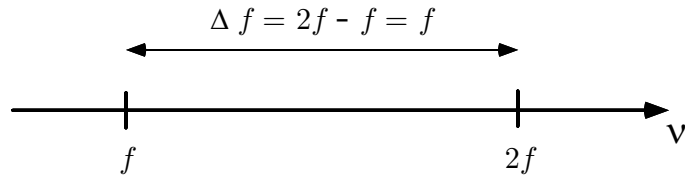


Figure 3.1: The new principle of absolute optical frequency measurements. The interval between Δf between f and $2f$ is just equal to the frequency f itself.

Extending our principle of determining frequency differences to the intervals between harmonics or subharmonics of an optical frequency leads naturally to the absolute measurement of optical frequencies. In the most simple case this is the interval between an optical frequency f and its second harmonic $2f$ as illustrated in Fig. 3.1. But of course other intervals can be used as well.

Such a frequency chain was first proposed by T. W. Hänsch in 1989 [104]. As no broad fs comb was available at that time, the idea was to successively divide the interval between f and $2f$ with optical frequency interval divider stages (introduced on page 6) in order to reduce the frequency gap until it could be measured with radio frequency techniques. To directly measure an optical frequency with divider stages only one would need 11 or 12 of these stages, each involving 2 nonlinear processes. This is not exactly an easy task but at least all the laser sources can be in the visible and near infrared where convenient laser diodes are available. The use of an optical frequency comb generator introduced earlier reduces the number of required stages to 5 or 6. With the broad fs combs this task is getting even easier, culminating in the single laser frequency chain –as discussed in this chapter– which actually is not really a “chain” any more but consists of one laser only.

3.2 Hydrogen $1S - 2S$ transition

3.2.1 Frequency chain from radio frequencies to vacuum UV

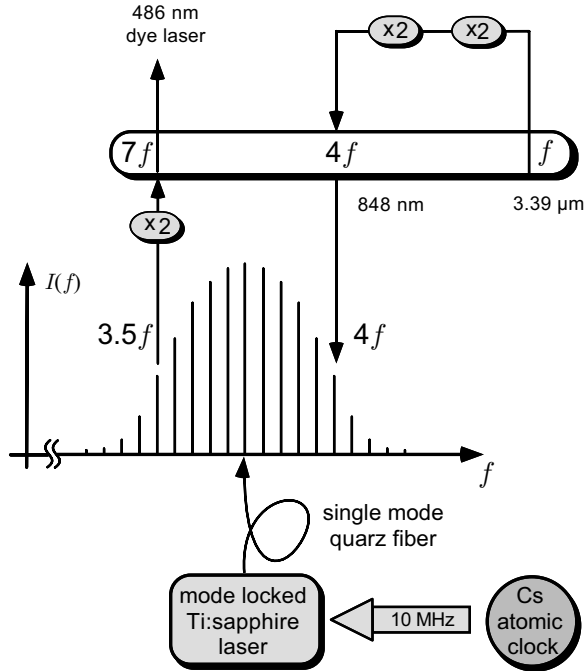


Figure 3.2: Frequency chain used for the frequency determination of the hydrogen $1S - 2S$ transition (simplified). The oval symbol represents an optical frequency interval divider as discussed earlier. It receives two input frequencies f and $7f$ and delivers the mean frequency $4f$.

We have used the first frequency chain following this principle in a determination of the hydrogen $1S - 2S$ transition. It measures the interval between $3.5f$ and $4f$ where f is the frequency of a HeNe laser at $3.39 \mu\text{m}$ (88 THz). Fig. 3.2 gives a simplified sketch: The He-Ne laser is operated at the 28th subharmonic of the hydrogen transition frequency which is driven by the forth harmonic of a dye laser at $7f$. The femtosecond laser, whose spectrum is broadened in a single mode optical fiber, measures the frequency difference between the output of the optical frequency interval divider at $4f$ and the subharmonic of the dye laser at $3.5f$. This frequency difference of $0.5f \approx 44.2 \text{ THz}$ equals one half of the absolute frequency of the He-Ne standard. Its frequency is therefore determined directly with the mode-locked laser by comparison with a local Cs clock that controls the mode spacing. Here the 10 MHz output from the Cs clock is multiplied in one step to 44.2 THz.

The actual setup shown in Fig. 3.3 looks a little bit more complicated. This is due to the fact that our $3.39 \mu\text{m}$ He-Ne laser could not be tuned far enough to reach the 28th subharmonic of the $1S - 2S$ transition. Instead we used an additional laser around $4f$

that was displaced by about 1 THz. The displacement was simultaneously measured with the frequency comb.

Note that this frequency chain can be explained as an extension to an already existing laser frequency chain that has been used for a previous 1997 measurement of the 1S-2S transition. At that time the $3.39\text{ }\mu\text{m}$ CH₄-stabilized He-Ne laser served as a transportable secondary frequency standard that had to be calibrated at the Physikalisch Technische Bundesanstalt (PTB) at Braunschweig, Germany [37, 6]. In the new chain, the He-Ne laser only acts as an optical flywheel. The reference standard is now a cesium atomic clock which controls the repetition rate of a commercial Kerr-lens mode-locked Ti:sapphire laser (Coherent, model Mira 900) and thus all the optical frequencies in the chain.

The dye laser for the hydrogen spectrometer operates at a frequency $7f - 2\Delta f$, where the offset $\Delta f \approx 1$ THz posed a major challenge in earlier experiments [6]. As before, we produce the fourth harmonic $4f$ of the He-Ne laser in two frequency doubling steps, using a phase-locked $1.70\text{ }\mu\text{m}$ NaCl:OH⁻ color center laser at $2f$ and a 848 nm diode laser at $4f$ as transfer oscillators (not shown in Fig. 3.3). An optical frequency interval divider between f and $7f - 2\Delta f$ generates the precise center frequency $4f - \Delta f$. The relatively small interval Δf between $4f$ and $4f - \Delta f$ can now be measured effortlessly with the much broader frequency comb of the mode-locked femtosecond laser.

To measure the absolute optical frequencies, we introduce a 973 nm diode laser whose second harmonic frequency (generated in a B-cut KNbO₃ crystal) is locked to the dye laser, so that it oscillates at the precise subharmonic $3.5f - \Delta f$. By bridging the interval of $0.5f$ between $4f - \Delta f$ and $3.5f - \Delta f$ with the frequency comb of the femtosecond laser, we are, in effect, measuring the frequency f of the He-Ne-laser directly in terms of the atomic clock frequency. Since the Mira laser has a rather moderate pulse length of 73 fs, we send its output through a 40 cm long single mode fiber which broadens the spectrum by self-phase-modulation so that it bridges the interval of 45.2 THz (see section 2.2.3).

The link between the 45.2 THz interval and the 10 MHz output frequency of the cesium clock is established in a single step by stabilizing the 200th harmonic of the pulse repetition rate to a 15.2 GHz signal provided by either by microwave synthesizer (Hewlett Packard, model 83623A) referenced to the cesium clock or to reduce phase noise by specially designed direct radio frequency link to the 9.2 GHz signal provided by the fountain clock. In addition to the mode spacing, we “fix” the entire comb by stabilizing the beat signal between the dye laser and the second harmonic of the 973 nm laser diode, which is phase-locked to a particular mode at $3.5f - \Delta f$. The simultaneous control of the mode spacing and the absolute position of our comparatively narrow frequency comb already enables us to measure any optical frequency between 848 nm and 973 nm.

For the phase-locked loops we employ digital phase detectors (see appendix A for details). Our well-tested cycle slip detection scheme introduced in section 2.3.2 prevents cycleslips from entering our data.

As shown in Fig.3.3 we measure the beat frequencies f_{c1} and f_{c2} at $4f$ and $4f - \Delta f$ with the modes of the comb. To ensure that the beat notes are counted correctly,

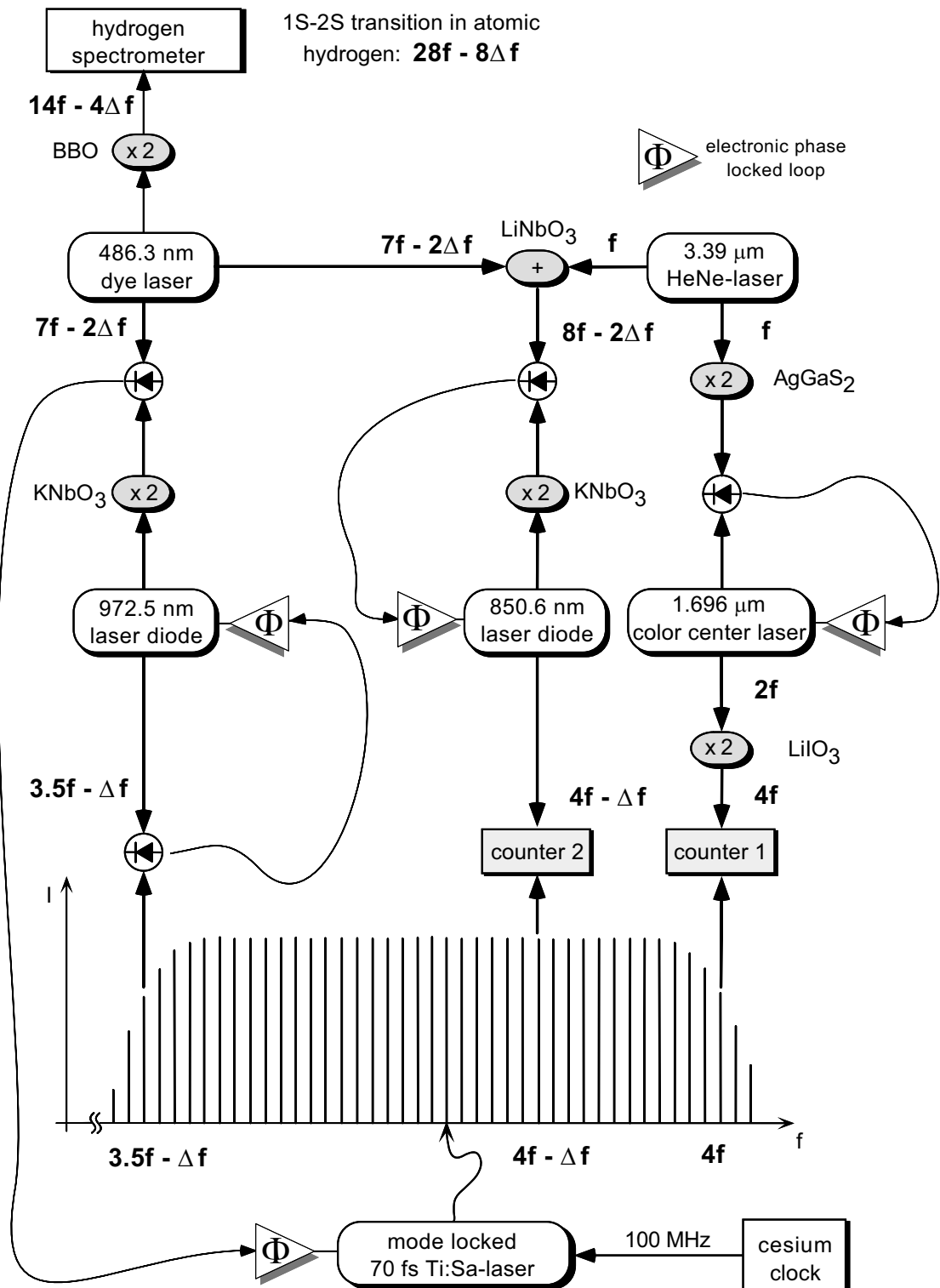


Figure 3.3: Detailed view of the first vacuum UV to rf frequency chain.

we use additional laser diodes (not shown in Fig. 3.3) phase-locked to these modes to provide enough power for a strong beat signal (signal to noise ratio ≥ 40 dB in 400 kHz detection bandwidth). In the phase-locked condition, the chain relates the frequency of the hydrogen 1S-2S transition ($28f - 8\Delta f$) to the measured radio frequencies f_{c1} and f_{c2} through

$$\begin{aligned} f_{1S-2S} &= -8f_{c1} - 64f_{c2} + (-8N_1 + 64N_2)f_r + f_{LO} \\ &= -8f_{c1} - 64f_{c2} + 2466.063\ 84 \text{ THz} \end{aligned} \quad (3.1)$$

where $N_1 = 595\ 351$ and $N_2 = 581\ 421$ are the number of modes between the 973 nm laser diode and the modes that produce the measured beat notes, $f_r = 76$ MHz is the pulse repetition rate and $f_{LO} = 5.504$ GHz contains all contributions from the local oscillator frequencies used for phase-locking.

This frequency chain has also been described in the preceding PhD thesis of J. Reichert [38] and published in Ref. [11].

3.2.2 The fountain clock reference

A prerequisite for precise optical frequency measurement is a stable and accurate reference. Since 1967 the SI second is defined as the time it takes for 9 192 631 770 oscillations of the microwave field connecting the two ground state hyperfine levels $F = 3$ and $F = 4$ of the cesium ^{133}Cs atom and every precise frequency measurement has to be traced back to this definition. The realization of this definition is accomplished by so called cesium atomic clocks.

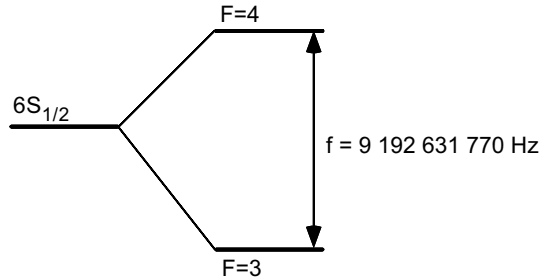


Figure 3.4: Hyperfine structure of the ^{133}Cs ground state. The hyperfine splitting defines the SI second.

Most modern atomic radio frequency standards utilize Ramsey–spectroscopy to resolve the clock transition [105]. Ramsey’s scheme uses two separated interaction regions. In the first interaction region the atoms are prepared in a superposition of ground and excited state. Between the interaction zones the atoms are oscillating with their intrinsic frequencies and in the second interaction zone they are either excited to the upper state or they are stimulated back to the ground state depending on the relative phase between the atomic dipole moment and the exciting microwave field. As a function

of the frequency of the driving field one observes a interference pattern, the so called Ramsey fringes. The resolution of this method depends only on the distance between the two zones and the velocity of the atoms, the width of the Ramsey fringes are given by $1/2T$ where T is the flight time between the interaction zones. Traditionally, cesium clocks have used a thermal beam of cesium atoms to perform Ramsey spectroscopy. The latest generation of cesium clocks uses slow laser-cooled atoms to enhance the flight times between the interaction zones and increase the accuracy dramatically.

In collaboration with the cesium fountain clock group at LPTF in Paris, France (P. Lemonde, G. Santarelli, M. Abgrall, P. Laurent, C. Salomon, and A. Clairon) we have used one of the currently most precise cesium frequency standard in the radio-frequency domain [106, 107] as a reference. For this purpose the (transportable!) fountain clock has been brought to Garching for 2 1/2 weeks in July 1999.

The fountain clock consists basically of three parts, the cold atom source, the interaction region and the detection region as shown in Fig. 3.5. Six red detuned laser beams are cooling and capturing the atoms in an optical molasses. The atoms are prepared in the $6S_{1/2}(F = 3, m_F = 0)$ state. Then the atoms are launched with a velocity of about 4 m/s in vertical direction on a ballistic trajectory. On their way up they are slowed down and eventually accelerated back down by gravity forming an atomic fountain. The atoms cross the same interaction region twice, on their way up and back down again. Finally the state population is analyzed in the detection region.

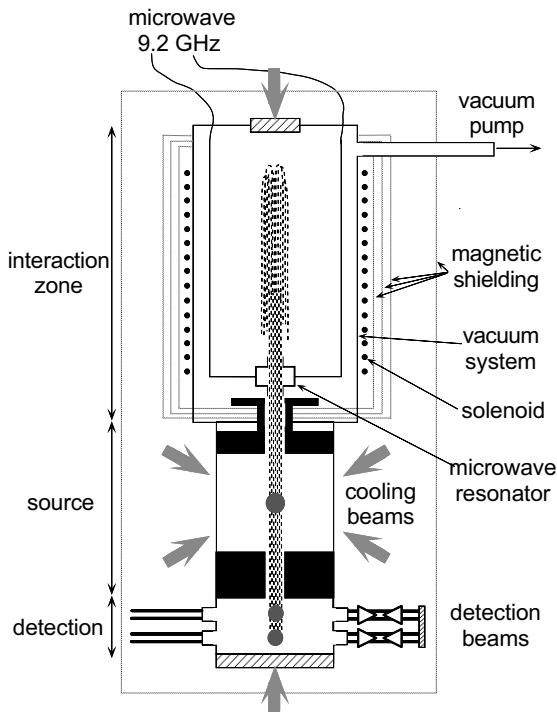


Figure 3.5: Setup of the cesium fountain clock. Cold atoms interact on their ballistic flight in a Ramsey scheme two times with a microwave field.

With this technique a quartz oscillator is frequency locked to the cesium resonance. The relative frequency stability of the device is $1.8 \times 10^{-13} (\text{Hz} \tau)^{-1/2}$, where τ is the averaging time, limited by the quartz oscillator phase noise. It has been measured by comparison with a hydrogen maser and corresponds to a relative stability per day of 6×10^{-16} . A preliminary accuracy evaluation of the fountain has been performed. The total uncertainty on the three major frequency shifts, namely the Zeeman effect, the shift due to blackbody radiation, and the shift due to collisions between cold atoms, is below 10^{-15} . To set an upper limit on other possible frequency shifts, the fountain has been compared to the other BNM-LPTF cesium fountain, FO1, before and after transportation to Garching. Both clocks are found to agree within the 10^{-15} statistical uncertainty of the comparison. A quoted uncertainty of 2×10^{-15} for the absolute frequency of the fountain is then a conservative value.

3.2.3 Hydrogen spectroscopy

The hydrogen 1S-2S transition is excited by Doppler-free two-photon spectroscopy with a standing laser wave near 243 nm in a cold atomic beam. The hydrogen spectrometer is operated by the hydrogen team in our group (M. Niering, M. Fischer, M. Weitz) and has been described in detail in the PhD thesis of M. Niering [108] and preceding works [109] and in Ref. [110]. It is situated in the laboratory next door to the frequency chain. The two laboratories are connected through an optical fiber that delivers 30 mW of the 486 nm dye laser light to the frequency chain.

The experimental setup is sketched in Fig. 3.6. The frequency of a dye laser at 486 nm is locked to an external high-finesse reference cavity. The light of this ultrastable laser

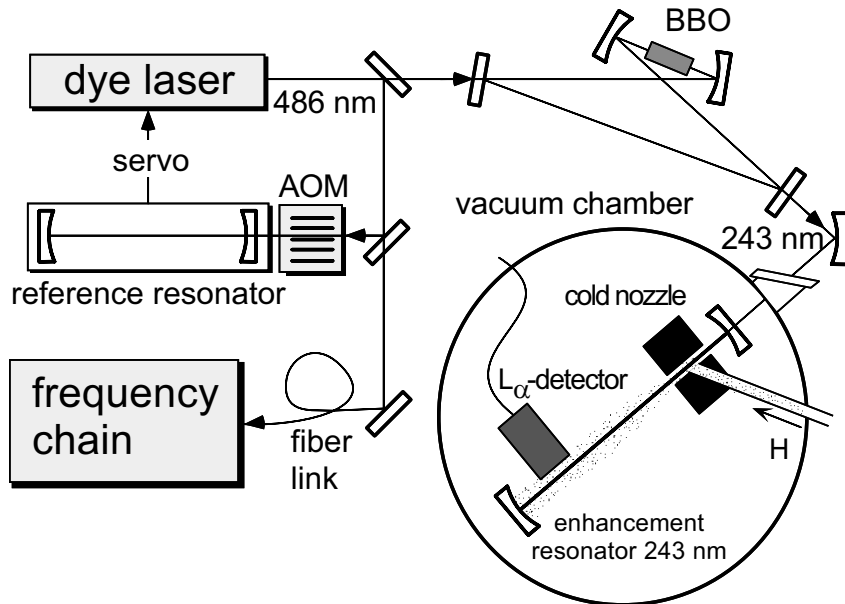


Figure 3.6: The hydrogen spectrometer.

is frequency doubled, and the resulting UV radiation at 243 nm is coupled into a linear enhancement cavity inside a vacuum chamber for excitation of the two-photon Doppler-free $1S$ - $2S$ transition. Hydrogen atoms escape from a nozzle cooled to 5-6 K by a liquid-helium flow-through cryostat and form an atomic beam. In the interaction region, shielded from stray electric fields by a Faraday cage, the atoms are excited from the $1S_{1/2}(F = 1, m_F = \pm 1)$ ground state to the excited $2S_{1/2}(F = 1, m_F = \pm 1)$ metastable state. After a distance $d \approx 13$ cm the atoms enter the detection region. A small electric field mixes the $2S$ and $2P$ states, forcing the excited atoms to decay and emit Lyman- α photons, which can be detected by a photomultiplier. Spurious background counts caused by the excitation light field are efficiently suppressed by periodically blocking the UV-light with a mechanical chopper (165 to 465 Hz) and reading out the photomultiplier only in dark times. In addition to cooling the nozzle, this technique further reduces the main systematic effects, which depend on the velocity of the atoms: the second-order Doppler-effect and the time-of-flight broadening. By enabling signal detection only after a certain delay time τ after blocking the UV-light, we select the signal of slow atoms from the thermal beam. With the help of a multi-channel photon-counter we detect photons time resolved and record them in a two-dimensional matrix as a function of laser detuning and discrete delay times τ . Fig. 3.7 shows a typical time resolved hydrogen $1S$ - $2S$ two-photon spectrum, as measured by comparison with the cesium atomic clock. We needed about 1 s to record one data point. Within ten days of measurement time we recorded about 600 such spectra, corresponding to some 2000 data points per day.

At this high level of accuracy, a detailed understanding of the hydrogen $1S$ - $2S$ two-

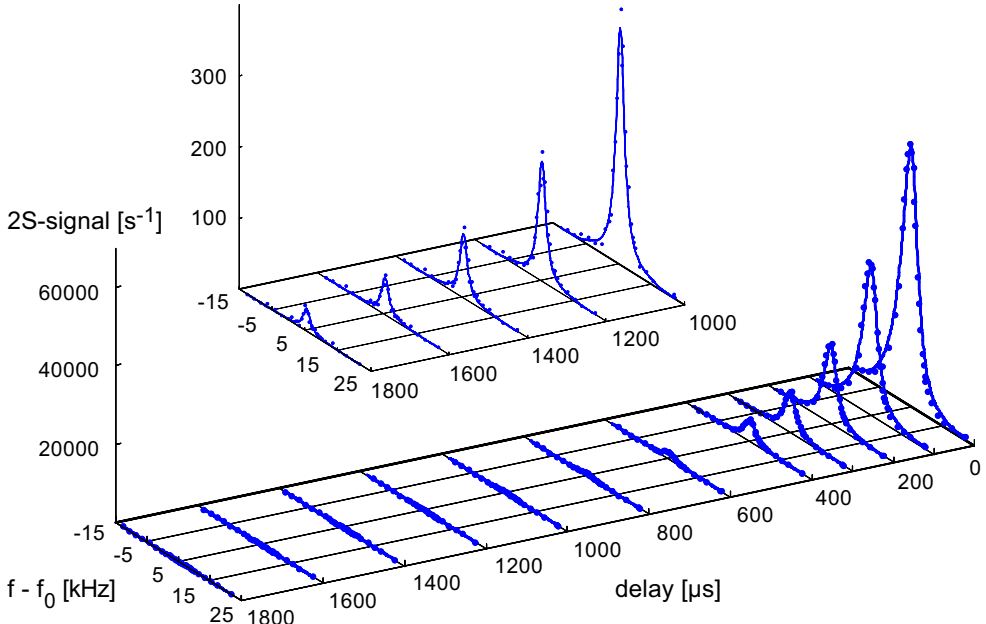


Figure 3.7: Time resolved $1S$ - $2S$ two photon spectrum. The recorded $2S$ count rate is plotted versus delay time and absolute frequency where $f_0 = 2\ 466\ 061\ 102\ 470$ kHz.

photon line-shapes and several systematic effects, notably the second-order Doppler-effect and the ac-Stark shift becomes necessary. The frequency stability of our chain is sufficient to resolve and explore the ac-Stark shift of this weak UV two-photon transition. With the laser intensities used, this shift amounts to 1 kHz at the most and is thus two or three orders of magnitude below that observed in hydrogenic $2S-nS$ and $2S-nD$ two-photon transitions [7, 120]. For an accurate determination of the hydrogen $1S-2S$ transition frequency, we apply a theoretical model for the line-shape taking into account both the excitation geometry and systematic effects [110]. We anticipate that the use of colder hydrogen atoms would allow a considerable further increase in resolution and accuracy.

To calculate the theoretical $1S-2S$ line-shape and fit the experimental data we have numerically integrated the Bloch equations for an atom starting at the nozzle in the $1S$ ground state, and travelling on a classical trajectory through the Gaussian 243 nm standing wave to the detector. In addition, we have integrated over all possible trajectories and the atomic velocity distribution $f(v)$. The line-shape model correctly predicts a dependence of the line center frequency on the delay time, as caused by the velocity dependence of the second-order Doppler-effect.

The time-resolved spectra, i.e., a whole set of experimental spectra with different delay times, is simultaneously fitted with the Levenberg-Marquart algorithm [121], which is performed with spline interpolated amplitude values from the line-shape model. The solid lines in Fig. 3.7 show the result of the described fitting procedure for a typical time-resolved $1S-2S$ spectrum. The described procedure is designed to correct for the second-order Doppler-shift.

This line shape model was part of the thesis work of A. Huber [109] and has been further refined in the thesis work of M. Niering [108]. Details are also published in [110].

3.2.4 Frequency measurements

A high-finesse reference-cavity is used as a fly-wheel in the optical region. During data analysis, we measure the frequency of the light standing in the cavity and eliminate the drift of the cavity, typically 100 Hz/s at 121 nm, by fitting the drift versus time with a third-order polynomial (Fig. 3.8). The absolute frequency of the dye laser is then calculated from the recorded time tags by adding the frequency difference between the dye laser and the cavity as selected by the acousto optical modulator. The best fit for the drift is obtained by including not only the time interval for a single recorded spectrum, but additional fifty data points before and after each spectrum as shown in Fig. 3.9. This procedure is repeated for each spectrum. The Allan variance of data points as seen in Fig. 3.8 and Fig. 3.9 is 2.3×10^{-13} . This reflects closely the measured Allan variance of the fountain clock of 2×10^{-13} for 1 sec. gate time. The frequency chain does therefore not contribute to the instability at the 10^{-13} level. Besides the second-order Doppler-shift, the ac-Stark shift introduces a significant systematic correction to our experimental $1S-2S$ two-photon spectra. Our theoretical

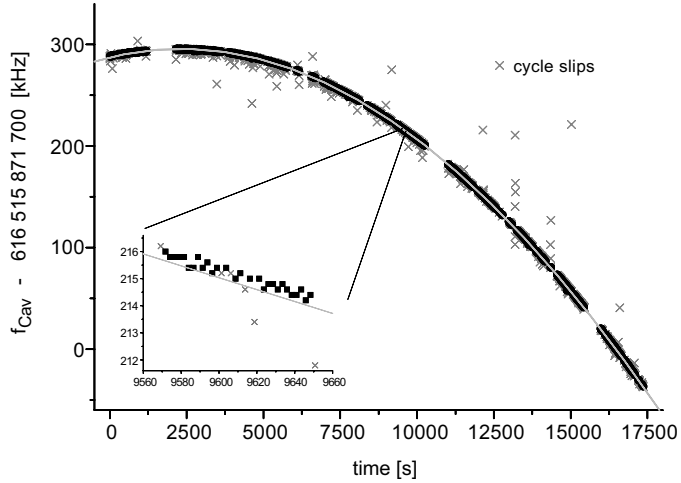


Figure 3.8: Drift of the high finesse resonator. Shown is the frequency of the light inside the cavity at 486 nm (616 THz) vs. time. The fit with a third order polynomial is not sufficient as shown in the inset.

line-shape model predicts a light shift of 2.45(5) Hz/mW for the chosen excitation geometry when averaging over all possible atomic trajectories. As the shift of the line center is linearly dependent on the excitation light intensity, we can correct for this shift by recording spectra at different light intensities and extrapolating to zero intensity. On a typical measurement day we have recorded 40-90 spectra for different powers of the excitation light field. In Fig. 3.10 the measured transition frequencies for a typical day of measurement, as derived from the fits with the theoretical line-shape model, are plotted versus the light power. The graph shows the linear extrapolation to zero intensity, which allows the correction for the ac-Stark shift. With this procedure we

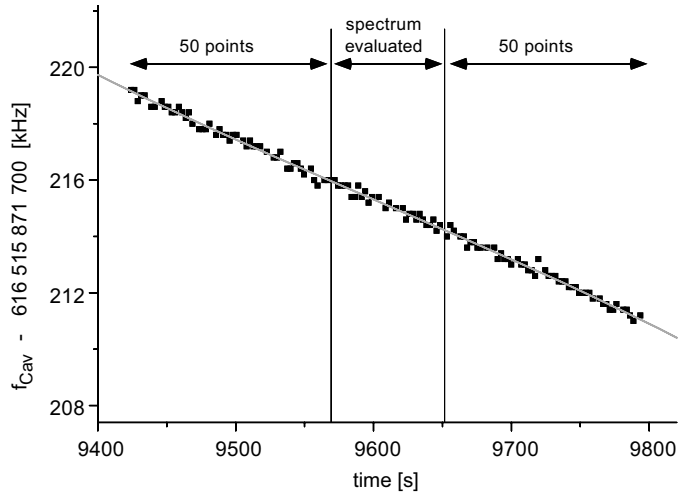


Figure 3.9: Resonator drift for a single spectrum. The solid line is a third order polynomial fit to the data.

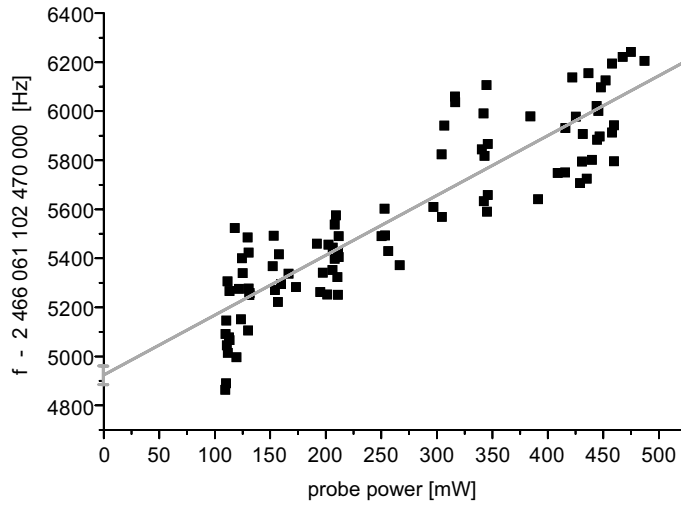


Figure 3.10: All spectra recorded on a typical measurement day at different power levels. The absolute frequency as derived from the line shape model is plotted vs. the excitation light field power.

derive ten values for the $1S-2S$ transition frequency and calculate the weighted mean value, as shown in Fig. 3.11. We find a frequency of $f_{1S-2S}^{hf} = 2\ 466\ 061\ 102\ 474\ 870$ Hz, with a statistical uncertainty of 36 Hz. We estimated the systematic uncertainty given by the line-shape to be 20 Hz [110], which is mainly determined by the uncertainty to which we can correct for second-order Doppler-shift and ac-Stark shift. The slope derived from the linear fit and the measured light power is given by 2.64(45) Hz/mW and is in good agreement with the theoretical value. Line-shifts due to blackbody radiation remain below 1 Hz [122]. Residual electric fields lead to a dc-Stark shift of the $1S-2S$ transition frequency of $\Delta\nu_{dc-Stark} = 3600 E^2$ Hz(V/cm) $^{-2}$ [123]. We estimate stray electric fields to be below 30 mV/cm, corresponding to a dc-Stark effect

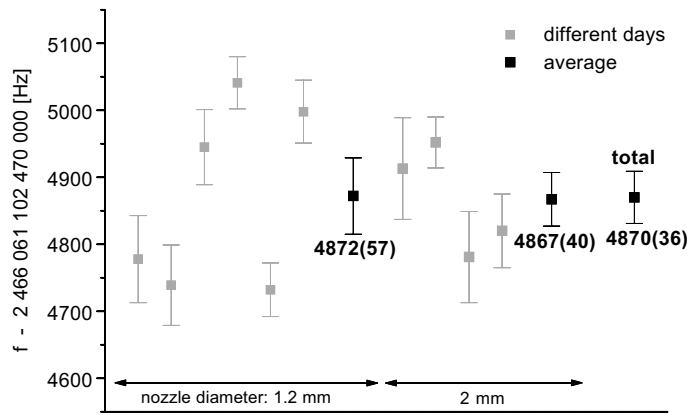


Figure 3.11: Complete set of data. The results of extrapolation to zero light intensity for ten different days are shown.

of less than 5 Hz. The pressure shift of the atomic hydrogen $1S$ - $2S$ line from molecular hydrogen has been previously measured in a gas cell to be $\Delta\nu_P = 8.4$ MHz/mbar [124]. In our apparatus, the background pressure of 10^{-6} mbar is mainly due to molecular hydrogen, leading to a pressure shift of about 10 Hz. However, the density in the relatively short nozzle region is certainly higher, which could lead to an additional collisional shift of the line center. We have recorded data sets for two different nozzle diameters to vary the pressure inside the nozzle. Fig. 3 shows, that no statistically significant difference in the results for the line center is observed at the present level of accuracy. Residual recoil shifts due to the finite size of the excitation field optical mode ($460\ \mu\text{m}$ diameter) can be estimated to be less than 10 Hz [110].

The frequency f_{1S-2S} of the hyperfine centroid is obtained by adding the well known hyperfine splitting of the $1S$ and $2S$ levels $f_{hf} = 310\ 712\ 223$ (13) Hz to the measured transition frequency f_{1S-2S}^{hf} [125]. Taking the pressure shift into account the obtained result is

$$f_{1S-2S} = 2\ 466\ 061\ 413\ 187\ 103\ (46)\ \text{Hz},$$

where the quoted uncertainty was obtained by quadratically adding the uncertainties of the frequencies f_{1S-2S}^{hf} and f_{hf} , the systematic uncertainty in the line-shape, and 100 % uncertainty for the pressure shift, the dc-Stark effect, the blackbody shift, and residual recoil shifts. This result represents the most precisely measured optical frequency in the ultraviolet and visible optical region. Further improvements should be possible by reducing the vacuum background pressure and the stability of the dye laser. Ultimately, a source of colder hydrogen atoms, e.g. in an atomic fountain could allow frequency measurements of the $1S$ - $2S$ transition with an accuracy exceeding 10^{-16} [126, 127].

Note that our new chain is providing the first phase coherent link from the vacuum UV (121 nm) to the radio frequency domain. The results presented here have been published in Physical Review Letters [12].

In Fig. 3.12 the more recent values of the $1S$ - $2S$ transition frequency measured in Garching are visualized. Note that the 1997 value was obtained with the help of the

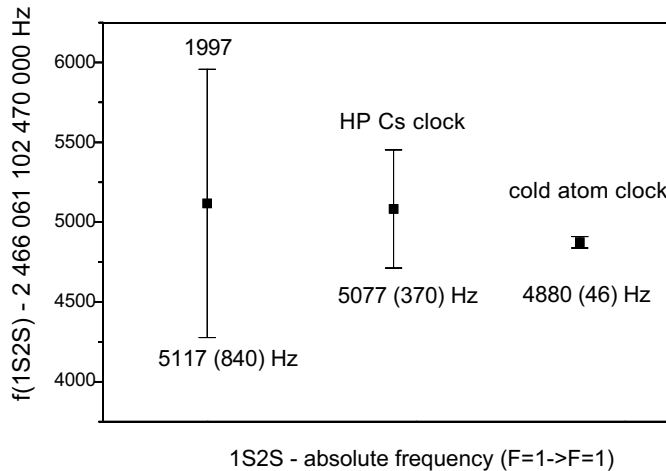


Figure 3.12: Recent measurements of the Hydrogen $1S$ $2S$ transition

harmonic frequency chain at PTB in Braunschweig by shuttling the methane stabilized He-Ne laser back and forth between Braunschweig and Garching. The second value was obtained in a test run (before inviting the cold atom clock crew from Paris) with our fs frequency chain and a commercial HP 5071A cesium clock as reference as presented in the thesis work of J. Reichert [38]. With exactly the same procedure to evaluate the data (fitting Lorentzians to the data obtained with slow atoms) we have been able to reproduce this value with our fs frequency chain and even reduce the error bar by a factor of 3.

This result has been the first indirect comparison between two independent frequency chains on the level of 3×10^{-13} . A comparison of a tradition harmonic chain and a fs chain by shuttling back and forth a iodine stabilized HeNe laser at 633 nm on the order of 2×10^{-12} has recently been reported by the group of J. Hall in Boulder [90]. A more rigorous proof from the direct comparison of two independent frequency chains is to follow in chapter 3.4.3.

3.2.5 Hydrogen and fundamental constants

Hydrogen is the most simple of all atoms and its properties have been calculated very precisely. For many years now high resolution spectroscopy has been performed on hydrogen to test QED and improve the precision of the Rydberg constant R_∞ . The Rydberg constant scales all the energy levels and can be determined from optical frequency measurements on atomic hydrogen with great precision. For highest precision the energy levels within atomic hydrogen are conventionally described as a sum of three contributions: The hyperfine interaction, which is very well known for the states discussed here and the Dirac energy $R_\infty e(nl)$ [111] which include all recoil corrections¹ up to the order $(Z\alpha)^4$. All that is left, e.g. QED contributions, remaining recoils contributions, nuclear size effects etc., is by definition [112] called the Lamb shift L_{nl} . The Lamb shift scales roughly as n^{-3} and is much smaller for P and D states than for S states. We write the frequencies of the most precisely known optical transitions [12, 113, 7], with the hyperfine structure removed, as follows:

$$\begin{aligned} f_{1S-2S} &= R_\infty (e(2S) - e(1S)) + L_{2S} - L_{1S} \\ f_{2S-8D} &= R_\infty (e(8D) - e(2S)) + L_{8D} - L_{2S} \\ f_{2S-12D} &= R_\infty (e(12D) - e(2S)) + L_{12D} - L_{1S} \end{aligned} \quad (3.2)$$

In these equations the left hand sides are determined experimentally to extract some values of the quantities on the right. The measurement of the $1S - 2S$ frequency is more than two orders of magnitude more precise than the other two [12]. Therefore the f_{2S-nD} measurements currently limit the precision of R_∞ . Now we have three equations and three unknowns, R_∞ , L_{1S} and L_{2S} , if we choose to use theoretical values for L_{8D} and L_{12D} . This is justified as they are comparatively small so that a very crude

¹Unlike the Schrödinger theory the Dirac theory does not allow to account for a finite mass nucleus simply by replacing m_e by the reduced mass. Instead an expansion in $Z\alpha$ is used.

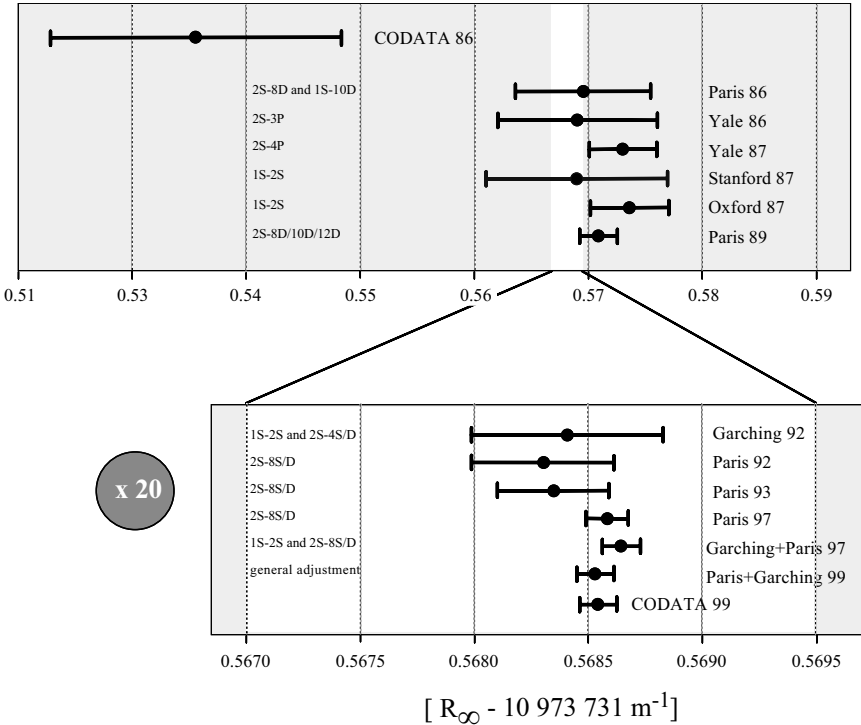


Figure 3.13: A history of measurements of the Rydberg constant

calculation is enough to avoid any influence on the result. On the other hand precise radio frequency determinations of the $2S_{1/2}-2P_{1/2}$ and $2S_{1/2}-2P_{3/2}$ splitting [114, 115] allow the determination of R_∞ and L_{2S} from the f_{2S-nD} measurements and R_∞ and L_{1S} from the $1S - 2S$ frequency if combined with one of the f_{2S-nD} measurements. Another possibility to replace L_{2S} is to use the $1/n^3$ scaling law of the Lamb shift which allows an accurate theoretical calculation of the small linear combination $L_{1S} - n^3 L_{nS}$ [116]. The differences $7f_{2S-8D} - f_{1S-2S}$ and $7f_{2S-12D} - f_{1S-2S}$ will yield the combination $L_{1S} - 2^3 L_{2S}$. To obtain even more precise results radio frequency beat measurements like $f_{2S-4S} - 1/4 f_{1S-2S}$ [120, 117, 118], which should be zero according to the Schrödinger theory, can be used as well as measurements in deuterium.

Most of the combinations to derive the interesting quantities, R_∞ , which is needed to fix the values of other constants (e.g. the fine structure constant), and L_{1S} , which allows one of the best tests of QED, yield a comparable accuracy. Therefore a general adjustment gives the best answers to date [7, 67]. In Fig. 3.13 a history of measurements is visualized. Note the substantially improved accuracy and the quite significant shift from the 1986 CODATA value. The 1999 CODATA value [67] $R_\infty = 10\ 973\ 731\ 568\ 549(83) \text{ m}^{-1}$ (7.6×10^{-12}) follows closely the 3 most recent measurements from the $1S - 2S$, $2S - 8D$ and $2S - 12D$ transitions made at Garching and Paris [12, 113, 7]. At this point improvements of the transition frequencies to higher excited states improve the accuracy of the Rydberg constant. To allow improved comparisons of the experimentally determined $1S$ Lamb shift with QED calculations a better value for proton charge radius, that enters the theory, is desperately needed [119].

3.3 Spectral broadening in photonic crystal fibers

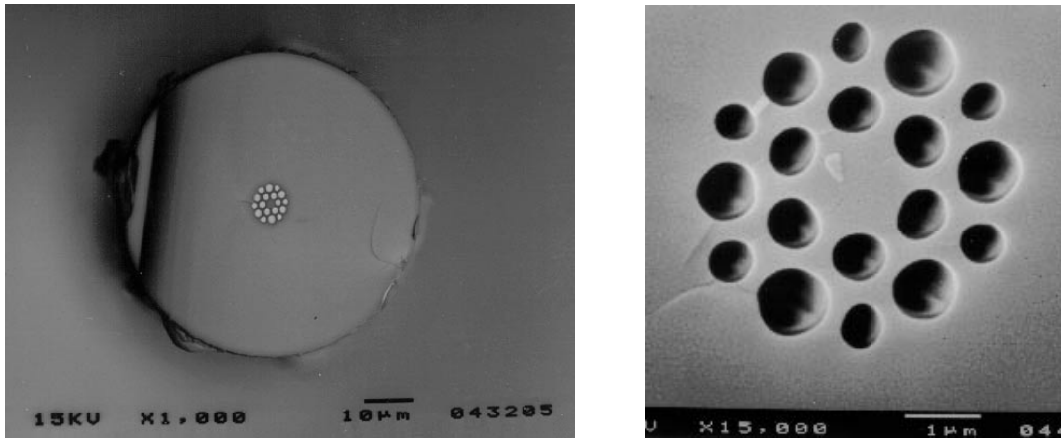


Figure 3.14: An electron micrograph of a photonic crystal fiber (PCF) used for spectral broadening (left) and close up of the core area (right). (“fiber 1” throughout this text.) Courtesy of J. Knight.

The first absolute measurement of an optical frequency with a fs frequency comb has inspired further rapid advances in the art of frequency metrology. This development was boosted by the sudden appearance of so called photonic crystal fibers. Although these fibers have been invented by P. Russell and collaborators in 1996 [22] it was not until the conference on lasers and electro optics (CLEO) 1999 that a group from Bell Labs reported to the surprised community the massive spectral broadening of relatively low power fs pulses in a photonic crystal fiber [128, 23].

It has been long known that a white light continuum is produced when amplified femtosecond pulses are focused into a $\chi^{(3)}$ medium. M Bellini and T. W. Hänsch have shown in 1997 that such white light continua can in fact be phase coherent [28]. However, pulses intense enough to observe this effect could only be produced in amplifying systems at a kHz repetition frequency – too dense a frequency grid to be used in frequency space.

From this point of view and after our initial efforts of spectral broadening in standard fibers it seemed obvious that such a fiber would deliver an octave spanning frequency comb. Soon afterwards the race to get a piece of this magic fiber begun. J. Hall’s group in Boulder won this race by a few weeks and received their first piece of fiber from Bell Labs in October 1999.

Being turned down by Bell Labs we teamed up with P. Russell, J. Knight and W. Wadsworth from the University of Bath (UK) and received our first photonic crystal fiber sample in November 1999.

The photonic crystal fiber (PCF) used for spectral broadening is a strongly-guiding fiber waveguide. An array of air holes running the length of a silica fiber confines the light to a pure silica region embedded within the array [22]. The large refractive

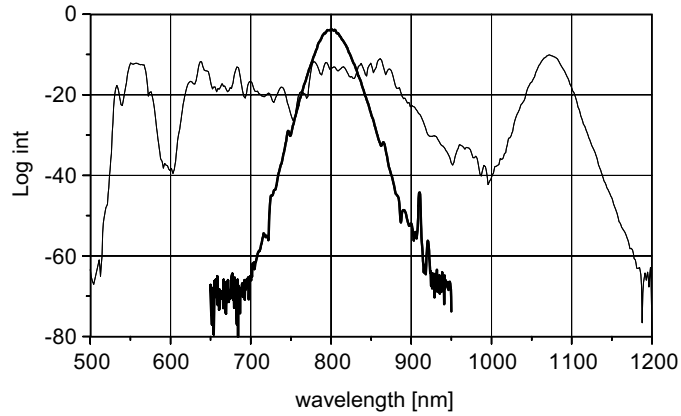


Figure 3.15: Spectral broadening of fs pulses in a photonic crystal fiber. The narrow peaked curve in the middle (bold) denotes the initial pulse directly from the fs laser (25 fs, 170 mW average power, 625 MHz repetition rate). The broadened spectrum stretches from 520 nm to 1100 nm (-10 dB width).

index contrast between the pure silica core and the “holey” cladding, and the resultant strong nature of the optical confinement, allows the design of fibers with very different characteristics to those of conventional fibers. In the fibers used here, a very small core size of $1 - 2\mu\text{m}$ leads to increased nonlinear interaction of the guided light with the silica. At the same time the very strong waveguide dispersion substantially compensates the material dispersion of the silica at wavelengths below 1 micron [129]. This gives an overall GVD which is zero around 700 nm as illustrated in Fig. 3.16. The magnitude of the GVD is also smaller than that in conventional fibers throughout the visible and near-infrared range, and is anomalous over much of this range. As a result, short optical pulses travel further in these fibers before being dispersed which further increases the nonlinear interaction. Consequently, very broad spectra can be generated in photonic

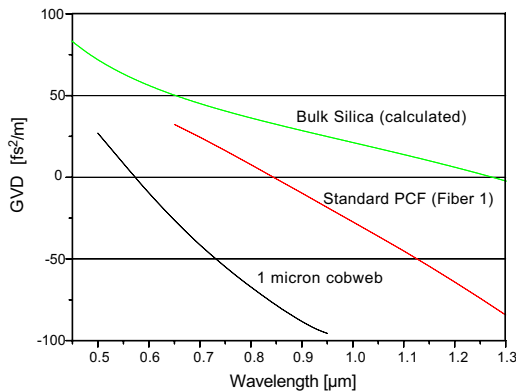


Figure 3.16: Group velocity dispersion (GVD) curves for bulk silica (theoretical), a typical PCF (Fiber 1, measured) and the 1 micron cobweb fiber (measured). Data courtesy of J. Knight.

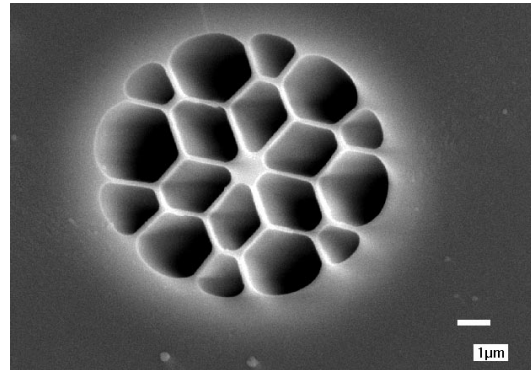


Figure 3.17: Core area of the 1 micron cobweb fiber.

crystal fibers at relatively low peak powers [23, 130]. Note that it is not a bandgap effect that is guiding the light here but rather the large mean refractive index contrast derived from the filling ratio of silica and air in the cladding surrounding the solid core. The parameters that can be varied to obtain a fiber with the desired properties are the core size and this filling ratio. The filling ratio in turn can be derived from the “pitch” and the size of the air holes. Another interesting variation of PCF’s is shown in Fig. 3.17, the cobweb fiber. In this fiber, light is confined to a small solid strand of silica in air by thin (100 – 150 nm width) threads of silica. This is getting remarkably close to a free strand of silica in air. Another technique for obtaining a strand of silica in air is tapering a standard single mode fiber. In this method, a fiber is heated and stretched in a flame until it forms a long narrow taper waist a few micron in diameter, joined to pigtails of untapered fiber by slow transition regions. Within the taper waist the original fiber core has been reduced to such a small diameter that it has no effect on the guidance of light, and light is guided at the cladding/air boundary. If the transition region are made shallow enough then there can be an adiabatic transformation of the fundamental mode of the untapered input fiber pigtail to the fundamental mode of the taper waist and back. Such tapers can be used for spectral broadening in just the same way as PCFs, as has recently been demonstrated by the Bath group [131].

For most of our frequency comb experiments reported here we have used the high repetition rate fs laser outlined in section 2.3.1 and schematically shown in Fig. 2.11. Depending on the pump parameters, the position of the quartz wedge and the alignment of the cavity the pulses from the laser showed slightly different pulse width and central wavelength. This resulted in slightly different broadened spectra and in a variation of the power needed to reach an octave spanning comb. The octave was reached at power levels ranging from 150 to 170 mW using our regular PCF. With approx. 600 mW average power from the Ti:Saph ring laser between 1/4 and 1/3 of the power have to be coupled into the fiber. This was achieved by selecting an aspheric lens from two lens sets (Thorlabs and New Focus). Our most widely used aspheric lenses are a $f = 4.5$ mm and $f = 3.1$ mm lenses from Thorlabs.

Besides the laser parameters other parameters influence the created spectrum. Most prominently this is the power coupled through the fiber. Fig. 3.19 illustrates how the

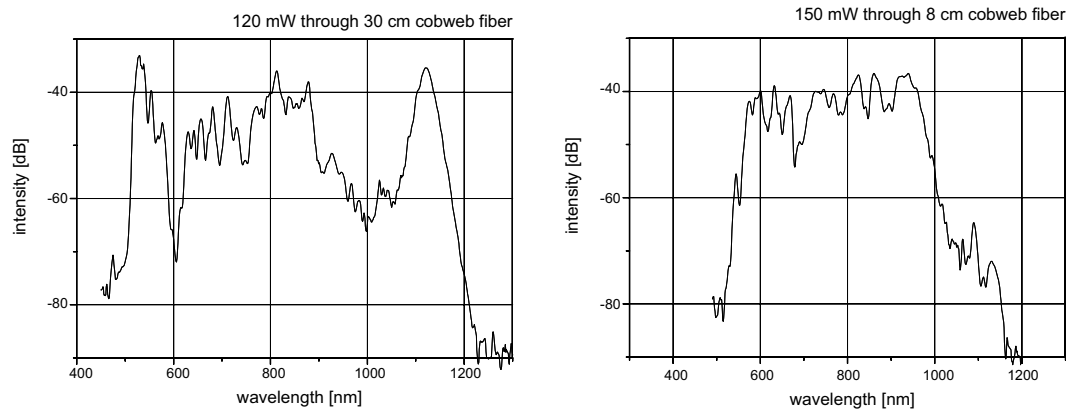


Figure 3.18: Broadening at different fiber length in the one micron cobweb fiber.

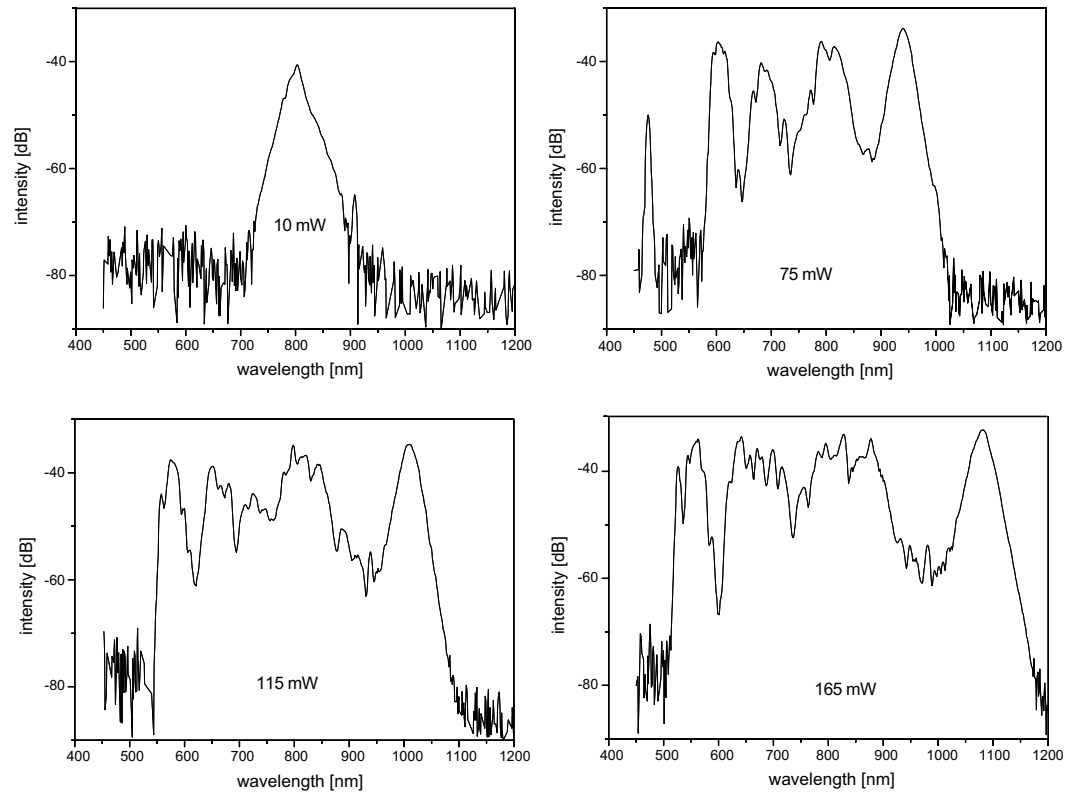


Figure 3.19: Broadening in the standard PCF (fiber 1) at different average power levels coupled through the fiber.

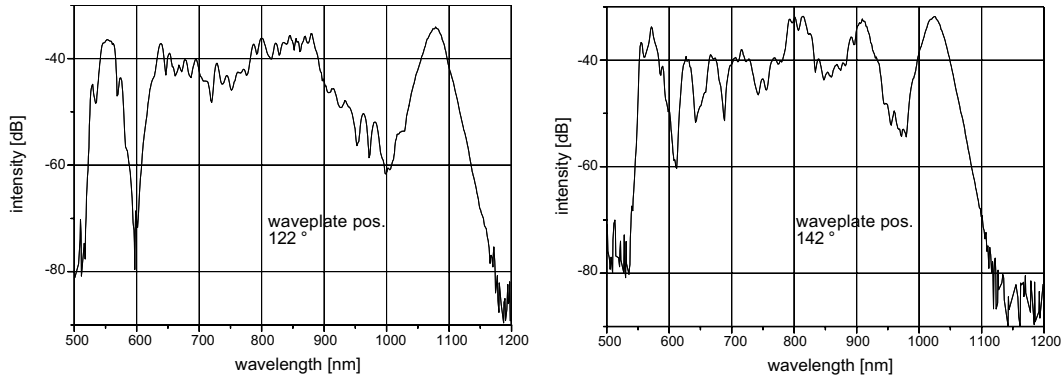


Figure 3.20: Broadening at different polarizations. The half wave plate at the fiber incoupling was rotated by 20 °, the power remained unchanged at 170 mW (fiber 1).

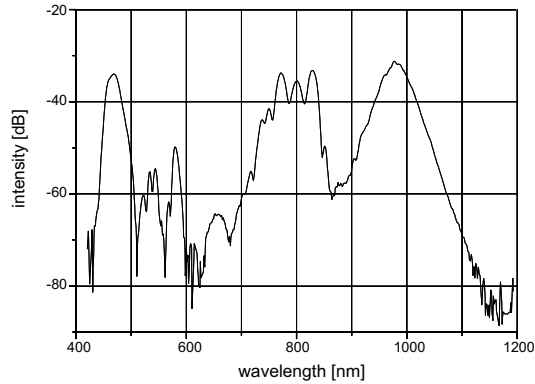


Figure 3.21: Broadening in a cobweb fiber with slightly larger core diameter. 140 mW are coupled are through 7 cm of fiber. Compared to Fig. 3.18 the spectrum is shifted to the blue.

frequency comb is getting broader and broader as the power increases. Again we used a regular PCF, similar to the one shown in Fig. 3.14 and 25 fs pulses at 750 MHz repetition rate. The use of different fibers also led to different spectra. An example is illustrated in Fig. 3.21. The cobweb fiber to generate this spectrum is similar to the 1 micron cobweb shown in Fig. 3.17 only with a slightly larger core diameter of 1.6 μm . Compared with the spectrum generated with the 1 micron cobweb the spectrum is shifted notably to the blue.²

Due to the anisotropies in the fiber design the broadening also depends on the polarization of the light pulses launched into the fiber. Fig. 3.20 illustrates how rotating a half wave plate at the fiber incoupling influences the spectrum without changing the power coupled through the fiber. This can be used to fine tune the heavily structured spectrum to achieve maximal signal to noise ratio when observing beats with cw lasers.

²This seems to be the ideal fiber for a future hydrogen measurement as the blue spectrum reaches the 482 nm of the laser whose 4 th harmonic excites the 1S-2S transition

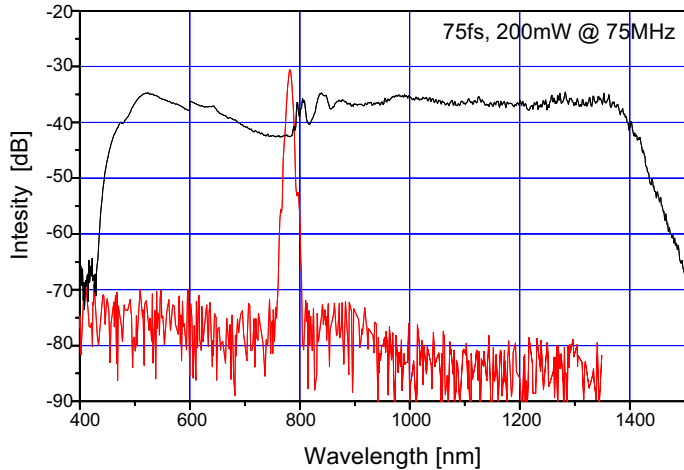


Figure 3.22: Spectrum from the mira and pcf.

Another interesting feature of the PCF's is that the broadening doesn't stop after a few cm as illustrated in Fig. 3.18 when the pulse should be dispersed even in a PCF. Even if the group velocity dispersion is zero at the center wavelength of the initial pulses the broadened pulses will disperse in time as the GVD is not zero across the whole octave. Therefore the model introduced in section 2.2.3 might be not fully valid. A simple picture might explain what's happening with local hot spots in the spectrum where a high enough peak intensity is maintained for efficient four wave mixing to redistribute the energy to outerlying modes. This would explain how the peaks in the infrared and green move outwards as the power is increased in Fig. 3.19. The highly efficient spectral broadening of the PCF compensates for the decrease of available peak power connected with a high repetition rate.

Although self phase modulation is likely the dominant mechanism of spectral broadening there are other processes like stimulated Raman and Brillouin scattering or shock wave formation that might spoil the usefulness of these broadened frequency combs. Indeed in an experiment using 8 cm of PCF and 73 fs pulses at 75 MHz repetition rate from a Mira 900 system (Coherent Inc.) we have seen an exceptionally broad spectrum from 450 to 1400 nm as shown in Fig. 3.22 but with excessive broadband noise. We did not observe these problems with the 25 fs pulses at 625 and 750 MHz repetition rate utilized for all other spectra shown in this section. Our colleagues in Boulder used in their experiments a 12 fs Ti:sapphire laser (KMLabs) and a fiber from Bell Labs as mentioned above. They report the creation of an optical octave at 25 mW power through the fiber. Further increase of the power also generated broadband noise. The exact source of this noise is still not completely understood. Taking further the heavily structured spectrum into account that might have a deep hole where one wants to measure an optical frequency there is still a certain amount of "art" connected with the use of these fibers.

All spectra in this section have been recorded with an optical spectrum analyzer (Ando corp. model AQ-6315A).

3.4 The $f : 2f$ frequency chain

3.4.1 $f : 2f$ Frequency chain with auxiliary laser

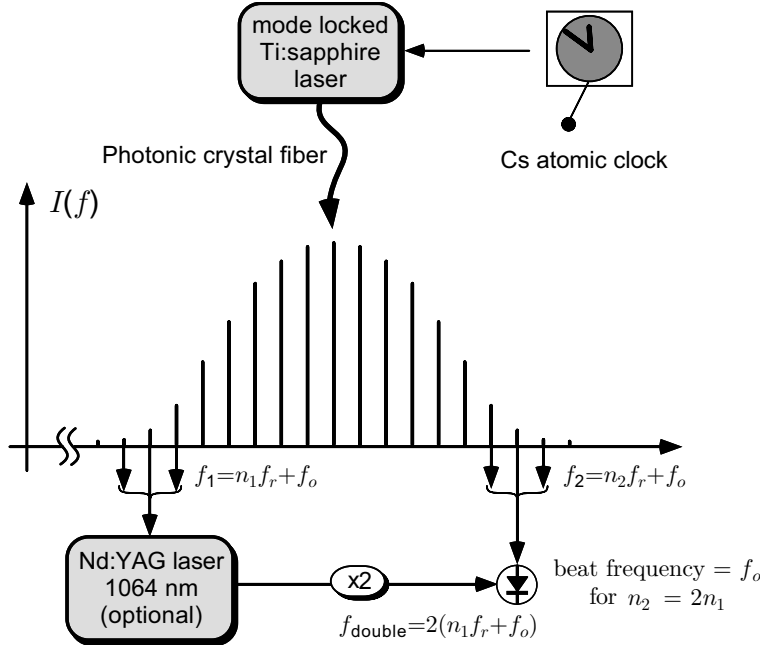


Figure 3.23: Principle of the $f : 2f$ frequency chain with photonic crystal fiber and auxiliary laser.

With the availability of photonic crystal fibers and broad frequency combs it is now straight forward to set up a frequency chain measuring the interval between an optical frequency f and its second harmonic. Due to the availability of the PCF this has first been demonstrated in Boulder resulting in a joint paper of J. Hall's group and our group [27] and shortly afterwards in our Garching laboratory.

Our implementation of the $f : 2f$ interval frequency chain sketched in figure 3.23 is based on a Ti:sapphire 25 fs ring laser with a high repetition rate (GigaOptics, model GigaJet). This laser has already been discussed in section 2.3.1.

While the ring design makes it almost immune to feedback from the fiber, the high repetition rate increases the available power per mode. The highly efficient spectral broadening of the PCF compensates for the decrease of available peak power connected with a high repetition rate. With 7 W of pump power we achieve above 600 mW average power from the fs laser. To generate an octave spanning comb we have coupled above 150 mW average power through 35 cm PCF. Fine adjustment of the spectrum can be achieved by rotating a $\lambda/2$ wave plate in front of the fiber incoupling. We have modified the original setup from Gigaoptics by mounting one of the mirrors on a translation stage for coarse control of the repetition rate and another mirror on a piezo transducer for fine tuning and phase locking of the repetition rate. In the final stage

of development the setup has further been modified by double folding the cavity to obtain more bounces on the chirped mirrors and by adding a fused silica wedge for coarse adjustment of the offset frequency. This is illustrated in Fig. 2.11 on page 17. Insertion of the wedge reduces the achieved output power slightly. We have inserted an electro optic modulator into the pump beam for fine adjustment and phase locking of the offset frequency. For this purpose we used an electro optics modulator (EOM) from Gsänger (model LM 0202) with an aperture of 3 mm. This turned out to be not enough for the Verdi pump beam. In initial experiments we used a telescope to focus through the EOM. Later on we used an EOM with an aperture of 5 mm. Usually the pump beam had approx. 7 W at the focusing lens into the crystal. Although we have not tried an AOM to modulate the pump power, there is no reason why this shouldn't work just the same way. We have operated this laser at a repetition frequencies of 1 GHz (single folded) 624 MHz and 750 MHz (double folded). Beat signals between the comb and cw lasers are usually observed with a signal to noise ration of better than 30 dB in 400 kHz bandwidth if the spectrum at the required frequency does not fall below a -10 dB line from the top peak of the spectrum. We utilize an adjustable beamsplitter and a grating to preselect some of the modes around the cw frequency as introduced in section 2.3.2.

In our setup a frequency doubled Nd:YAG laser (Prometheus, Innolight) defines the interval between f and $2f$ that is subsequently measured with the help of the frequency comb.

In a different interpretation the YAG laser serves to pick and amplify one of the modes by phase locking it to that particular mode. The Nd:YAG laser is internally frequency doubled in a periodically poled KTP crystal and a beat signal in the green with another mode of the comb is observed. This beat signal gives direct access to the offset frequency f_0 introduced earlier and as shown in Fig. 3.23. The offset frequency f_o is phase locked with the help of an electro optic modulator in the pump beam while the repetition rate f_r is phase locked with a PZT mounted folding mirror. Both are referenced to our cesium atomic clock. By this means the absolute frequency of each of the modes is phase coherently linked to the rf reference and known with the same relative precision.

Different locking schemes can be applied. Fig. 3.24 shows the natural locking scheme for an optical frequency synthesizer. In this case we first lock the pulse repetition frequency f_r to a stable radio frequency reference (circuit I in Fig. 3.24). In our laboratory we utilize for this purpose a stable quartz oscillator (Oscilloquartz, model 8607-BM, specified Allan standard deviation 2×10^{-13}) and a cesium atomic frequency standard (Hewlett Packard, model HP5081A). Locking is accomplished by controlling the fs laser cavity length with a piezo mounted folding mirror. A fast photo detector is used to detect the repetition rate. In order to reduce noise in the detection process we use a 12.5 GHz signal provided by a synthesizer (Hewlett-Packard, model 8360) to mix the two signals to dc with a radio frequency mixer and phase lock the 10th or 20th harmonic of f_r [5, 44]. By referencing the synthesizer to the quartz oscillator its frequency is multiplied in one step to 282 THz (1064 nm).

The next step is to phase lock the fundamental wave of the Nd:YAG laser to one of the modes of the frequency comb [44] (circuit II). This is done by forcing their beat note to

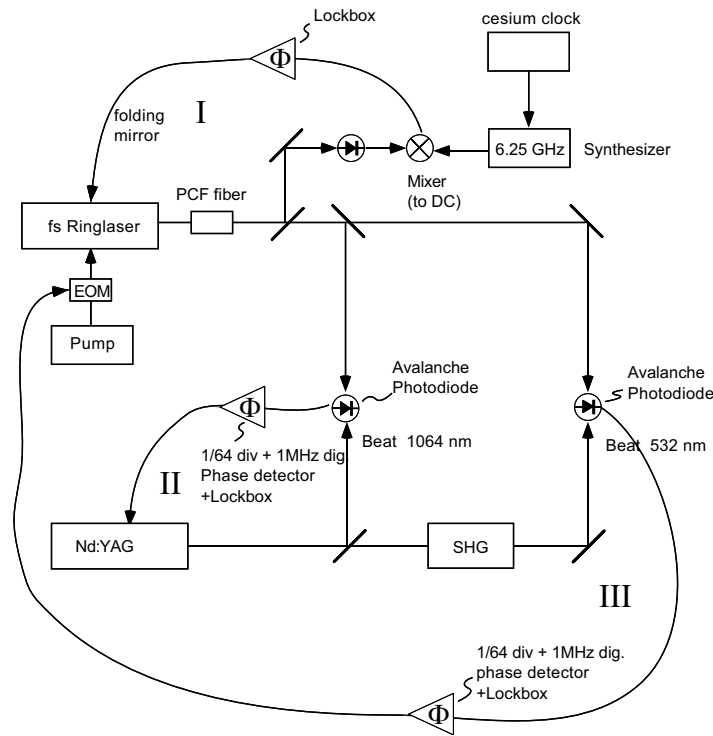


Figure 3.24: The “optical frequency synthesizer” locking scheme

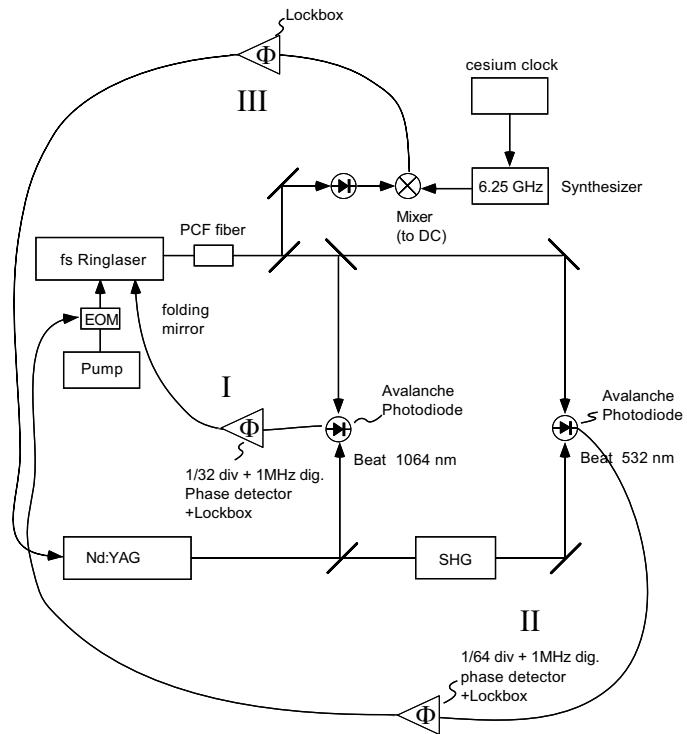


Figure 3.25: The “optical to rf clockwork” locking scheme

oscillate in phase with a radio frequency reference LO_{1064} , the local oscillator [61]. The absolute frequency of this laser is then given by Eqn. 2.3 ($f_{1064} = nf_r + f_o + LO_{1064}$) with unknown n and f_o . As shown in figure 3.23 we then observe a beat note at $2f_{1064} = f_{532} = 2(nf_r + f_o + LO_{1064})$ with the frequency comb whose closest mode frequency is given by $2nf_r + f_o$. The beat frequency is $f_o + 2LO_{1064}$ and is locked to another radio frequency offset: $f_o + 2LO_{1064} = LO_{532}$. This is accomplished by adjusting the power of the pump laser (Coherent, model Verdi) with an electro-optic modulator as described in chapter 2.3.1 (circuit III). For locking the two beat signals we employ digital phase locks that have a $\pm 16\pi$ locking range and are operated at a lock oscillator frequency of 1 MHz (see appendix A for details). To further increase the locking range we additionally divide the input beats signals with a standard digital TTL circuit by 64 or 32. A comparator at the input generates clear digital signals. When operating the frequency chain we count the in lock beat signal with a different bandwidth to detect possible cycle slips. As threshold we usually utilize 1 Hz for 1 s gatetime.

Note that for the case $f_o = 0$ Hz according to Eqn. 2.3 the mode frequencies are exact harmonics of the repetition rate. By choosing the value of $2LO_{1064} - LO_{532} = f_o = \Delta\varphi/T2\pi$ we can adjust the pulse to pulse phase shift $\Delta\varphi$ to a selected value (e.g. $\Delta\varphi = 0$). To achieve this we have operated the frequency chain with settings of $LO_{1064} = 32$ MHz and $LO_{532} = 64$ MHz. We have therefore precise control of the time evolution of the absolute carrier phase versus the envelope. Stabilization of f_o is in turn a prerequisite for the next generation of ultrafast experiments as discussed in section 3.5. However, the ultimate carrier-to-envelope phase control, i.e. the control over φ rather than $\Delta\varphi$ has not yet been achieved.

The second locking scheme as shown in Fig. 3.25 is the natural locking scheme for application as a clockwork for counting the rapid oscillations of a stable optical oscillator. In this scheme a mode of the comb is locked to the auxiliary laser (I), in this case the fundamental wave of our Nd:YAG laser by controlling the fs laser cavity length with a piezo mounted folding mirror. Then the beat signal between the second harmonic of the YAG laser and the green part of the fs frequency comb is phase locked by adjusting the pump power as described above (II). This fixes the offset frequency. The frequency of the YAG laser now determines the repetition frequency (III).

3.4.2 Single laser optical frequency synthesizer

The Nd:YAG laser can be omitted (as again first demonstrated by J. Hall's group at JILA in Boulder and shortly afterwards in our laboratory [27, 25, 24]), if one does not take a single mode of the comb but several modes and generates the sum and second harmonic frequencies directly from the infrared part of the fiber output. We have therefore arrived at the single laser frequency chain which actually is not a chain any more but just a self referenced frequency comb.

As sketched in Fig. 3.28 the infrared part of the spectrum is separated from the green part with the help of a dichroic mirror. Sum and second harmonic frequencies of the

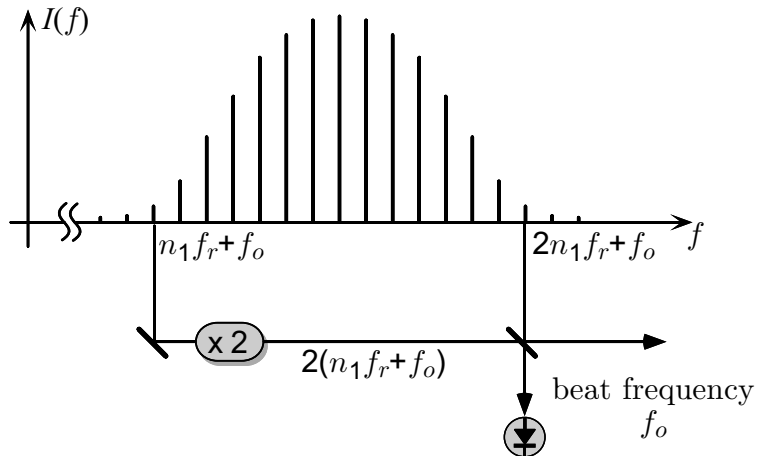


Figure 3.26: Principle of the $f : 2f$ frequency chain using a frequency comb spanning an optical octave .

modes in the infrared are generated in a 7 mm long KTP crystal properly cut and AR coated. This frequency doubled pulse is recombined with the green part of the original pulse on a polarizing beam splitter. For the green part an optical delay line was included to match the optical path length. Three different types of delay lines have been used in the experiments reported here and below. The polarization axes of the recombined light are mixed using a rotatable polarizer. A grating with 2100 Lines/mm serves as a bandpass filter to select two overlapping portions of the spectra. A beat signal exceeding 40 dB in 400 kHz bandwidth has been achieved, sufficient for phase locking.

The necessity of the delay line is easily understood in the time domain. We have two green pulses that need to arrive at the same time at the detector in order to interfere. In the frequency domain all the possibilities to create the f_o beat signal have to interfere constructively. The phase matching condition can be adjusted with the delay line. Three different possibilities that have all been used in the Garching and Vienna experiments without noticeable differences in performance are illustrated in Fig. 3.27.

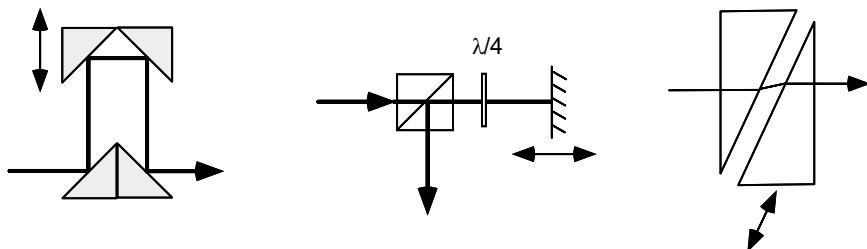


Figure 3.27: Three different ways to implement a delay line to match the path difference.

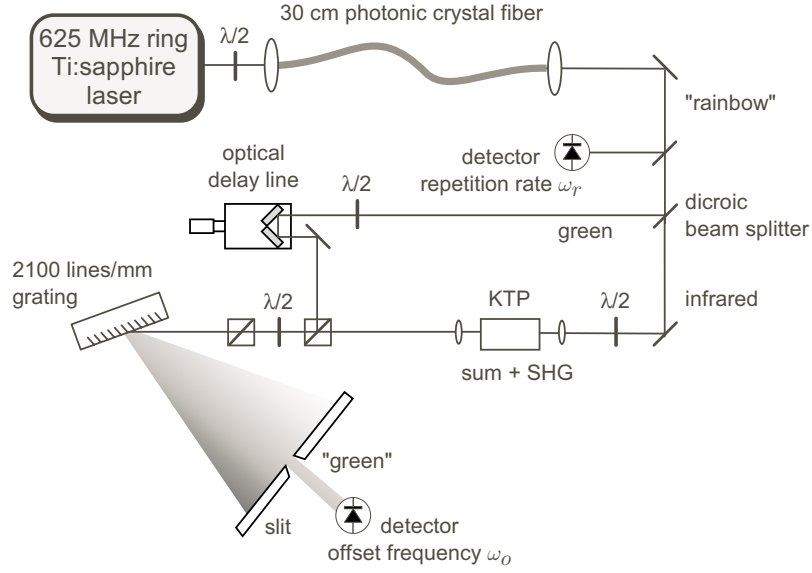


Figure 3.28: Frequency chain consisting of one single laser (and pump).

Fig. 3.29 visualizes a typical rf spectrum at the “offset frequency” detector in Fig. 3.28 under locked condition. The offset beat has a small sidebands that strongly depend on the adjustment of fiber and laser. The origin of this substructure is not yet fully understood but does not seem to influence the locking procedure and therefore the accuracy of the frequency comb.

In this way we have direct access to the offset frequency f_0 . Here we have locked it to 64 MHz using the digital offset locking technique described above although any other value is possible. The repetition rate can be locked independently as described above. Note that both parameters, i. e. f_r and f_0 are controlled after broadening in the

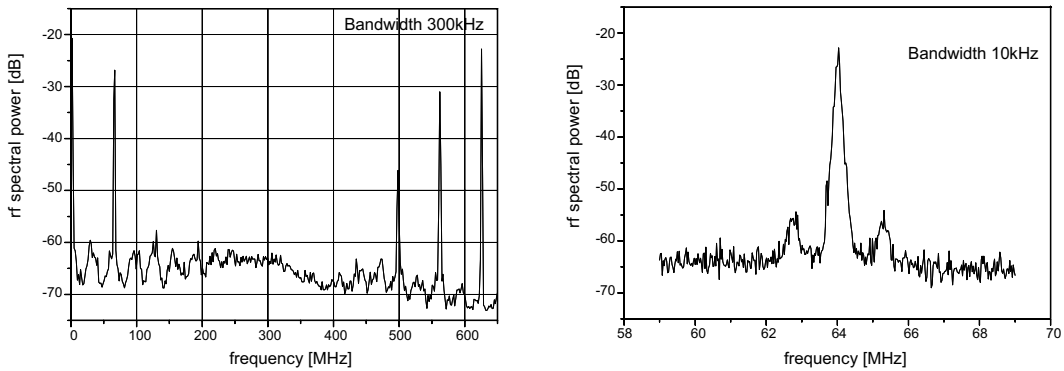


Figure 3.29: Left: the radio frequency spectrum as seen with the “offset frequency” detector in Fig. 3.28. Besides the offset frequency f_0 at 64 MHz and the repetition frequency f_r at 640 MHz also $f_r - f_0$ and $f_r - 2f_0$ can be seen. Right: close up of the locked offset beat at 64 MHz.

fiber. Also beat signals with cw lasers are observed after broadening. The fiber will certainly introduce additional phase noise and even Doppler shifts due to temperature variations. All this is taken care of in the stabilization techniques.

We have now arrived at a frequency chain that consists of one fs laser (and optional Nd:YAG) only and nevertheless links a 10 MHz rf reference phase coherently in one step with the optical region. It occupies only 1 square meter on an optical table with the potential for further miniaturization. At the same time it supplies us with a reference frequency grid across much of the visible and infrared spectrum with comb lines that are separated by 625 MHz and can easily be distinguished with a commercial wavemeter. This makes it a ideal laboratory tool for precision spectroscopy and a compact solid state system that is ready to serve as a clockwork in future optical clocks. In the reverse direction we expect this clockwork to transfer not only the accuracy but also the superior stability of optical oscillators to the rf domain.

3.4.3 Validation of the $f : 2f$ frequency chain

To check the integrity of the broad frequency comb and evaluate the overall performance of the $f : 2f$ interval frequency chain we have compared it with the $3.5f : 4f$ frequency chain used for the measurement of the hydrogen $1S - 2S$ transition frequency as described above. This represents the first direct comparison of two independent frequency chains. We find agreement between the two chains on the level of 5.1×10^{-16} .

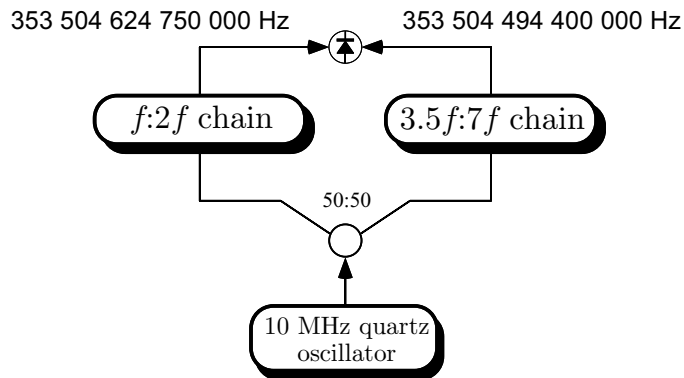


Figure 3.30: Comparision of two frequency chains.

The $f : 2f$ chain has been described in detail in the preceding section. The other frequency chain (“ $3.5f : 4f$ ”) has been used in the hydrogen experiment of section 3.2. The fs comb used here is only 44.2 THz wide and has been thoroughly tested in section 2.3.2. This chain was modified to replace the dye laser (in the laboratory next door) by a frequency doubled diode laser/tapered amplifier combination at 969 nm [133]. An output of 20 mW from a laser is diode amplified in a tapered amplifier to 500 mW and subsequently frequency doubled in a bow tie cavity featuring a Hänsch–Couillaud lock [132]. About 80 mW of blue light are produced. The additional frequency gap of 1 THz in the previous setup has been removed by operating the diode laser at exactly

gate time	Allan standard deviation	mean deviation from 130.35 MHz	relative uncertainty	approved readings
1 s	3.3×10^{-13}	-1.2 ± 1.8 Hz	5.1×10^{-15}	4310
3 s	7.0×10^{-14}	-0.54 ± 1.8 Hz	5.1×10^{-15}	181
10 s	2.6×10^{-14}	207 ± 376 mHz	1.1×10^{-15}	574
30 s	1.1×10^{-14}	551 ± 441 mHz	1.6×10^{-15}	65
100 s	3.9×10^{-15}	-82 ± 233 mHz	6.6×10^{-16}	39

Table 3.1: Summary of results from the frequency chain comparison with statistical uncertainties derived from the data. Two additional points have been removed from the 1 sec data set that have been more than 50 kHz off but have not been detected as cycle slips. The weighted mean of column 3 yields 71 mHz ± 179 mHz (5.1×10^{-16}).

$3.5f$. Without this additional frequency gap the frequency chain is identical to the simplified Fig. 3.2. To compare the two frequency chains we use the 848 nm laser diode and a second 848 nm laser diode locked to the frequency comb of the $f : 2f$ chain. The frequency f_1 of the 848 nm laser diode locked to the $f : 2f$ chain can be expressed through

$$f_1 = N_1 f_r + f_0 + 20 \text{ MHz} = 353\,504\,624\,750\,000 \text{ Hz} \quad (3.3)$$

where $N_1 = 565725$, $f_r = 624.87$ MHz, $f_0 = 64$ MHz and a 20 MHz contribution from the local oscillator employed for phase locking the laser diode. The frequency f_2 of the 848 nm laser diode in the $3.5f : 4f$ chain can be written as

$$f_2 = N_2 f_r + f_0 + 20 \text{ MHz} = 353\,504\,494\,400\,000 \text{ Hz} \quad (3.4)$$

where $N_2 = 4\,675\,985$, $f_r = 75.6$ MHz, $f_0 = 8.4$ MHz and again a 20 MHz contribution from the local oscillator used for the phase lock. We expect a beat signal at 848 nm of $f_{beat} = f_1 - f_2 = 130.35$ MHz. The setup is schematically shown in Fig. 3.30. The data presented here have been taken with these parameters to make data evaluation easier. However we also operated the $f : 2f$ chain with repetition rate $f_r = 625$ MHz and a offset frequency $f_0 = 0$ Hz as well as with and without a auxiliary laser defining the $f : 2f$ interval.

We have taken data with different gatetimes (1 sec through 100 sec.) After averaging all data we obtained a mean deviation from the expected beat frequency of 71 ± 179 mHz at 353 THz. This corresponds to a relative uncertainty of 5.1×10^{-16} . No systematic effect is visible at this accuracy [24] (Fig. 3.33).

The results are summarized in table 3.1 and visualized in Fig. 3.31. Fig. 3.32 shows the measured Allan standard deviation³ for counter gate times of 1, 3, 10, 30 and 100 sec. As both 354 THz signals are phase locked to each other (via the quartz oscillator) and the rms phase fluctuation is expected to be constant in time, the Allan standard

³For a definition see footnote on page 35.

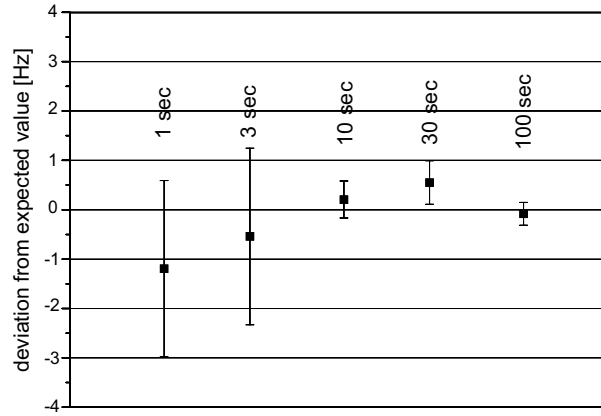


Figure 3.31: Comparision of two frequency chains. The results for different gate times presented in table 3.1 are visualized.

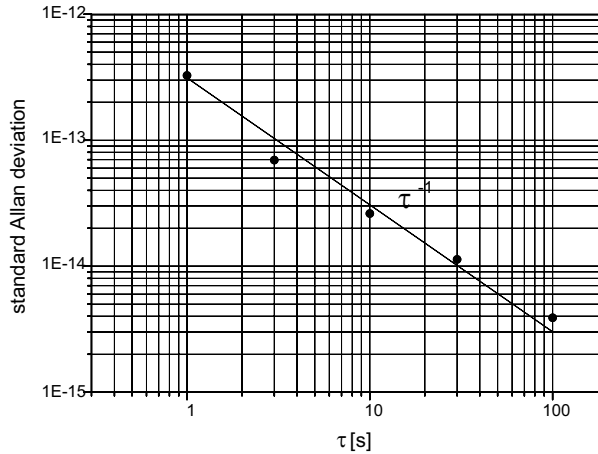


Figure 3.32: Allan standard deviation derived from the data for different gate times.

deviation should fall off like the inverse counter gate time. The large margin phase detector together with the slow servo controlling the phase of the HeNe laser relative to the diode lasers causes frequency fluctuations of 14 Hz at 1 sec gate time as measured from the in-lock beat signal. This would correspond to fluctuations of 4×14 Hz at the beat note comparing the two chains. According to table 3.1 this fluctuation is larger by more than a factor of 2 suggesting that other instabilities contribute. These instabilities could be caused not only by the large margin phase locked loops but also by mechanical vibrations or thermal expansion. Note that the large frequency chain of Fig. 3.2 is resting on two separate optical tables whose relative position is not controlled. Another source of instability could be the specified 1.5×10^{-13} Allan standard deviation (within 1 sec) of the quartz oscillator together with time delays present in both systems. To check whether or not the synthesizers introduce additional noise we operated both chains with the same synthesizer to stabilize the repetition rates without any significant difference.

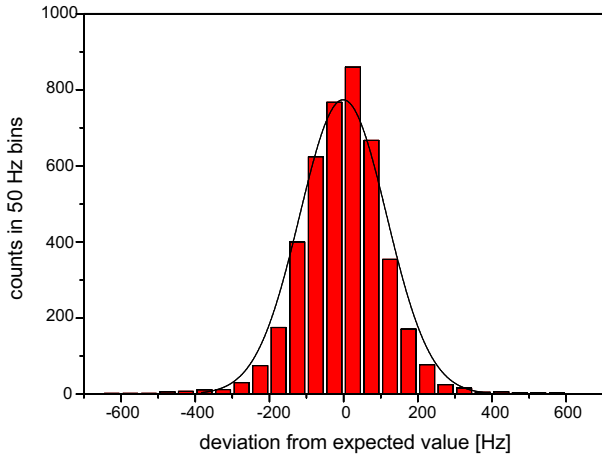


Figure 3.33: Histogram of the 1 s data.

Note that the Allan standard deviation for longer gate times can not be derived from the 1 s data by juxtapositioning [134].

The results from this first comparison of two independent frequency chains have been published in Physical Review Letters [24].

3.4.4 Application to Iodine

To demonstrate the usefulness and broad applicability of this technique we have used a single laser femtosecond frequency chain together with a widely tunable Nd:YAG laser to measure the absolute frequency of several absorption lines in molecular Iodine around 532 nm. The use of two different repetition frequencies allows us to determine the number of modes used for the frequency measurement unambiguously. The lines also provide data for the determination of improved ro-vibrational constants of the Iodine molecule.

The iodine spectrometer was developed at the Institute of Laser Physics (ILP) (Novosibirsk, Russia) and has been described in chapter 2.6 in detail. Here we exploit the large tuning range of more than 500 GHz of this laser to measure previously unmeasured lines in iodine.

From the precise knowledge of more than 100 000 iodine lines studied by Gerstenkorn and Luc by Fourier transform spectroscopy [87], certain molecular constants can be derived [135]. The accuracy of these calculations, based on experimental data, is presently limited by the resolution of Fourier transform spectroscopy, which, in spite of its versatility, does not resolve the Doppler broadened hfs transitions. High-resolution saturated absorption spectroscopy together with precise absolute frequency measurements of the hfs transitions of the R and P branches with common upper or lower vibrational manifold can be used for improving the values of rotational and vibrational constants of the X and B iodine states as well as to study the J-dependence of quadrupole coupling

constant eqQ [136]. With the fs comb technique described here there is no fundamental obstacle to perform accurate measurements all across the visible and near infrared part of the spectrum to collect data for this evaluation. The data presented here are a first step in this direction and demonstrate the versatility of this new technique.

Optical frequency measurements with fs laser frequency combs are always accomplished by observing a beat signal f_{beat} of the laser frequency to be measured with a corresponding mode f_n of the comb. Therefore optical frequencies are always measured modulo the repetition rate and the remaining problem is to unambiguously identify the mode number n of the mode that is used for the measurement in equation 2.3 $f_n = f_0 + n f_r$.

If the optical frequency f_{light} to be measured is already known to a precision much higher than the mode spacing the mode number can simply be determined by solving the corresponding equation $f_{light} = f_0 + n f_r \pm f_{beat}$ for n and demanding n to be integer. This has been the case for the measurements in Hydrogen (section 3.2), Indium (section 2.5) and our previous iodine measurements (section 2.6).

In our first experiment using fs frequency combs (section 2.4 and Ref. [5]) we solved this problem in a different way. We used a passive cavity with a free spectral range of exactly 20 times the repetition rate [5]. So in the time domain the repetition rate was increased 20 fold as every pulse bounced back and forth in the cavity 20 times before the next pulse arrived.

For the measurements presented here we are following another approach. We have measured the same optical frequency with different settings for the repetition rate. This gives us two equations:

$$\begin{aligned} f_{light} &= f_0 + n_1 \times f_{rep_1} + f_{beat_1} \\ f_{light} &= f_0 + n_2 \times f_{rep_2} + f_{beat_2} \end{aligned} \quad (3.5)$$

For a given optical frequency a relation between the mode numbers n_1 and n_2 can be extracted. Consider now the two repetition frequencies 750 MHz and 751 MHz. The two do not share a common divider and therefore if a mode from the first comb coincides with another mode from the second comb this will happen again after 750×751 MHz = 563.25 GHz. Even with a rather poor wavemeter performance the coincidence can be identified unambiguously. We used in our experiment a commercial wavemeter (Burleigh WA1500 Series) to find the lines and determine the mode number within ± 1 . Equations 3.5 resolve that last ambiguity.

The frequency chain has been described in detail in the preceding section. Once the offset frequency and repetition rate are phase locked to our cesium clock (HP 5071A), all the modes in the comb can be used for optical frequency measurements.

We have operated the iodine spectrometer using cell 13/97PTB⁴ with the parameters $T = -5^\circ\text{C}$ ($p = 2, 42$ Pa), $P = 0.8$ mW, $I = 40$ mW/cm².

⁴This iodine cell was filled, sealed and labeled at the Physikalisch Technische Bundesanstalt (PTB) at Braunschweig, Germany.

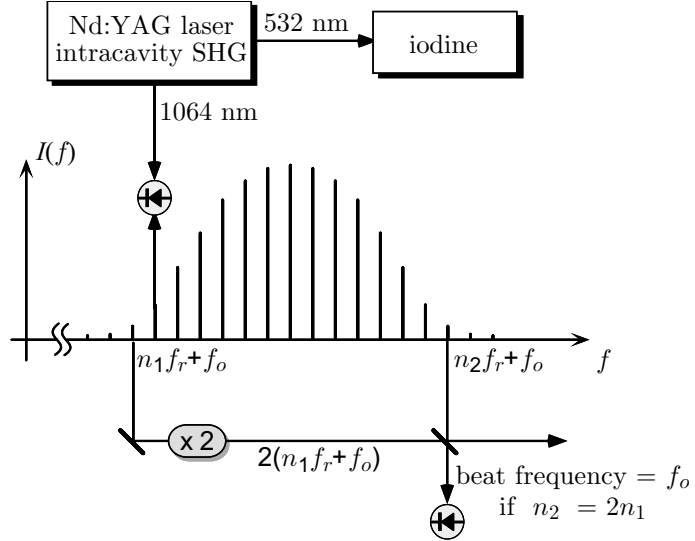


Figure 3.34: Application of the $f : 2f$ frequency chain. Once the offset frequency and repetition rate are locked, all the modes in the comb can be used for optical frequency measurements. Here modes near 1064 nm are used to measure a iodine stabilized Nd:YAG laser.

For the measurement presented here we have coupled 1 mW from the 1064 nm radiation through a fiber that connects the spectrometer and the frequency chain and observed directly a beat signal with a corresponding mode of the comb with a signal to noise ratio exceeding 30 to 35 dB in 400 kHz bandwidth. For each line and repetition rate a different beat frequency has to be counted with $0 < f_{beat} < f_{rep}/2$. To make this task easier we have shifted all beat notes above 100 MHz by mixing it with a known radio frequency to the vicinity of 40 MHz where a convenient band pass filter has been available. Beat frequencies close to 0 Hz or $f_{rep}/2$ have been shifted to a more convenient frequency by slightly increasing or decreasing the phase locked repetition frequency. Slightly changing the repetition frequency also gives a handle to determine the sign of the beat frequency in equation 1. In three measurement sessions on three different days the different lines have been measured with repetition rates of 624 MHz, 750 MHz and 751 MHz. The change from 624 MHz to 750 MHz involves major realignment of the laser cavity whereas the change from 750 to 751 MHz can be done easily without leaving the mode-locked operation. For this task one of the cavity mirrors is mounted on a translation stage. For each line and repetition rate at least 200 data points with a gate time of 1 sec. have been collected. The results are summarized in Table 3.2. Each line has been measured with at least 2 different repetition rates and associated mode numbers have been determined.

To illustrate this procedure let us look at one sample measurement: in the first session the a_1 component of line 1105 has been measured with a repetition rate of 624 MHz. The chain equation reads as follows:

$$f(1110, a_{10}) = 2 \cdot (N f_{rep} + f_0 + f_{beat}) \quad (3.6)$$

line	assignment	component	frequency [kHz]
1082	R61,32-0	a1	562 998 761 600.5
1083	P58,32-0	a1	563 002 588 735.1
1087	R60,32-0	a1	563 052 807 019.5
1088	P57,32-0	a1	563 056 434 053.9
1093	R59,32-0	a1	563 105 854 235.6
1095	P56,32-0	a1	563 109 440 893.3
1098	R58,32-0	a1	563 158 063 529.7
1099	P55,32-0	a1	563 161 456 916.8
1104	R57,32-0	a1	563 209 276 621.5
1105	P54,32-0	a1	563 212 634 608.9
1109	P83,33-0	a1	563 243 620 975.4
1110	R56,32-0	a10	563 260 223 508.7
1110	R56,32-0	a1	563 259 651 965.5
1115	R55,32-0	a1	563 309 032 997.2
1116	P52,32-0	a1	563 312 173 684.1
1122	R54,32-0	a1	563 357 576 493.6
1123	P51,32-0	a1	563 536 360 675.1

Table 3.2: Summary of the frequency measurements. 16 lines within the tuning range of the Nd:YAG laser have been measured. Each line has been measured with at least two different settings for the repetition frequency. The line numbering follows [87]. The data are presented as measured with parameters $T = -5^\circ\text{C}$ ($p = 2,42 \text{ Pa}$), $P = 0.8 \text{ mW}$, $I = 40 \text{ mW/cm}^2$. Absolute uncertainty for each line is 5.1 kHz.

with $N = 451\,292$, $f_{beat} = 45\,304\,250 \text{ Hz} \pm 78 \text{ Hz}$, $f_0 = 64 \text{ MHz}$ and $f_{rep} = 624 \text{ MHz}$ we derive a frequency $f(1105, a_1) = 563\,212\,634\,608\,500 \text{ Hz}$. From a second measurement with $f_{rep} = 750 \text{ MHz}$ we get in the same manner $563\,212\,634\,609\,330 \text{ Hz}$. Stated in Table 3.2 is the average value of $563\,212\,634\,608\,915 \text{ Hz}$. The difference between the two measurements of approximately 800 Hz is a typical value. This difference can be as big as 2.2 kHz and 2.1 kHz for the outer-lying lines 1082 and 1122 respectively, but usually the difference is well below 1 kHz. Note that only between 200 and 300 data points with a gate time of 1 sec have been collected per line and repetition frequency setting.

The contributions to the estimated standard uncertainty are 140 Hz (2.5×10^{-13}) from the optical synthesizer, limited by the short term stability of our cesium atomic clock, 50 Hz on average from the measurement statistics and 1.5 kHz from our spectroscopy setup. As we are moving out from the Nd:YAG gain center near line 1105 the probe power and the signal to noise ratio are somewhat reduced. To account for this we have increased our error estimation to 1.5 kHz compared to 1.1 kHz stated in chapter 2.6. The measured power shift in our setup is -340 Hz/mW . The average power in our spectrometer is $P = 0.6 \text{ mW} \pm 0.2 \text{ mW}$ with lower power (-0.2 mW) for the outer lying lines and higher power near the gain maximum ($+0.2 \text{ mW}$). Therefore the lines

are slightly shifted to the red (by $200 \text{ Hz} \pm 70 \text{ Hz}$) as compared to the unperturbed line.

In addition we face a well known problem with impurities in the iodine cells. For a set of iodine cells the one with the smallest impurities will lead to the highest measured transition frequency of a given iodine line. Our recent experiments with different iodine cells have shown that the cell used in this experiment usually yields an approximately 1 kHz lower value for a given transition compared to cleaner cells (e.g. PTB reference cell 16/98). We cannot exclude that even higher frequencies will be measured in the future (see also chapter 2.6. This would lead to a blue shifted value and we attribute a safe 5 kHz uncertainty to that. The pressure shift in our apparatus has been measured to be $-4.2 \text{ kHz/Pa} \pm 0.2 \text{ kHz/Pa}$. To compare our results to previously published data taken at $T = -20^\circ\text{C}$ ($p = 0.46 \text{ Pa}$) [10] one might want to add $9.4 \text{ kHz} \pm 0.4 \text{ kHz}$ to the values stated in Tab. 3.2. This extrapolation comprises a pressure shift of 8.2 kHz, a power shift of 0.2 kHz and a (possibly higher) shift due to iodine impurities of 1.0 kHz. As all lines are similarly affected by impurities in the iodine cell the relative distance between the lines can be stated with an uncertainty of 2.1 kHz derived from twice the spectrometer uncertainty. The uncertainty in the absolute frequency data of our measurement adds up to a total of 5.2 kHz.

The a_{10} hfs component of the R(56)32-0 iodine absorption line (1110) is recommended by the Comité International des Poids et Mesures (CIPM) for the realization of the meter [10].

The measurement presented here is in good agreement with a recent measurement done in our laboratory where we used a methane stabilized He Ne laser as a reference presented in chapter 2.6 and independent measurements at JILA (Boulder, USA) with another fs frequency chain [27]. The frequency value for the a_1 component of line 1105 also nicely reproduces the value from chapter 2.6. In earlier experiments the difference between the lines 1104 to 1111 and the a_{10} hfs component of line 1110 have been measured [88]. We have remeasured 3 of these lines (1104, 1105, 1109) and find moderate agreement within a few kHz. All other lines have never before been measured at this level of accuracy.

Note that none of the new iodine measurements with fs chains are in disagreement with measurements made with harmonic chains (section 2.6 and also Ref. [90]).

The work presented here has been submitted for publication.

3.4.5 $f : 2f$ chain with a Cr:LiSAF laser

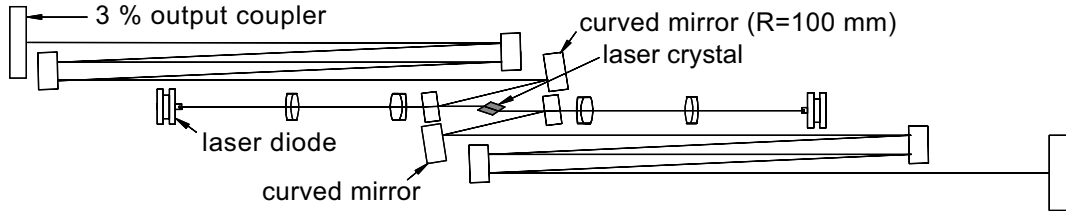


Figure 3.35: The laser setup with 26 reflections per round trip to fit everything in a $15 \times 60 \times 20$ cm box. For details see text.

On the search for an alternative to Ti:Sapphire lasers that require a costly green pump source we have launched pulses from a battery operated Cr:LiSAF laser into a photonic crystal fiber to create an octave spanning frequency comb. Despite the massive broadening in the fiber the comb structure of the spectrum is preserved and this frequency comb is perfectly suited for optical frequency metrology applications.

The Cr:LiSAF laser was set up by K. Gäbel and P. Rußbüldt in the group of R. Poprawe at the Fraunhofer Institut für Lasertechnik in Aachen, Germany and delivered as a turn key system to our laboratory in Garching.

Kerr-lens mode locked Ti:sappire lasers represent convenient laboratory work horses and come in a variety of different pulse lengths, repetition rates and peak powers. However, one of the drawbacks of these lasers is that they need a green pump source and as no green high power laser diodes are available at the moment they can not be directly diode pumped. Costly large frame Ar-ion or frequency doubled Nd:YAG lasers are used for pumping instead. This also excludes applications where portability and low power consumption are required.

The relatively new laser crystals of the colquittites $\text{Cr}^{3+}\text{LiSAF}$, $\text{Cr}^{3+}\text{LiSGaF}$, $\text{Cr}^{3+}\text{Li-CaF}$, etc. which can be directly pumped by laser diodes at 670 nm offer a low cost high performance alternative to Ti:sapphire. These crystals have only a slightly smaller gain bandwidth, and even a two times lower saturation intensity than Ti:sapphire. However, there are some disadvantages: The colquittites are soft, the thermal conductivity is more than 10 times lower than in sapphire, at a crystal temperature above 60°C thermal quenching substantially lowers the gain, and the nonlinearity (needed for Kerr lens mode locking) is 5 to 10 times smaller than in sapphire. To get a high gain and a high nonlinearity in a standard Z-fold cavity one has to focus tightly into the laser crystal. The laser diodes in the required power range have a rather poor beam quality with an M^2 of about 2×8 measured behind the collimating micro lens. To maximize the gain the overlap of the pump beam with the resonator mode was numerically optimized for both axes [137]. To implement the calculated improvements we used the setup in Fig. 3.35. The plane folding mirrors between the crystal and the curved mirrors and micro lenses in front of the laser diodes allow for an almost aberration free imaging into the laser crystal and a compact setup. For dispersion compensation one of the high reflective mirrors was substituted by a chirped one.

All mirrors in the setup have been custom designed and coated by Layertec GmbH (Mellingen, Germany). Because of the low power level of 2×350 mW available from the pump diodes the high intracavity power required for Kerr-lens mode locking can only be achieved with low output coupling of 3 % and dense low scatter sputtered mirror coatings with losses of 0.02 % per bounce. The optimized pumping scheme and the low losses enable an overall optical slope efficiency of 39 %.

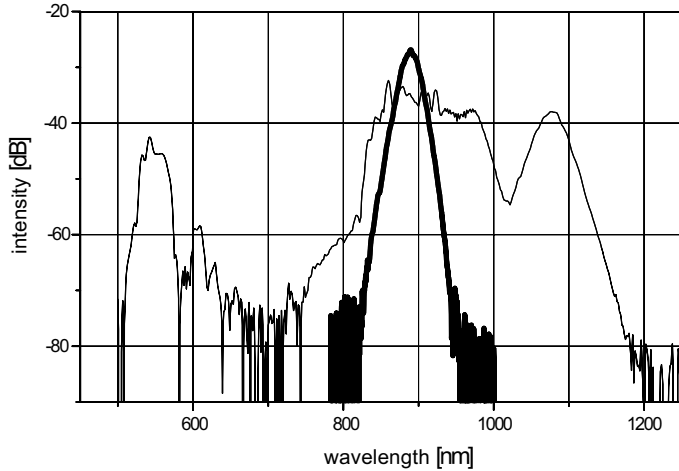


Figure 3.36: Spectrum obtained with the Cr:LiSAF laser. Repetition rate 93 MHz, 40 fs, 42 mW through 20 cm 1 micron cobweb fiber.

Theoretical and experimental data predict best performance of soft aperture KLM Ti:sapphire lasers if the laser crystal is moved out of the center between the curved mirrors in such a way that the beam-waist is located on one crystal surface [138]. But our Cr:LiSAF laser experiments and numerical calculations [139], taking into account the strong gain saturation, show that the best performance is accomplished with a higher eccentricity (2.5 mm for a 5 mm Cr:LiSAF crystal and radius of curvature of 100 mm). We obtained up to 150 mW mode-locked power at a 100 MHz repetition rate and dispersion controlled central wavelengths of 835 - 895 nm. The mode-locked bandwidth varies between 20 - 30 nm FWHM with a corresponding pulse duration of 40 - 60 fs respectively.

In the reported experiments the laser was operated with 115 mW mode locked power at 93 MHz, 894 nm central wavelength, 24 nm FWHM bandwidth (Fig. 3.36, bold curve), supporting a 40 fs pulse width. The pulses launched into the fiber without compression had a 57 fs pulse width and a pulse-bandwidth product of $\tau\Delta\nu = 0.45$. To obtain a good long-term stability and low noise special attention has been paid to the mechanical setup. The internal base plate is mechanically, thermally and electrically isolated from the environment and the power supplies. The completely shielded power supplies are hosted in the same air tight box, so that only 12 V DC (< 1 A) from a battery and a water flow for thermal stabilization has to be externally supplied. The use of a single tension free material ensure the long-term stability of the resonator setup.

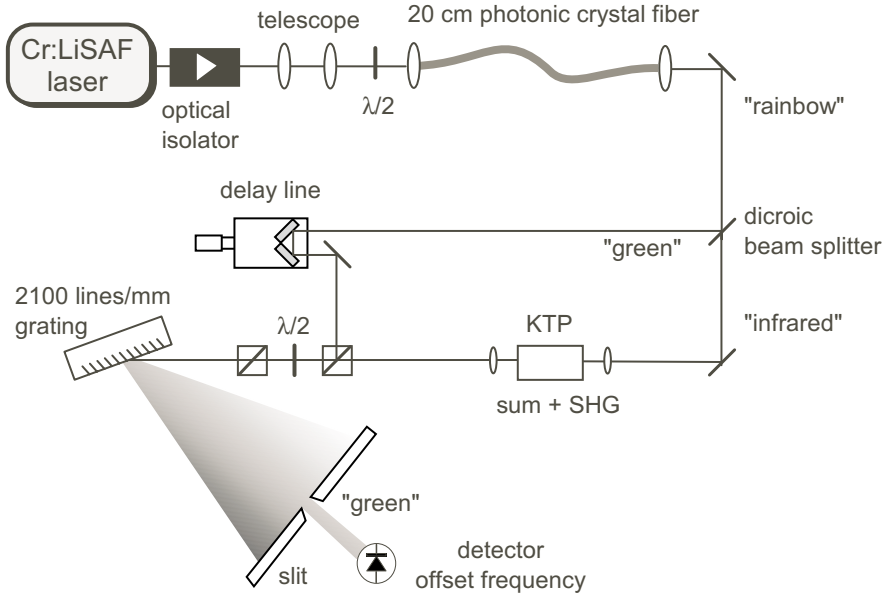


Figure 3.37: The $f : 2f$ interval frequency chain with a Cr:LiSAF laser. An optical isolator is needed to reduce back reflections from the fiber.

The only objections from an end-user point of view would be the rather uncertain life time estimates for the pump diodes and the relatively low output power level achieved.

We have used the PCF with the smallest core diameter available ($1 \mu\text{m}$, see Fig. 3.17) with zero GVD near 580 nm to increase the nonlinear interaction. The spectra generated in PCFs with small cores and short GVD zero wavelengths generally cover a very broad range, but exhibit deep spectral holes, governed by the GVD zero and the pump wavelength. This is due to the complicated phase structure of the pulse propagation in the fiber which also has so far prohibited the recompression of such ultrabroad spectra. A very pronounced example is shown in Fig. 3.36. It has despite the deep holes in the red part the advantage of having peaks at 530 nm and 1060 nm that we need for self referencing the frequency comb with the setup described above and shown in Fig. 3.37. Starting with 115 mW from the laser 20 mW are lost in a optical isolator (Gsänger, DLI 1) and 42 mW average power are coupled through 20 cm of PCF to generate the octave spanning comb. To maximize the coupling efficiency a telescope has been included in front of the microscope objective. As in earlier experiments the infrared part of the spectrum has been separated from the green part with the help of a dichroic mirror, doubled in a $3 \times 3 \times 7 \text{ mm}^3$ KTP crystal properly cut and AR coated and recombined with the green part on a polarizing beam splitter. For the green part an optical delay line was included to match the optical path length. The polarization axes of the recombined light are mixed using a rotatable polarizer. A grating with 2100 lines/mm serves as a bandpass filter to select the overlapping portions of the spectra. Fig. 3.38 shows the resulting rf spectrum at the photo detector in Fig. 3.37. A beat signal with a signal to noise ratio exceeding 40 dB in 100 kHz bandwidth has been achieved. The signal to noise ratio is sufficient to phase lock both f_0 and f_r .

Without any stabilization the Allan standard deviation of the repetition frequency of the free running laser at 1 sec was 2.2×10^{-10} . We have not actually stabilized it due to the limited access to the sealed box of the LiSAF laser. With an additional piezo to control the cavity length and a direct control of the pump power both parameters can be controlled in a future frequency chain application. This will result in a compact and transportable single laser optical frequency synthesizer without the need for large frame pump lasers.

The results presented here have been submitted for publication.

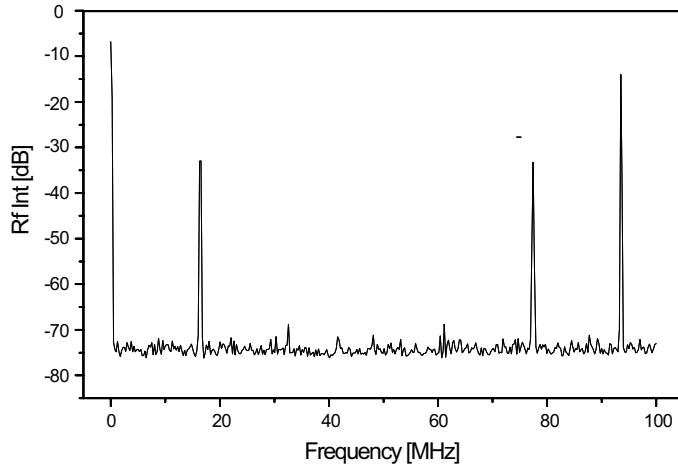


Figure 3.38: The radio frequency spectrum showing the offset frequency beat f_0 as well as the repetition frequency f_r and $f_r - f_0$. Detection bandwidth was 100 kHz.

3.5 Applications in the time domain

In collaboration with A. Poppe, A. Apolonski, G. Tempea and F. Krausz at the Technical University (TU) in Vienna we have applied the frequency domain techniques discussed so far to an ultra short pulse laser capable of emitting pulses of a duration below 6 fs.

In the course of this work we have demonstrated the generation of sub-6-fs light pulses with their pulse to pulse carrier-envelope phase locked to within less than 0.3 radians to an electronic oscillator and their field amplitude stabilized to within less than 0.05% for extended periods of time, indicating the emerging experimental capability of synthesizing few-cycle light waves with reproducible field evolution.

Exposing matter to a few oscillation cycles of intense optical radiation permits bound electrons to survive in the vicinity of the nucleus up to unprecedented intensity levels, allowing to enter previously inaccessible, extreme regimes of nonlinear optics [54].

Observed and predicted consequences include optical-field ionization rates comparable to the light frequency [140], making atoms radiate high-order harmonics of the driving laser up to photon energies exceeding by more than a factor of 300 the energy of the laser photons [141], and the possibility of generating isolated X-ray pulses of attosecond duration [142].

These phenomena emerge in the strong-field, low-frequency regime of nonlinear optics, where the electronic motion is directly controlled by the electric and (at relativistic intensity levels also) magnetic fields. In a few-cycle laser pulse, with an electric field

$$E(t) = A(t)\cos(\omega_0 t + \varphi), \quad (3.7)$$

the fields sensitively depend on the parameter φ , determining the position of the carrier wave (oscillating at frequency ω_0) with respect to the amplitude envelope $A(t)$.

Triggered by the recent availability of intense few-cycle laser pulses [143] down to pulse durations as short as 4 fs [144, 54] several methods have been proposed for gaining access to either the so called absolute phase φ or its variation $\Delta\varphi$ [54]. These include techniques drawing on strong-field processes, such as optical field ionization [145, 146, 147] or high harmonic generation [148], and last but not least the frequency domain techniques discussed in this work and by other authors [25, 64, 149].

The generation of electromagnetic waveforms in a controlled and reproducible manner, i. e. control of φ , can be routinely accomplished at radio frequencies but could not be achieved in the optical region so far. Rapid changes of φ in the pulse train delivered by mode-locked oscillators [59] and failure of gaining access to this parameter prevented this in the past. Measurement of the interferometric cross-correlation of successive sub-10-fs laser pulses revealed that φ suffers a shift upon each round trip of the pulse in the resonator due to a difference in the phase and group velocities in the laser components [59]. This round-trip phase shift typically accumulates to several hundred times 2π plus a physically relevant component $\Delta\varphi$, which obeys $0 < \Delta\varphi < 2\pi$ and accounts for a corresponding shift of the carrier with respect to the envelope as discussed in section

2.2. We have seen that as a result the carrier is slipping under the envelope at the carrier-envelope-offset frequency $f_{ceo} = f_0 = (\Delta\varphi/2\pi)f_r$. With the frequency domain techniques discussed earlier we gain access to f_0 and are thus able to freeze the time evolution of φ .

To be more quantitative the carrier envelope phase shift of the n th pulse versus its predecessor pulse can be written as $\Delta\varphi_n = \varphi_n - \varphi_{n-1}$ where φ_n evolves from a initial value φ_0 according to $\varphi_n = \varphi_0 + \sum_N \Delta\varphi_i$. Phase locking f_0 will keep the time average $\Delta\varphi_0 = \langle \Delta\varphi_n \rangle$ constant, but waveform synthesis can only be claimed if φ evolved reproducibly over the measurement time T_m under consideration, typically on the order of seconds to minutes. To achieve this the carrier envelope phase jitter

$$\sigma_\varphi(T_m) = \langle (\varphi_n - \varphi_0 - n\Delta\varphi_0)^2 \rangle^{1/2} \quad (3.8)$$

(the angle brackets indicate averaging over $N = f_r T_m$ pulses) must not exceed a tiny fraction of π . Although phase locking of the carrier-envelope offset frequency f_0 to a stabilized rf local oscillator can substantially reduce this random deviation, the availability of a frequency comb stable enough for accurate frequency metrology does not automatically imply fulfillment of the condition $\sigma_\varphi \ll \pi$. In fact, random phase excursion of phase-locked signals may exceed 2π without compromising the utility of the signal for frequency metrology as long as these large-amplitude excursions are detected and subsequently corrected for by the feed-back loop (cycle-slip-free operation). In contrast, random excursions of φ on the order of π may completely prevent phase-sensitive nonlinear effects from being observed in the time domain. Especially cumbersome are small phase noise contributions δ_n to the pulse to pulse phase shift $\Delta\varphi_n$ ($= \Delta\varphi_0 + \delta_n$) that can accumulate up to the response time (i.e. the inverse bandwidth) of the servo loop which may range from milliseconds to tens of microseconds depending on the technique used for adjusting f_0 (i.e. piezo controlled alignment vs. electro optic or acousto optic modulation of the pump power) and on the bandwidth of the driving electronic circuitry.

What is therefore needed is a fs oscillator producing few cycle pulses with high peak powers and very low pulse energy fluctuations. To this end, a specially-designed Kerr-lens-mode-locked, mirror-dispersion-controlled Ti:sapphire laser has been developed. Fig. 3.39 shows the schematic. More details can be found in the PhD thesis of A. Poppe [145]. The resonator is made up of broadband chirped mirrors and incorporates a 1:1 imaging telescope consisting of two curved mirrors (radius 1 m) and several plane folding mirrors (not shown in Fig. 3.39) to extend its length to ≈ 6 meters. Pumped with a single-frequency, frequency-doubled Nd:YVO₄ laser ($P_{pump} \approx 4.5$ W, Coherent Inc., model Verdi), the laser generates a highly-stable train of 9-fs, 20-nJ pulses at a repetition rate of 24 MHz (Fig. 3.39). These megawatt pulses produce substantial spectral broadening by self-phase modulation in a 3 mm piece of standard single mode optical fiber (FS-SC-3314, Thorlabs). Fig. 3.40 depicts the broadened spectrum, which spans from less than 500 nm to more than 1100 nm, as well as the pulse before spectral broadening (bold, middle). The spectrally broadened pulses are passed through a chirped-mirror compressor, yielding sub-6-fs, 6-nJ pulses in a diffraction-limited beam.

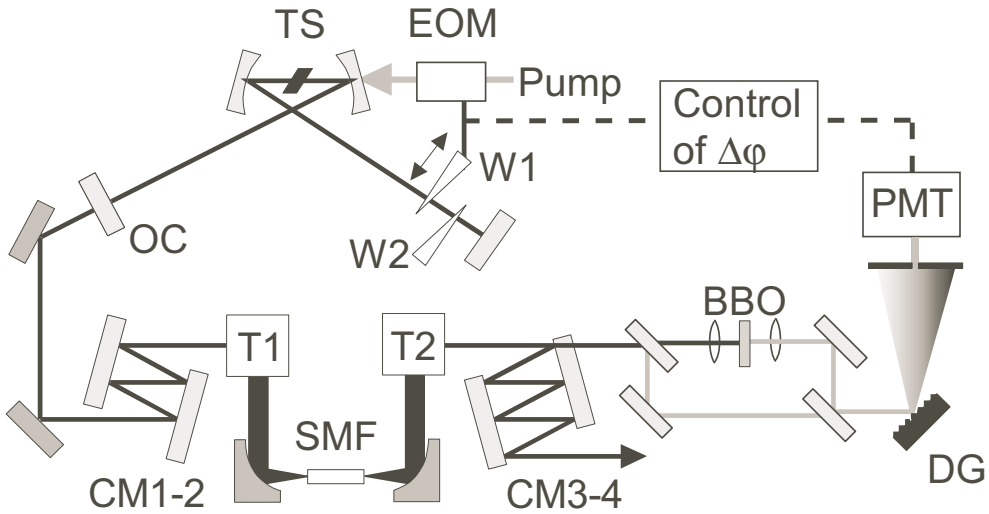


Figure 3.39: The fs laser used in the Vienna experiment. It features pulses below 6 fs, with a peak power exceeding 1 MW and a 24 MHz repetition frequency. Not shown is the intra cavity telescope to reach the 24 MHz repetition rate. (TS Ti:sapphire crystal, EOM electro optic modulator, OC output coupler, W Wedges, CM chirped mirrors for compression, SMF single mode fiber for self phase modulation, T telescope for mode matching, DG diffraction grating, PMT photo multiplier)

A dichroic chirped mirror CM4 in the compressor transmits the spectral components near 1080 nm and 540 nm.

In a first experiment a 1-mm-thick BBO doubling crystal oriented for type-I phase matching at ≈ 1080 nm has been placed in close proximity of the fiber output to maximize frequency doubling efficiency. In an improved version a nonlinear interferometer has been inserted as already described in the preceding sections, which beats the second harmonic of the 1080-nm wave packet with the 540-nm wave packet selected from the fundamental spectrum. The resultant beat note arises at f_0 and exhibits an improved signal-to-noise ratio (> 30 dB in 100 kHz bandwidth). The overlapping portions of the spectra are dispersed by a diffraction grating and directed through a polarizer and a slit onto a photomultiplier. The polarizer has been aligned to permit interference between the orthogonally polarized fundamental and frequency-doubled laser fields.

We have phase locked the carrier-slip beat note to $f_{local} = 1$ MHz by adjusting the pump power with an electro-optic modulator (EOM) as introduced in chapter 2.3. This servo loop relies on intra cavity nonlinearities, translating a minor change of W into a significant change of $\Delta\varphi$ and hence that of f_0 . Once f_0 is manually adjusted by translating a thin fused-silica wedge (W2 in Fig. 3.39) to be within $f_{local} \pm 100$ kHz the servo loop pulls f_0 to f_{local} and phase-locks the carrier-slip beat note to the signal of the local oscillator using our digital phase lock electronics described in appendix A. The same nonlinearities are used as a diagnostic tool, for determining the sub-cycle jitter of φ , which is indispensable for reproducible waveform generation as discussed below.

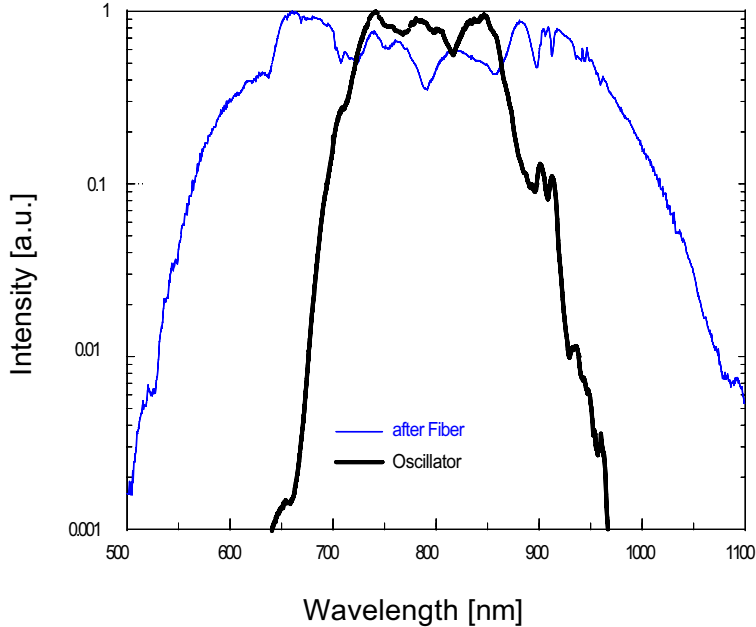


Figure 3.40: Spectrum of the Vienna laser before (bold, middle) and after broadening in a short piece (3 mm) of standard single mode fiber.

The phase locked f_0 beat signal is depicted in Fig. 3.41. Our cycle slip detection scheme (i.e. counting the in lock beat signal to make sure that there is no deviation between f_0 and f_{local}) assures us that the servo loop works properly over extended periods of time.

It is important to note that the generation of phase-stable few-cycle pulses at the output of the fiber/chirped-mirror compressor by locking f_0 to zero or an preset offset in the present scheme does not strictly imply phase stabilization directly at the output of the mode-locked oscillator as well. This is because drift or fluctuations in the pulse parameters at the fiber input and in the fiber parameters (e.g. temperature, refractive index) may be translated into a corresponding change in φ by linear and nonlinear effects [59]. The resultant time-dependent shift of φ then emerges with opposite sign at the output of the oscillator, if φ is stabilized at the fiber output. Nevertheless, in the present case these external fluctuations and drifts in φ are estimated as very low ($< \pi/50$) owing to the high pulse energy stability, moderate spectral broadening in the fiber, and the short fiber length.

Also note that this degree of control can be achieved without stabilizing f_r to an rf local oscillator. Minor variations in f_r merely shift the instants at which a pulse exits the laser without affecting phase locking, because the latter is performed at $f_{local} \ll f_r$ and is hence incapable of resolving this event. With f_r freely floating the absence of synchronism of the pulse train with f_{local} has some negative implications. This source of carrier envelope phase uncertainty can be fully eliminated by deriving f_{local} from f_r via frequency division.

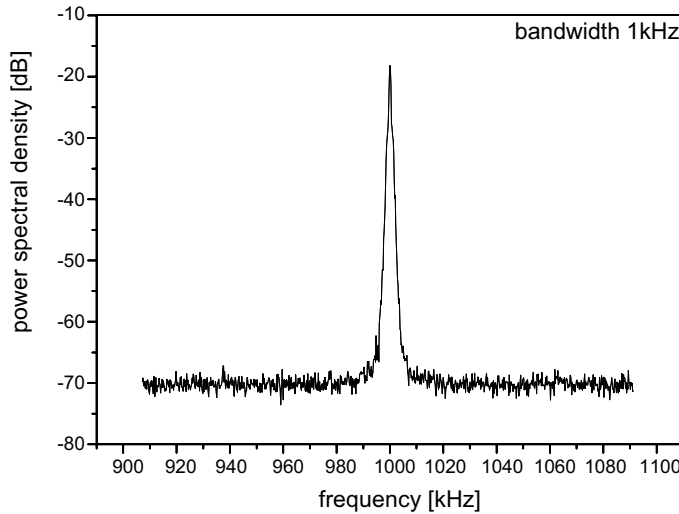


Figure 3.41: Carrier envelope offset beat f_0 phase locked to 1 MHz.

As discussed above, cycle slip free operation is necessary but not sufficient for synthesizing reproducible waveforms in the time domain. To gain direct optical access to the sub-cycle jitter of φ_n , we utilize that the parameter primarily controlled by the servo loop, namely the pulse energy W_n , can be directly and permanently monitored and is directly connected to $\Delta\varphi_n$. As a consequence, the carrier-envelope phase jitter $\sigma_{\varphi(W)}$ that accumulates over the measurement time T_m due to (controlled or random) variation of W_n can be determined from the power spectral density $S_W(f)$ of pulse energy variations [59] as

$$\sigma_{\varphi(W)}(T_m) = \frac{W_0}{\sqrt{2}\pi} \left| \frac{\partial \Delta\varphi}{\partial W} \right|_{W_0} \left(\int_{1/T_m}^{f_r/2} S_W(f) \frac{f_r^2}{f^2} df \right)^{1/2}, \quad (3.9)$$

where W_0 is the average intracavity pulse energy and we have made use of the approximately linear dependence of $\Delta\varphi$ on $\Delta W/W$ with a slope of $W_0 |\partial \Delta\varphi / \partial W|_{W_0} = 2$ rad at $W_0 = 60$ nJ⁵.

Fig. 3.42 depicts the measured $S_W(f)$ (lower left) and the calculated $\sigma_{\varphi(W)}(T_m)$ (upper right) for phase-locked (thin black) as well as unlocked (thick gray) operation. For more details see Ref. [145]. The increase of $\sigma_{\varphi(W)}$ with T_m well beyond 2π for $T_m > 0.1$ s can be reconciled with the observation of cycle-slip-free operation by assuming substantial carrier-envelope phase jitter originating from effects other than pulse energy fluctuations at frequencies $f_{noise} < 100$ Hz. In this range a significant fraction of the pulse energy fluctuations have to be “rephased” by the control loop to compensate a jitter from other sources and $\sigma_{\varphi(W)}$ mirrors this jitter.

Although the phase jitter originating from effects other than energy noise rapidly increases with T_m (see upper thick grey line in Fig. 3.42), energy-noise-induced phase

⁵Expression (3.9) is obtained by replacing in Eq. (3) of Ref. [59] the lower boundary of integration with $1/T_m$, rather than the higher boundary, as mistakenly stated in the context of Fig. 3 in Ref. [59].

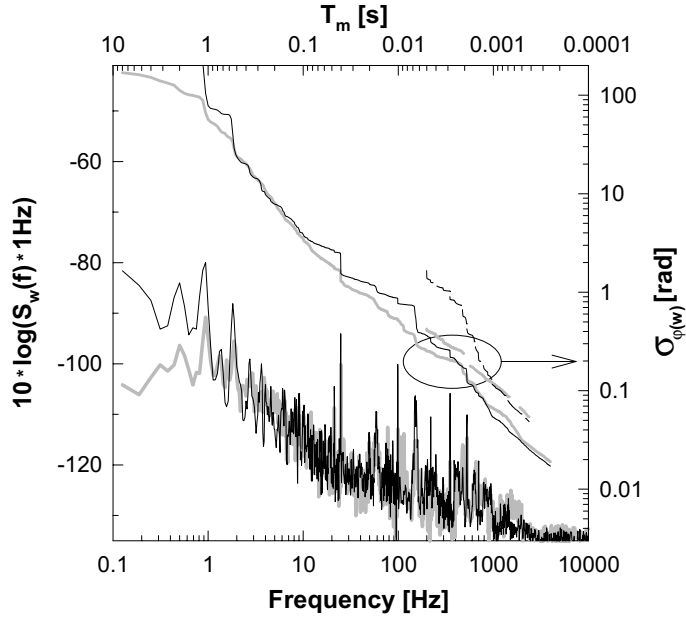


Figure 3.42: Lower traces: power spectral density $S_W(f)$ of the pulse energy fluctuations at the output of the Ti:sapphire laser with the servo loop opened (thin black line) and closed (thick grey line). Upper traces: carrier envelope phase jitter $\sigma_{\varphi(W)}$ as a function of the measurement time T_m introduced by pulse energy fluctuations, with the servo loop open (thin black full and dashed lines) and closed (thick grey lines). The dashed lines represent a different data set with a somewhat noisier laser. The arrow indicates the phase jitter level (≈ 0.2 rad) at which the servo loop starts responding.

jitter becomes dominant for measurement times $T_m > 1$ sec., as indicated by the dramatic noise reduction under locked conditions at frequencies below 1 Hz. This leads to a root mean square of the residual pulse energy fluctuations of $\sigma_W \approx 0.01\%$ over the spectral range of 0.1 Hz - 0.1 MHz at the output of the carrier-envelope-phase-locked oscillator, which is, to our knowledge, an unprecedented value. This is enhanced by somewhat less than a factor of 10 at the fiber output (due presumably to mechanically-induced beam pointing instabilities at the fiber input), resulting in a reproducibility of the field amplitudes to within less than 0.05% (corresponding to $\sigma_W \approx 0.1\%$) in the sub-6-fs pulse train.

As compared to the sub-Hz regime, smaller but clearly notable and reproducible damping of pulse energy fluctuations is caused by the servo loop in the range from 10 Hz to 1 kHz, as it is evident from a corresponding suppression of $\sigma_{\varphi(W)}$, indicating the dominance of energy noise in this range. In repeated measurements (see also dashed lines), $\sigma_{\varphi(W)}$ gets reproducibly suppressed at frequencies where it approaches ≈ 0.3 rad for increasing T_m . The highest frequency at which the suppression of $\sigma_{\varphi(W)}$ sets in has ranged from 500 Hz to 1000 Hz in our experiments, depending on the relevant noise level (with the loop opened), which has varied somewhat in repeated measurements. Because energy-noise-induced jitter appears to dominate for $T_m < 10$ ms, from these

observations we may infer that the jitter of the carrier-envelope phase is kept safely below 0.3 rad by the servo loop, corresponding to a phase error of less than $\pi/10$. It will be interesting to see, whether the carrier-envelope phase jitter can be further lowered by reducing f_{ceo} , increasing the servo bandwidth and by deriving f_{local} from f_r via frequency division in the future.

Note that optical waveform synthesis is only useful if the pulses merely comprise a few oscillation cycles of the light field. Only in this case becomes the absolute phase relevant in light matter interactions. To this end the broad spectra created with the help of photonic crystal fibers would have to be recompressed which has not been done to date due to the higher order dispersion that these fibers introduce.

To conclude we have seen that phase locking of the carrier offset frequency reduces the intensity noise of a few cycle fs laser and freezes the time evolution of absolute phase φ . Although this absolute phase is still unknown, a pulse picker can now be triggered to pick pulses that have the same (unknown) absolute phase. By varying the trigger phase the absolute phase can be scanned and this opens the door for exploring nonlinear phase sensitive optical effects. In spite of the similarities in the techniques we have discussed different requirements for synthesizing frequencies and waveforms. Note that the requirements on the stability seem to converge again as the fs frequency combs are used to transfer the superior stability of optical sources down to the rf regime.

Upon their observation, phase-sensitive nonlinear optical effects can immediately be exploited for determining the absolute value of φ and assigning it to the corresponding trigger phase in the demonstrated few-cycle waveform generator. This step will, in combination with shaping the amplitude envelope and tailoring the chirp by frequency-domain techniques [150], allow the synthesis of few-cycle light with arbitrary waveforms. Extending this capability from radio frequencies to the optical regime opens up new prospects in a number of fields where light is used for triggering, tracing and controlling microscopic processes.

The ideas and results presented here have been published in part in Physical Review Letters [32] and have in part been accepted at Applied Physics B for publication.

Chapter 4

Conclusion and Outlook

The single laser $f : 2f$ frequency chain appears as the natural endpoint of a 30 year long development to measure optical frequencies. It uses a single fs laser and is nevertheless capable of phase coherently linking the rf and the optical domain.

It has now reached a stage where it can be easily and reliably operated over extended periods of time as a clockwork for future all optical clocks. Here it will transfer the superior accuracy and stability of an optical clock to the rf domain.

As a good candidate for an optical oscillator in such a clock application are ions trapped in rf traps. In section 2.5 we have investigated an indium ion towards its use as an optical frequency standard and this work is to be continued. Other groups around the world are working towards the same direction with other ions like strontium [16] and mercury [4]. As of the writing of this text the groups of L. Hollberg and J. Bergquist are measuring a suitable clock transition in mercury now rivaling the 1S-2S transition in hydrogen for the most precise optical frequency measurement [26] with just the same setup as described in here.

Patents for this new technology are pending and we expect that a final turn key “Optical Frequency Synthesizer” is not too far down the road.

For the first time precise optical frequency synthesis is now available even for small scale spectroscopy laboratories.

The hydrogen spectroscopy setup is now the limiting factor for the determination of the 1S-2S transition. Further improvements in our setup are underway and a future source of ultracold hydrogen atoms for spectroscopy might be a Bose Einstein condensate as investigated in D. Kleppner's group at MIT, Boston, USA [127]. Nonetheless, after more than a century of spectroscopic experiments, the hydrogen atom still holds substantial challenges and opportunities for further dramatic advances. In the future, it may reveal possible slow changes of fundamental constants or, with the antihydrogen experiments now under preparation at CERN [31], conceivable differences between matter and antimatter.

We believe that the development of accurate optical frequency synthesis marks only the beginning of an exciting new period of ultra-precise physics.

And also ultra-fast physics is starting out into a new age. The presented results in the time domain open the way to generating few-cycle light pulses focusable to intensities up to 10^{18} W/cm² and beyond with precisely reproducible electric and magnetic fields. Exposing matter to these ultraintense electromagnetic transients will allow unprecedented control of optical field ionization of atoms and subsequent motion of the freed electron wave packets in strong fields. Anticipated impacts of this new experimental capability include the controlled generation of isolated attosecond bursts of coherent soft-X-ray radiation and highly-collimated relativistic electron pulses with sub-laser-cycle duration.

Appendix A

Phase locking optical frequencies

Some technical details about phase locking of optical frequencies that might be of interest to some readers are collected here. The digital phase detectors applied in many of our experiments and illustrated in Fig. A.2 are extensively described in Ref. [61]. Phase locked loops allow us to transfer frequency information from one oscillator to another without loosing accuracy. This is subject of many textbooks. An excellent one is the text of Gardner [151].

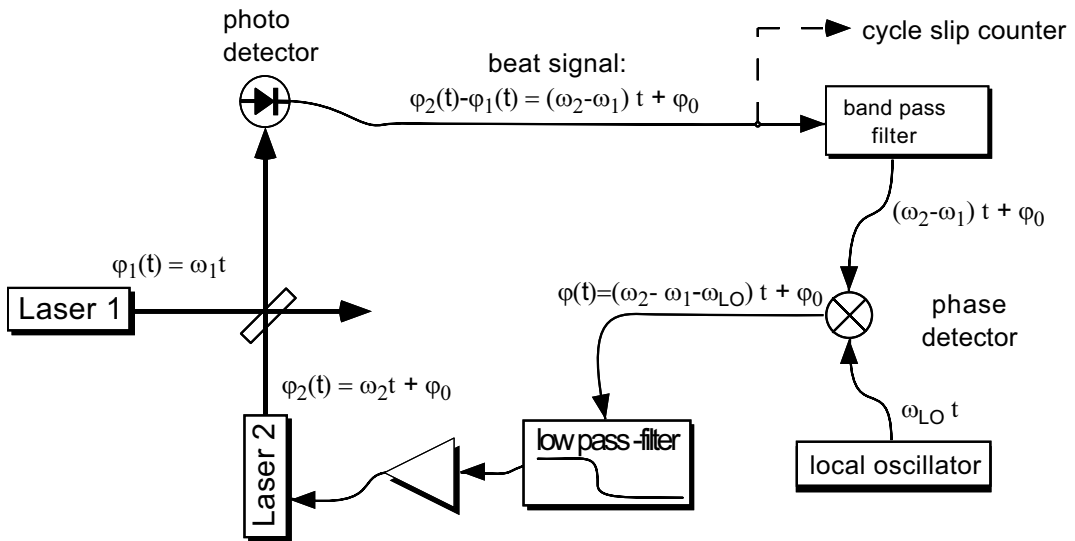
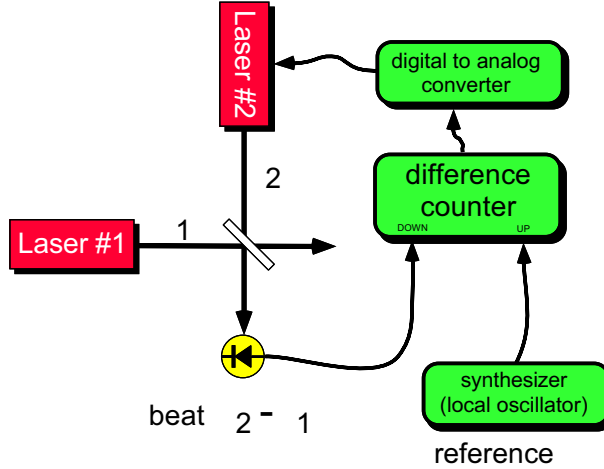


Figure A.1: Principle of a phase locked loop.

A typical setup for a phase locked loop is described in Fig. A.1. The beat signal between two laser beams $E_1(t) = E_1 e^{-i\omega_1 t}$ and $E_2(t) = E_2 e^{-i\omega_2 t - \varphi_0}$ is observed on a photo detector. A signal proportional to $I(t) \propto |E_1(t) + E_2(t)|^2 = E_1^2 + E_2^2 + 2E_1 E_2 \cos((\omega_2 - \omega_1)t + \varphi_0)$ is created. In a phase detector the phase difference between this signal and a local oscillator is formed. The loop is closed by feeding back the signal to one of the lasers in order to keep the phase constant.



$$f_2 = f_1 + f_{LO}$$

Figure A.2: Principle of a digital phase locked loop.

Fig. A.2 illustrates the principle of our digital phaselocks. By permitting a larger RMS phase error than analog detectors, it can be operated at substantially lower locking bandwidth and allows very stable phase locking. The basic element of this phase detector is a counter where the local oscillator counts up and the beat signal counts down. The counter has a range from 0 to 16 and is initialized at 8. Therefore the phase detector can track a $\pm 16\pi$ phase difference between the two sources. Fig. A.3 illustrates the output signal for two slightly different input signals. This signal is fed into a digital to analog converter to generate a signal proportional to the relative phase.

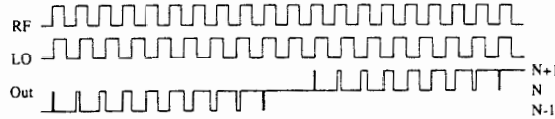


Figure A.3: Two slightly different input signals at the digital PLL and the corresponding output.

Appendix B

Helium Neon standard

The transportable Helium Neon standard was developed at the Institute of Laser Physics in Novosibirsk, Russia. During the measurements reported here it was operated by P. Pokasov who has been a visiting scientist from Novosibirsk, Russia at that time.

It actually consists of three lasers. One of them, the so called reference laser is locked onto a methane resonance at relatively high power (≈ 1 mW) and relatively high methane pressure ($\approx 5 \times 10^{-3}$ mbar to obtain a strong error signal. This laser tube provides the stability of the system. The second tube is operated at lower power with a larger beam diameter and smaller methane pressure and resolves the hyperfine structure of the transition. This laser tube delivers the accuracy of the system. Finally a third laser (heterodyne laser) serves as connection between the two and delivers ≈ 1 mW of output power. Details are elaborated in [65], and the PhD thesis of Th. Udem gives an extensive overview [37].

It was previously (1996) calibrated for a measurement of the hydrogen 1S - 2S absolute frequency [6, 37] by transporting it to the harmonic frequency chain at the Physikalisch Technische Bundesanstalt (PTB) in Braunschweig, Germany. In repeated sessions the frequency was determined to be $f_{He-Ne} = 88\,376\,182\,599\,937\,(23)$ Hz.

As a side result of the Hydrogen measurement described in chapter 3.2 we have at the same time also measured the He–Ne frequency as part of the frequency chain against the cesium fountain clock to

$$f_{He-Ne} = 88\,376\,182\,599\,976\,(10) \text{ Hz}$$

This value deviates from the previous one by 39 Hz (1.6 combined standard deviations), most likely because the operating parameters were not exactly maintained for several years.

The new calibration was done 4 months before the measurement of the In^+ clock transition and the iodine lines. Unlike in the previous calibration, the laser was not moved between its calibration and the measurement so that alignment dependent operating parameters are better conserved.

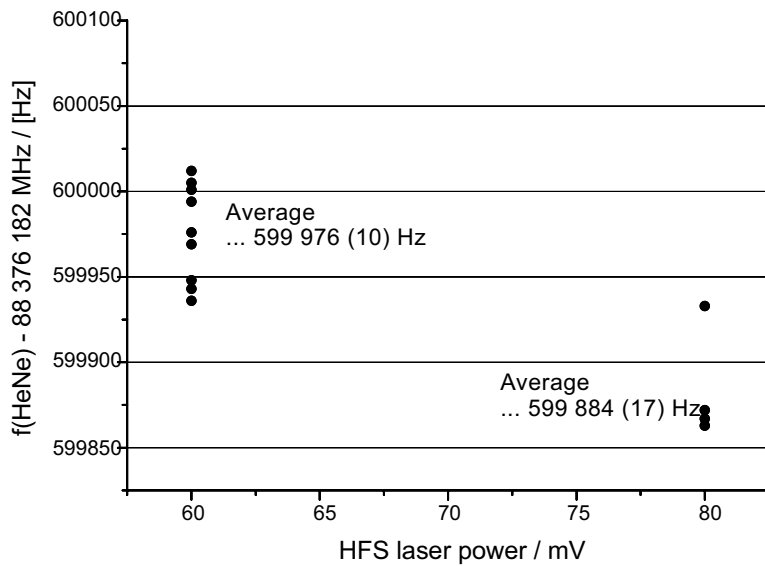


Figure B.1: Calibration of the HeNe standard during the measurement of the hydrogen 1S-2S transition with a cesium fountain clock. For operation parameters see text.

Bibliography

- [1] N. Bloembergen, ed., *Nonlinear Spectroscopy*, Proceedings of the International School of Physics “Enrico Fermi”, North Holland Publ. Co., (1977)
- [2] G. F. Bassani, M. Inguscio, and T. W. Hänsch (eds.), *The Hydrogen Atom*, Springer-Verlag, Berlin (1989).
- [3] T. W. Hänsch and M. Inguscio, eds., *Frontiers in Laser Spectroscopy*, Proceedings of the International School of Physics “Enrico Fermi”, North Holland Publ. Co., (1994)
- [4] B.C. Young, F.C. Cruz, W.M. Itano and J.C. Bergquist, Phys. Rev. Lett. **82**, 3799 (1999).
- [5] Th. Udem, J. Reichert, R. Holzwarth and T. W. Hänsch, Phys. Rev. Lett. **82**, 3568 (1999).
- [6] Th. Udem, A. Huber, B. Gross, J. Reichert, M. Prevedelli, M. Weitz and T. W. Hänsch, Phys. Rev. Lett. **79**, 2646 (1997).
- [7] C. Schwob, L. Jozefowski, B. de Beauvoir, L. Hilico, F. Nez, L. Julien, F. Biraben, Phys. Rev. Lett. **82**, 4960 (1999).
- [8] V.A. Dzuba, V.V. Flambaum and J.K. Webb, Phys. Rev. Lett. **82**, 888 (1999); V.A. Dzuba and V.V. Flambaum, Phys. Rev. A **61**, 034502 (2000).
- [9] See, for example, N. Ramsey, *Proc. of the XXXth Rencontre de Moriond*, p. 357, Eds.: B. Guiderdoni, G. Greene, D. Hinds, J. Tran Thanh Van, Editions Frontieres, Gif-sur-Yvette (1995).
- [10] Recommendation adopted by the Comité International des Poids et Mesures at its 86th meeting: T. J. Quinn, Metrologia, **30**, 523, (1993/1994); T. Quinn, Metrologia, **36**, 211, (1999).
- [11] J. Reichert, M. Niering, R. Holzwarth, M. Weitz, Th. Udem, and T.W. Hänsch, Phys. Rev. Lett., **84**, 3232, (2000).
- [12] M. Niering, R. Holzwarth, J. Reichert, P. Pokasov, Th. Udem, M. Weitz, T. W. Hänsch, P. Lemonde, G. Santarelli, M. Abgrall, P. Laurent, C. Salomon, A. Clairon, Phys. Rev. Lett., **84**, 5496, (2000).

- [13] F. Riehle, H. Schnatz, B. Lippardt, G. Zinner, T. Trebst, and J. Helmcke, IEEE Trans. Instrum. Meas., **48**, 613, (1999); see also: H. Schnatz, B. Lippardt, J. Helmcke, F. Riehle, and G. Zinner, Phys. Rev. Lett., **76**, 18, (1996).
- [14] S. N. Bagayev, V. P. Chebotayev, Usp. Fiz. Nauk, **148**, 143 (1986)
- [15] J. von Zanthier, Th. Becker, M. Eichenseer, A. Yu. Nevsky, Ch. Schwedes, E. Peik, H. Walther, R. Holzwarth, J. Reichert, Th. Udem, T. W. Hänsch, P. V. Pokasov, M. N. Skvortsov, S. N. Bagayev, Opt. Lett. **25**, 1729 (2000).
- [16] J. E. Bernard, A. A. Madej, L. Marmet, B. G. Whitford, K. J. Siemsen, and S. Cundy, Phys. Rev. Lett., **82**, 3228, (1999).
- [17] H. Schnatz, B. Lippardt, J. Helmcke, F. Riehle and G. Zinner, Phys. Rev. Lett. **76**, 18 (1996).
- [18] B. de Beauvoir, F. Nez, L. Julien, B. Cagnac, F. Biraben, D. Touahri, L. Hilico, O. Acef, A. Clairon and J. J. Zondy, Phys. Rev. Lett. **78**, 440 (1997).
- [19] Th. Udem, J. Reichert, R. Holzwarth, and T. W. Hänsch, Opt. Lett., **24**, 881, (1999).
- [20] J. N. Eckstein, A. I. Ferguson, and T. W. Hänsch, Phys. Rev. Lett. **40**, 847 (1978).
- [21] V. P. Chebotayev and V. A. Ulybin, Appl. Phys. B **50**, 1 (1990).
- [22] J. C. Knight, T. A. Birks, P. St. J. Russell and D. M. Atkin, Opt. Lett. **21** 1547 (1996)
- [23] J. K. Ranka, R. S. Windeler and A. J. Stentz, Opt. Lett. **25**, 25 (2000).
- [24] R. Holzwarth, Th. Udem, T. W. Hänsch, J. C. Knight, W. J. Wadsworth, P. St. J. Russel, Phys. Rev. Lett., **85**, 2264 (2000).
- [25] D. J. Jones, S. A. Diddams, J. K. Ranka, A. Stentz, R. S. Windeler, J. L. Hall, S. T. Cundiff, Science **288**, 635 (2000).
- [26] L. Hollberg, Private communication.
- [27] S. A. Diddams, D. J. Jones, Jun Ye, S. T. Cundiff, J. L. Hall, J. K. Ranka, R. S. Windeler, R. Holzwarth, Th. Udem, T. W. Hänsch, Phys. Rev. Lett., **84**, 5102, (2000).
- [28] M. Bellini and T. W. Hänsch, Opt. Lett. **25**, 1049 (2000).
- [29] M. Bellini, C. Lynga, A. Tozzi, M. B. Gaarde, T. W. Hänsch, A. L'Huillier, C. G. Wahlstrom, Phys. Rev. Lett. **81**, 297 (1998).
- [30] A. Huber, Th. Udem, B. Gross, J. Reichert, M. Kourogi, K. Pachucki, M. Weitz, and T. W. Hänsch, A. Huber, Phys. Rev. Lett. **80**, 468 (1998).

- [31] J. Eades and F. J. Hartmann, Rev. Mod. Phys. **71**, 373 (1999).
- [32] A. Apolonski, A. Poppe, G. Tempea, Ch. Spielmann, Th. Udem, R. Holzwarth, T. W. Hänsch, f. Krausz Phys. Rev. Lett. **85**, 740 (2000).
- [33] D. McIntyre and T. W. Hänsch, *Digest of the Annual Meeting of the Optical Society of America*, paper ThG3, Washington D.C. (1988). See also T.W. Hänsch in Proceedings of *The Hydrogen Atom*, edited by G. F. Bassani et al., Berlin: Springer 1989, or H. R. Telle, D. Meschede, and T. W. Hänsch, Opt. Lett. **15**, 532 (1990).
- [34] M. Kurogi, T. Enami, and M. Ohtsu, IEEE Photon. Technol. Lett. **6**, 214 (1994).
- [35] M. Kurogi, B. Widjyatomo, Y. Takeuchi, and M. Ohtsu, IEEE J. Quantum Electron. **31**, 2120 (1995).
- [36] M. Kurogi, T. Enami, and M. Ohtsu, IEEE Photon. Technol. Lett. **8**, 1698 (1996).
- [37] Th. Udem, PhD thesis, Ludwig-Maximilians-Universität, Munich (1997)
- [38] J. Reichert, PhD thesis, Ludwig-Maximilians-Universität, Munich (2000)
- [39] J. von Zanthier, J. Abel, Th. Becker, M. Fries, E. Peik, H. Walther, R. Holzwarth, J. Reichert, Th. Udem, T. W. Hänsch, A. Yu. Nevsky, M. N. Skvortsov, and S. N. Bagayev, Opt. Comm., **166**, 57, (1999).
- [40] A. I. Ferguson, J. N. Eckstein, and T. W. Hänsch, Appl. Phys. **18**, 257 (1979).
- [41] Y. V. Baklanov and V. P. Chebotayev, Appl. Phys. **12**, 97 (1977).
- [42] D. J. Wineland, J. C. Bergquist, W. M. Itano. F. Diedrich and C. S. Weimer, Proceedings of *The Hydrogen Atom*, edited by G. F. Bassani, M. Inguscio and T. W. Hänsch, Berlin: Springer 1989.
- [43] D. M. Kane, S. R. Bramwell and A. I. Ferguson, Appl. Phys. **B 39**, 171 (1986).
- [44] J. Reichert, R. Holzwarth, Th. Udem, T.W. Hänsch, Opt. Comm., **172**, 59, (1999).
- [45] C. Rulliere (Ed.), *Femtosecond laser pulses*, Springer, Berlin (1998).
- [46] J. C. Diels and W. Rudolph, *Ultrashort Laser Pulse Phenomena*, Academic Press, San Diego (1996).
- [47] A. Kasper, PhD thesis, Technische Universität München (1997).
- [48] G. P. Agrawal, *Nonlinear Fiber Optics*, 2nd edition, Academic Press, San Diego (1995).
- [49] H. A. Haus and A. Mecozzi, IEEE J. Quant. Electron. **29**, 983 (1993).

- [50] F. Krausz, M.F. Fermann, T. Brabec, P.F. Curley, M. Hofer, M.H. Ober, C. Spielmann, E. Wintner and A.J. Schmidt: IEEE J. Quant. Electron. **28**, 2097 (1992)
- [51] R. Szipöcs, and R. Kohazi-Kis, Appl. Phys. B **65**, 115 (1997).
- [52] U. Morgner, F.X. Kärtner, S.H. Cho, Y. Chen, H.A. Haus, J.G. Fujimoto, E.P. Ippen, V. Scheuer, G. Angelow and T. Tschudi, Opt. Lett. **24**, 411 (1999).
- [53] D.H. Sutter, L. Gallmann, M. Matuschek, F. Morier-Genoud, V. Scheuer, G. Angelow, T. Tschudi, G. Steinmeyer and U. Keller, Appl. Phys. B **70**, 5 (2000).
- [54] T. Brabec and F. Krausz, Rev. Mod. Phys. **72**, 545 (2000).
- [55] R. L. Fork, O. E. Martinez, and J. P. Gordon, Opt. Lett. **9** 150 (1984).
- [56] J. A. Valdmanis, R. L. Fork, IEEE J. Quantum Electron. **22**, 112 (1986).
- [57] D.E. Spence, CP.N. Kean and W.Sibbett, Opt. Lett. **16**, 42 (1991)
- [58] M.T. Asaki, C.P. Huang, D. Garvey, J.P. Zhou, H.C. Kapteyn and M.M. Murnane, Opt. Lett. **18**, 977 (1993)
- [59] L. Xu, Ch. Spielmann, A. Poppe, T. Brabec, F. Krausz, T. W. Hänsch, Opt. Lett. **21**, 2008 (1996).
- [60] L. Ricci, M. Weidemüller, T. Esslinger, A. Hemmerich, C. Zimmermann, V. Vuletic, W. König and T. W. Hänsch, Opt. Comm. **117**, 541 (1995).
- [61] M. Prevedelli, T. Freegarde, and T. W. Hänsch, Appl. Phys. B **60**, 241 (1995).
- [62] F. L. Walls et al., IEEE Trans. Instrum. Meas. **24**, 210 (1975).
- [63] S. A. Diddams, D. J. Jones, L. S. Ma, S. T. Cundiff and J. L. Hall, Opt. Lett. **25**, 186 (2000).
- [64] H. R. Telle, G. Steinmeyer, A. E. Dunlop, J. Stenger, D. H. Sutter and U. Keller, Appl. Phys. B **69**, 327 (1999).
- [65] S. N. Bagayev, A. K. Dmitriyev and P. V. Pokasov, Laser Physics, **7**, 989, (1997).
- [66] Kinoshita T., Rep. Prog. Phys. **59**, 1459 (1996), and references therein.
- [67] P. J. Mohr and B. N. Taylor, Rev. Mod. Phys. **72**, 351 (2000).
- [68] B. C. Young, PhD thesis, Stanford University (1997).
- [69] D. L. Farnham, R. S. Van Dyck, and P. B. Schwinberg, Phys. Rev. Lett. **75**, 3598 (1995).

- [70] M. P. Bradley, J. V. Porto, S. Rainville, J. K. Thompson, and D. E. Pritchard, Phys. Rev. Lett. **83**, 4510 (1999).
- [71] K. H. Weber, and C. J. Sansonetti, Phys. Rev. A **35**, 4650 (1987).
- [72] A. Peters *et al.*, Phil. Trans. R. Soc. Lond. A **355**, 2223 (1997).
- [73] R. Grimm, and J. Mlynek, Appl. Phys. B **49**, 179 (1989).
- [74] V. Vuletić *et al.*, Opt. Comm. **99**, 185 (1993).
- [75] R. J. Rafac, and C. E. Tanner, Phys. Rev. A **56**, 1027 (1997).
- [76] *Proc. of the 5th Symp. on Freq. Standards and Metrology*, Woods Hole, MA, USA, 15-19 Oct. 1995, Ed.: J.C. Bergquist, World Scientific, Singapore (1996).
- [77] J.C. Bergquist, W.M. Itano, F. Elsner, M.G. Raizen, D.J. Wineland, *Light Induced Kinetic Effects on Atoms, Ions and Molecules*, p. 291, Eds.: L. Moi, S. Gozzini, C. Gabbanini, E. Arimondo, F. Strumia, ETS Editrice, Pisa (1991).
- [78] J.E. Bernard, L. Marmet, A.A. Madej, Opt. Comm. **150**, 170 (1998).
- [79] J.E. Bernard, A.A. Madej, L. Marmet, B.G. Whitford, K.J. Siemsen, S. Cundy, Phys. Rev. Lett. **82**, 3228 (1999).
- [80] E. Peik, G. Holleman, H. Walther, Phys. Rev. A **49**, 402 (1994).
- [81] E. Peik, G. Holleman, H. Walther, Phys. Scr. T **59**, 403 (1995).
- [82] E. Peik, J. Abel, Th. Becker, J. von Zanthier, H. Walther, Phys. Rev. A **60**, 439 (1999).
- [83] Th. Becker, J. von Zanthier, A.Yu. Nevsky, Ch. Schwedes, M.N. Skvortsov, H. Walther, E. Peik, to be published.
- [84] H. Dehmelt, IEEE Trans. Instrum. Meas. **31**, 83 (1982).
- [85] A. N. Goncharov, A. Y. Nevsky and M. N. Skvortsov, Appl. Phys. B **62**, 427 (1996).
- [86] A. N. Goncharov, A. Y. Nevsky and M. N. Skvortsov, Appl. Phys. B **60**, 43 (1995).
- [87] S. Gerstenkorn and P. Luc, “Atlas du spectre d’absorption de la molecule d’iode 14800 - 20000 cm⁻¹”. Complement: Identification des transitions du systeme (B-X), *Editions du CNRS*, Paris, (1985).
- [88] J. Ye, L. Robertson, S.Picard, L. S. Ma and J.Hall, IEEE Trans. Instrum. Meas., **48**, 544 (1999).
- [89] B. Bodermann, M. Klug, U. Winkelhoff, H. Knöckel and E. Tiemann, Eur. Phys. J. D, **11**, 213 (2000).

- [90] J. Ye, T. H. Yoon, J. L. Hall, A. A. Madej, J. E. Bernard, K. J. Siemsen, L. Marmet, J. M. Chartier and A. Chartier, Phys. Rev. Lett. **85**, 3797 (2000).
- [91] J. A. Barnes, A. R. Chi, L. S. Cutler, D. J. Healey, D. B. Leeson, T. E. McGunigal, J. A. Mullen, W. L. Smith, R. L. Sydnor, R. F. C. Vessot and G. M. R. Winkler, IEEE Trans. Instrum. Meas. **IM-20**, 105 (1971).
- [92] J. Ye, L. Robertsson, S. Picard, L.-S. Ma and J. L. Hall, IEEE Trans. Instrum. Meas., **48**, 544, (1999).
- [93] H. Darnedde, W. R. C. Rowley, F. Bertinetto, Y. Milleroux, H. Haitjema, S. Wetzel, H. Piree, E. Prieto, M. Mar Perez, B. Vaucher, A. Chartier, J.-M. Chartier, Metrologia, **36**, 199, (1999).
- [94] M. Eickhoff and J. L. Hall, IEEE Trans. Instrum. Meas., **44**, 155, (1995).
- [95] R. Storz, C. Braxmeier, K. Jäck, O. Pradl, and S. Schiller, Opt. Lett., **23**, 1031, (1998).
- [96] A. Arie, S. Schiller, E. K. Gustafson, and R. L. Byer, Opt. Lett., **17**, 1204, (1992).
- [97] A. Arie and R. L. Byer, J. Opt. Soc. Am. B **10**, 1990, (1993).
- [98] P. A. Jungner, S. Swartz, M. Eickhoff, J. Ye, J. L. Hall, and S. Waltman, IEEE Trans. Instrum. Meas., **44**, 151, (1995).
- [99] J. L. Hall, L.-S. Ma, M. Taubman, B. Tiemann, F.-L. Hong, O. Pfister, and J. Ye, IEEE Trans. Instrum. Meas., **48**, 583, (1999).
- [100] R. W. P. Drever, J. L. Hall, F. V. Kowalski, J. Hough, G. M. Ford, A. J. Munley, H. Ward, Appl. Phys. B, **31**, 97, (1983).
- [101] P. Cordiale, G. Galzerano, and H. Schnatz, Metrologia, **37**, 177, (2000).
- [102] F. Bayer-Helms, J. M. Chartier, J. Helmcke, and A. Wallard, PTB Bericht, vol. ME-17, 139, (1977).
- [103] A. Nevsky, R. Holzwarth, J. Reichert, Th. Udem, T. W. Hänsch, J. von Zanthier, H. Walther, H. Schnatz, F. Riehle, P. V. Pokasov, M. N. Skvortsov and S. N. Bagayev, submitted for pulication
- [104] see articles in *The Hydrogen Atom*, G. F. Bassani, M. Inguscio and T. W. Hänsch (eds.), (Springer-Verlag, Berlin, 1989).
- [105] N. F. Ramsey, Rev. Mod. Phys. **62**, 541 (1990).
- [106] G. Santarelli, Ph Laurent, P. Lemonde, A. Clairon, A. G. Mann, S. Chang, A. N. Luiten and C. Salomon, Phys. Rev. Lett. **82**, 4619 (1999).
- [107] P. Lemonde *et al.*, in *Frequency Measurement and Control*, A. N. Luiten (ed.), (Springer-Verlag, Berlin, 2000).

- [108] M. Niering, PhD thesis, Ludwig-Maximilians-Universität, Munich (2000)
- [109] A. Huber, PhD thesis, Ludwig-Maximilians-Universität, Munich (1998)
- [110] A. Huber, B. Gross, M. Weitz and T. W. Hänsch, Phys. Rev. A **59**, 1844 (1999).
- [111] K. Pachucki et al., J. Phys. **B** **29**, 177 (1996) + erratum p. 1573.
- [112] J. R. Sapirstein and D. R. Yennie, *Quantum Electrodynamics*, edited by T. Kinoshita, Singapore: World Scientific, 1990.
- [113] B. de Beauvoir, F. Nez, L. Julien, B. Cagnac, F. Biraben, D. Touahri, L. Hilico, O. Acef, A. Clairon and J. J. Zondy, Phys. Rev. Lett. **78**, 440 (1999).
- [114] S. R. Lundeen and F. M. Pipkin, Phys. Rev. Lett. **46**, 232 (1981).
- [115] E. W. Hagley and F. M. Pipkin, Phys. Rev. Lett. **72**, 1172 (1994).
- [116] S.G. Karshenboim, Z. Phys. **D** **39**, 109 (1997).
- [117] D. J. Berkeland, E. A. Hinds and M. G. Boshier, Phys. Rev. Lett. **75**, 2470 (1995).
- [118] S. Bourzeix, B. de Beauvoir, F. Nez, M. D. Plimmer, F. de Tomasi, L. Julien, F. Biraben and D. N. Stacey, Phys. Rev. Lett. **76**, 384 (1996).
- [119] D. Taqqu et al., Hyperfine Interactions **119**, 311 (1999).
- [120] M. Weitz, A. Huber, F. SchmidtKaler, D. Leibfried, W. Vassen, C. Zimmermann, K. Pachucki, T. W. Hänsch, L. Julien and F. Biraben, Phys. Rev. **A** **52**, 2664 (1995).
- [121] W. H. Press et al., *Numerical Recipes in Pascal* (Cambridge University Press, Cambridge, 1989).
- [122] J. W. Farley and W. H. Wing, Phys. Rev. A **23**, 2397 (1981).
- [123] H. A. Bethe and E. E. Salpeter, *Quantum Mechanics of One- and Two-Electron Atoms* (Plenum, New York, 1977).
- [124] D. H. McIntyre et al., Phys. Rev. A **39**, 4591 (1989).
- [125] L. Essen et al., Nature (London) **229**, 110 (1971); J. W. Heberle, H. A. Reich and P. Kusch, Phys. Rev. **101**, 612 (1956).
- [126] R. G. Beausoleil and T. W. Hänsch, Phys. Rev. A **33**, 1661 (1986).
- [127] D. G. Fried, T. C. Killian, L. Willmann, D. Landhuis, S. C. Moss, D. Kleppner, and T. J. Greytak , Phys. Rev. Lett. **81**, 3811 (1998).

- [128] J. K. Ranka, R. S. Windeler, A. J. Stentz: "Efficient visible continuum generation in air-silica microstructured optical fiber with anomalous dispersion at 800 nm". Conference on Lasers and Electro-optics (CLEO), postdeadline paper CD-8, Washington D.C. (1999).
- [129] M. J. Gander, R. McBride, J. D. C. Jones, D. Mogilevtsev, T. A. Birks, J. C. Knight and P. St. J. Russell, Electron. Lett. **35**, 63 (1999).
- [130] W. J. Wadsworth, J. C. Knight, A. Ortigosa-Blanch, J. Arriaga, E. Silvestre and P. St. J. Russell, Electron. Lett. **36**, 53 (2000).
- [131] T. A. Birks, W. J. Wadsworth and P. St. J. Russell, Opt. Lett. **25**, 1415 (2000).
- [132] T. W. Hänsch and B. Couillaud, Opt. Comm. **35**, 441 (1980).
- [133] C. Zimmermann, V. Vuletic, A. Hemmerich and T. W. Hänsch, Applied Phys. Lett. **66**, 2318 (1995).
- [134] P. Lesage, IEEE Trans. Instrum. Meas. **32**, 204 (1983).
- [135] S. Gerstenkorn and P. Luc , J. Physique **46**, 867 (1985).
- [136] J. P. Wallerand, F. du Burck, B. Mercier, A. N. Goncharov, M. Himbert and C. J. Borde, Eur. Phys. J. D **6**, 63 (1999).
- [137] K. Gäbel, P. Rußbühl, R. Lebert and R. Poprave, "New concepts for compact diode-pumped fs-lasers" poster Laser 97 Munich
- [138] V. Magni, G. Cerullo and S. De Silvestri, Opt. Comm. **101**, 365 (1993)
- [139] K. Gäbel, P. Rußbühl, R. Lebert and R. Poprave, "The influence of gain-saturation on Kerr-lens mode locking of a Cr:LiSAF laser" Conference digest CLEOEurope 2000, 144
- [140] C. Kan, N. H. Burnett, C. E. Capjack and R. Rankin , Phys. Rev. Lett. **79**, 2971 (1997).
- [141] Z. Chang, A. Rundquist, H. Wang, M. M. Murnane, and H. C. Kapteyn, Phys. Rev. Lett. **79**, 2967 (1997); Ch. Spielmann *et al.*, Science **278**, 661 (1997); M. Schnürer, Ch. Spielmann, P. Wobrauschek, C. Streli, N. H. Burnett, C. Kan, K. Ferencz, R. Koppitsch, Z. Cheng, T. Brabec, and F. Krausz, Phys. Rev. Lett. **80**, 3236 (1998).
- [142] I. P. Christov, M. M. Murnane and H. C. Kapteyn, Phys. Rev. Lett. **78**, 1251 (1997).
- [143] M. Nisoli, S. De Silvestri, O. Svelto, R. Szipöcs, K. Ferencz, Ch. Spielmann, S. Sartania, and F. Krausz, Opt. Lett. **22**, 522 (1997); S. Sartania, Z. Cheng, M. Lenzner, G. Tempea, Ch. Spielmann, F. Krausz, K. Ferencz, Opt. Lett. **22**, 1526 (1997).

- [144] Z. Cheng, *et al.*, in *Ultrafast Phenomena XI*, T. Elsässer, J. G. Fujimoto, D. A. Wiersma, and W. Zinth, eds., (Springer, Berlin, 1998), p. 8.
- [145] A. Poppe, PhD thesis, Technische Universität Wien, Vienna (2000)
- [146] I. P. Christov, Opt. Lett. **24**, 1425 (1999).
- [147] P. Dietrich, F. Krausz, P. B. Corkum, Opt. Lett. **25**, 16 (2000).
- [148] F. Krausz *et al.*, Opt. Photon. News **9** (7), 46 (1998); A. de Bohan, P. Antoine, D. B. Miloevi, and B. Piraux, Phys. Rev. Lett. **81**, 1837 (1998).
- [149] M. Mehendale, S. A. Mitchell, J. P. Likforman, M. Villeneuve and P. B. Corkum, Opt. Lett. **25**, 1672 (2000).
- [150] A. M. Weiner, Rev. Sci. Instr. **71**, 1929 (2000).
- [151] F. M. Gardner, *Phaselock techniques*, 2nd Edition, John Wiley & Sons, New York (1979).

Danke

Ich möchte mich bei Allen ganz herzlich bedanken, die diese Arbeit möglich gemacht haben und mich in den letzten drei Jahren tatkräftig unterstützt haben.

Mein besonderer Dank gilt an dieser Stelle Herrn Professor T. W. Hänsch, der die guten Ideen für die Frequenzkette nur so aus dem Ärmel geschüttelt hat und mir alle Möglichkeiten für diese Arbeit eröffnet hat.

Die „Frequenzkette“ war in den letzten drei Jahren sozusagen meine Heimat. Mit Thomas Udem und Jörg Reichert habe ich mir nicht nur die Meßnächte um die Ohren geschlagen, sondern auch so manche denkwürdige Bergtour gemacht und dabei noch eine Ganze Menge gelernt. Vielen Dank. Der Dank gebührt natürlich auch dem Jüngsten im Team, Marcus Zimmermann und unserem Sommergast Eva Rittweger.

Vielen Dank auch dem Wasserstoff-Team im Labor nebenan, in wechselnder Besetzung Andreas Huber, Bruno Gross, Markus Niering, Marc Fischer und natürlich Martin Weitz. Auch den „Indianern“ im Stockwerk über uns, Eckehard Peik, Joachim von Zanthier, Mario Eichenseer und Thomas Becker danke ich für die hervorragende Zusammenarbeit.

Helmut Brückner, unserem Elektroniker, der allzeit gut gelaunt die Wackelkontakte in Angriff nahm, unseren Technikern Charly Linner und Wolfgang Simon die schon die Hände über Kopf zusammenschlagen wenn mal wieder schnell was gemacht werden soll, vielen Dank. Ebenso geht mein Dank an Frau Lechner und Gabi Gschwendtner, unseren Sekretärinnen, die die Arbeitsgruppe am Laufen gehalten haben.

Der ganzen Gruppe danke ich für die gemütliche und gleichzeitig produktive Atmosphäre. Michael Mei für den Ausflug zu Businessplänen und ähnlichem, Kjeld Eikema für seinen Humor und seine unvergleichliche Art Vorträge zu halten, Anette Pahl, Jochen Walz, Reiner Scheunemann, Susanne Friebel, dem Rest der Gruppe aus der Stadt für die freundschaftliche Zusammenarbeit und natürlich das Freizeitprogramm. Viele Personen außerhalb unserer Arbeitsgruppe haben zum Gelingen dieser Arbeit beigetragen, allen voran natürlich unsere Engländer mit der „Wunderfaser“: Jonathan Knight, William Wadsworth und Phillip Russell, die Wiener Andreas Poppe, Sascha Apolonski, Gabriel Tempea und Ferenc Krausz, die Kollegen an JILA und NIST in Boulder, Scott Diddams, David Jones, John Hall, Jun Ye, Leo Hollberg, in freundschaftlicher Konkurrenz verbunden, die Pariser mit ihrer Fontänenuhr, Giorgio Santarelli, Pierre Lemonde und Michel Abgrall, ebenso aus Novosibirsk Sascha Nevsky, Pavel Pokasov, Mischa Skortsov, und schließlich aus Japan Takeshi Ikegami und Atsushi Onae,

ihnen allen danke ich für die gute Zusammenarbeit und für den Spaß (und den gelegentlichen Frust) den wir zusammen hatten.

Allen meinen Freunden in und außerhalb von München, die mich manchmal schon im Labor verschollen glaubten, danke ich für die moralische und anderweitige Unterstützung.

Nicht zuletzt bin ich meinen Eltern sehr dankbar dafür, daß sie mir das alles ermöglicht haben.

Vielen Dank!

Lebenslauf

Ronald Holzwarth

geb. am 9.9.1969 in Stuttgart

1976-1980	Grundschule in der Taus Backnang
1980-1989	Max Born Gymnasium Backnang
1989	Abitur
1989-1990	Wehrdienst
1990-1997	Studium der Physik, Universität Tübingen
1992	Vordiplom in Physik
1993-1994	Auslandsaufenthalt an der University of Oregon (Eugene Oregon)
1996-1997	Diplomarbeit bei Carl Zeiss, Oberkochen und Universität Tübingen
1997	Diplom
1997	Beginn der Promotion an der Ludwig-Maximilians-Universität München und am Max-Planck-Institut für Quantenoptik